UNIVERSITÀ DEGLI STUDI DI NAPOLI
FEDERICO II

Università degli Studi di Napoli Federico II

Ph.D. THESIS
in
Measurements

IoT for measurements and measurements for IoT

Alessandro Tocchi

Tutor: Prof. Mauro D'Arco

Coordinator: Prof. Riccio Daniele

XXXIII Ciclo

Scuola Politecnica e delle Scienze di Base
Dipartimento di Ingegneria Elettrica e delle Tecnologie dell'Informazione

Contents

Sommario

Introduction

More than 50 years have passed since the birth of the Internet and more than 20 since the expression Internet of Things (IoT) was coined. In these years, IoT technologies have multiplied and developed, as well as many application areas have deeply evolved: smart home, smart building, smart metering, smart factory, smart car, smart city, and so on to follow with smart environment, smart agriculture, smart logistics, smart lifecycle, smart retail and smart health. All areas made possible by the interconnection of smart objects. IoT can often be referred to the technological development whereby, through the Internet, potentially every object of daily experience acquires its own identity in the digital world. As mentioned, the IoT is based on the idea of "smart" objects interconnected in order to exchange information owned, collected and/or processed. But the meaning of IoT goes far beyond the simple definition and translates into: the IoT goes beyond smart objects and takes full meaning in the network that interconnects these objects. The examples of Internet of Things, as mentioned before, in this sense, are countless. Just think of cars, initially made connected "only" through GPS-GPRS boxes for insurance purposes and that today leave the factories already equipped with connectivity on board. Or the home, where we have witnessed the evolution from "only" wired home automation to wireless solutions that are increasingly affordable for everyone, characterized by cloud services and the growing use of Artificial Intelligence. Or think about the factory, an area in which IoT technologies are contributing both in terms of distribution of system intelligence. To give even simpler examples of IoT, let us think about the very common street lamps in our cities, able to adjust their brightness based on visibility conditions, or traffic lights that synchronize to create a safe path for the passage of an emergency vehicle. Thanks to IoT, the concepts of Cyber Physical System and Digital Twin become pervasive,

according to which objects acquire a virtual soul with a perfect correspondence between the physical and digital worlds. A cyber-physical or cyber-physical system is a computer system capable of continuous interaction with the physical system in which it operates. A digital twin is a digital replica of a physical entity, which can be a simple or complex object, an asset or a process. It is used to understand the state of the asset, simulate situations, monitor its operation, and troubleshoot problems. Digital twin technology uses cloud-connected sensors embedded in machines to upload real-time operational data, producing up-to-date virtual simulations of real machines. Particularly in the Smart Factory environment, the IoT paradigm together with the possibilities offered by Machine Learning opens up promising new scenarios for predictive maintenance. This new approach fuels important technological challenges of great interest to the scientific community:

- management of large amounts of data (Big Data);
- data storage and processing (Cloud);
- optimizations through machine learning methods (Machine Learning);
- data security (Cyber Security).

There are several challenges that are associated with the implementation and deployment of IoT solution. Some of the challenges are security and privacy, lack of interoperability, heterogeneity of IoT device, uncertainty in business models. Some of the technical issues are:

- Choice of Technology (The right choice of IoT technology is a big challenge because a lot of capital is needed to the use of new technologies. Key factors are support for roaming, suitability of technology to small-scale, medium-scale and large-scale, suitability to different geographical location and climatic conditions)
- Reliability (IoT devices must withstand severe weather conditions, such as flood and hurricanes.)

- Scalability (Existing protocols have to withstand a large number of IoT devices/nodes.
- Interference (The deployment of massive IoT devices will cause interference problems particularly with the IoT devices using the unlicensed spectrum.)

In this thesis work many approaches are shown, some of them specialized to implement innovative IoT measurement system:

- Fire-IoT is a conceptual IoT framework that best suits the issues related to fire Propagation Map simulation and Evacuation Plan Model of animals to support the activities of the Regional Veterinary referral Center for non-epidemic emergencies (CeRVEnE) in the Campania Region;
- RadIoT is an integrated platform based on a cost-effective wireless sensor network (WSN) for monitoring environmental radioactive pollution. This solution has fascinating features like scalability and flexibility to overcome the drawback of a classic monitoring system;

others to develop a different research path suited to find new technics to allow measurements on IoT systems, in particular on protocol such as LoRa/LoRaWAN

- An innovative approach based on compressive sampling has been shown, capable of extracting valuable parameters like “Bandwidth and Spreading factor” from signal that represents LoRa signal as locally sparse signal.
- A promising technic that allows the estimation of instantaneous frequency (IF) of signals characterized by interfering IF trajectories, has been shown. It could be a very useful methodology for maintenance and troubleshooting of LoRa networks sharing the same operating frequency range.

Part I-Internet of Things

Chapter 1- State of art

1.1 Introduction

The Internet of Things (IoT) is considered the third wave of information technology after internet and mobile communications [1]. The IoT is a collection of connected objects, embracing electronics, software, sensors that accumulate and exchange information with applications through wireless networks connected to the Internet. By allowing connected objects to remotely communicate and being remotely controlled, the IoT represents a direct integration between the physical and the digital worlds [2].
The IoT concept was formally proposed for the first time twelve years ago in 2005 in a Report of the International Telecommunication Union (ITU) where it was postulated that all objects can exchange information via Internet [1]. Since then, the number of connected objects has grown up quickly. Within 2020, 50 billion devices will be connected to the network (Figure 1). To that extent, the opportunities to reinvent existing objects into connected devices, that include sensors and transmitters, are theoretically countless. The Internet of Things (IoT) has found its application in several areas, such as connected industry, smart-city [3], [4], smart-home [5] smart-energy, connected car [6], smart-Agriculture [7], connected building and campus [8], healthcare [9], logistics [10], among other domains. IoT aims to unite the physical world with the virtual world via the Internet as a means of communicating and distributing information [11].

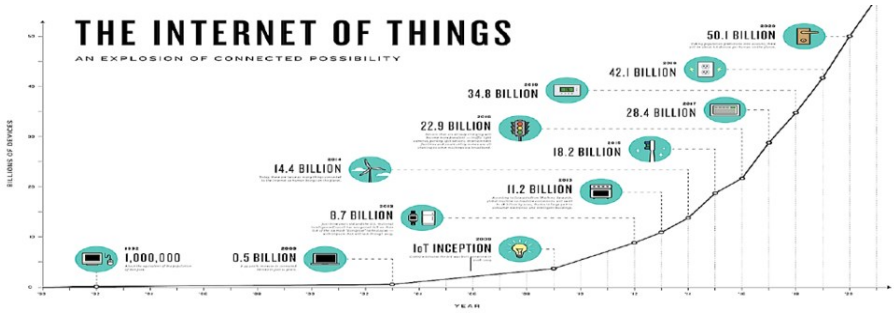

Figure 1-Growth of connected objects [3]

The IoT is seen as a system of interconnected computing devices, objects, mechanical and digital machines, animals or people with unique identifiers and the characteristic of transferring data over a network without requiring human-human or human-computer interaction. A key area of interest is the application of IoT in agriculture. It is estimated that the world's population will grow to about 9.7 billion people in 2050, so there will be a need for food, which along with diminishing natural resources, arable land, and unpredictable weather conditions, make food security a major concern for most countries. The world is increasingly making use of IoT combined with data processing (DA) to meet the world's food needs in the coming years [12]. The 'use of IoT devices in the agricultural sector is expected to increase from 30 million in 2015 to 75 million by 2020. The use of IoT and DA will lead to smart agriculture that is expected to provide high operational efficiency and high yield [13], [14]. IoT is the marriage of several existing technologies such as WSN, RF identification, cloud computing, middleware systems, and end-user applications. The IoT devices consist of embedded processing and storage systems that communicate with sensors and actuators and require wireless connectivity. These IoT devices are sometimes referred to as IoT sensors or IoT device. The embedded system consists of field

programmable gate array or microprocessor, communication modules, memory, and input/output interfaces. Sensors are used to monitor and measure a variety of variables (e.g., in agriculture, soil nutrients, weather data, in industry, air quality in warehouses, in the home, lighting in a room, etc.) and help manage factors that affect production. Sensors can be divided into macro areas based on their use, namely: into position sensors, optical sensors, mechanical sensors, electrochemical sensors and airflow sensors. Sensors are used to provide the atomic or complex information required for processing such as air temperature, soil temperature at various depths, precipitation, humidity, wind speed, pollutant rates, wind direction, relative humidity, solar radiation, and atmospheric pressure. There are key characteristics of IoT devices that make them suitable for different usage sectors: 1) energy efficiency; 2) memory; 3) computation efficiency; 4) portability; 5) durability; 6) coverage; 7) reliability; and 8) cost. Communication technology contributes massively in the successful implementation of IoT systems. It can be classified based on standards, spectrum, and application scenarios. Communication standard is divided into short-range and long-range communication standards. Communication spectrum can be grouped into licensed and unlicensed spectrum. The unlicensed spectrum has several disadvantages: security issues, the cost of infrastructure, and electromagnetic interference generated by radio devices using the same band, and makes use of the scientific and medical industrial RF band known as ISM band. On the other hand, the licensed spectrum that are allocated to the cellular network offer more efficient traffic management, less interference, better reliability, increased quality of service (QoS), high level of security, wider coverage and less infrastructure costs for users. The disadvantage for using licensed spectrum is the subscription cost for data transmission and the consumption of transmission power on IoT devices. The existing standards for wireless communications, are many. They can be classified based on the distance achieved into: short-range and long-range communication standards. Examples of

short-range standards are near-field communication-enabled devices, Bluetooth, ZigBee, Z-Wave, passive and active radio frequency identification systems (RFID), and they can cover distances within 100 m. Long-range communication standards can cover distances up to tens of kilometers and are referred to as low power wide area (LPWA) (examples are LoRa, Sigfox, NB-IoT). LPWA makes use of low power and can cover a wide area [16], [17]. The choice of communication technology also depends on the applications of the IoT device, whether they act as nodes or gateways. Nodes transmit little data and cover very short distances with low power consumption, while gateways support high data rates and reach much longer distances. Some of the communication technologies are bidirectional, allowing error correction, data encryption, over-the-air firmware updates, and communication between devices. From [18] It is possible to extrapolate the comparison between LoRa and NB-IoT, which shows that each technology has its own advantages and disadvantages, so the most appropriate technology depends on the application. The Internet is the primary network layer used to transport and exchange data and network information between multiple subnets. Connection to the Internet allows data to be available anywhere, anytime. However, it is necessary to ensure adequate security in the handling of sometimes sensitive data, real-time data support and ease of accessibility. The internet has enabled cloud computing, where big data is collected for storage and processing. To enable different systems and devices to connect over the Internet, IoT connectivity protocols and middleware are being developed, such as service-oriented architecture (SOA), cloud-based IoT middleware, and actor-based IoT middleware. SOA for IoT consists of a multi-layered architecture. Some of the IoT architectures that we have indicated have the following layers: sensing, access, network, middleware, and application layers. An example of IoT protocol is MQTT, which is a lightweight application protocol that allows devices to effectively and asynchronously communicate [19]. A software component which is used in a

publisher/subscriber communication model, is the broker that is responsible to data transmitting and receiving from the platform. It is a messaging server that deals with matching between Subscriber and Publisher with subsequent dispatching of the message according to topic of interest. In other words, a publisher sends a message on a specific topic to the broker. A subscriber (i.e. a consumer who subscribes to messages posted on the same topic) receives them from the broker when available. This communication model greatly simplifies the protocol and turns out to be one of the main application layer protocol for IoT applications. IoT applications involve the collection of huge amounts of data, dynamic, complex and spatial, which require storage and processing. They can be unstructured, structured data with complexity varying. They can be text, images, audio, and video. The data can vary from historical data, sensor data, livestreamed data, business etc. The use of IoT cloud platforms allows the amount of data collected from sensors to be stored in the cloud. This includes hosting critical applications across services. Recently, edge computing is advocated, where IoT devices and gateways perform computation and analysis in order to reduce latency for critical applications, reduce cost, and promote QoS [21], [22]. As an example the application of IoT in agriculture involves enriching farmers with decision-making tools and automation technologies that seamlessly blend products, knowledge, and services to ensure quality and profit are achieved. However, these opportunities are coupled with technical challenges. The point is how to transform common objects that have not changed in form or function for decades into smart devices Internet-connected. In order to achieve such a result, node cost, network cost, battery lifetime, data rate (throughput), latency, mobility, range, coverage, and deployment model are the most significant parameters to consider in the first instance. Recent surveys on IoT have focused on the challenges and constraints for large-scale pilots across the supply chain in the agribusiness sector [7], [15], but this can be simply extended to other sector. Some of the recurring issues are the need

for new business models, security and privacy, and data governance and ownership resolution. There are several security issues that need to be considered at different levels of the IoT ecosystem.

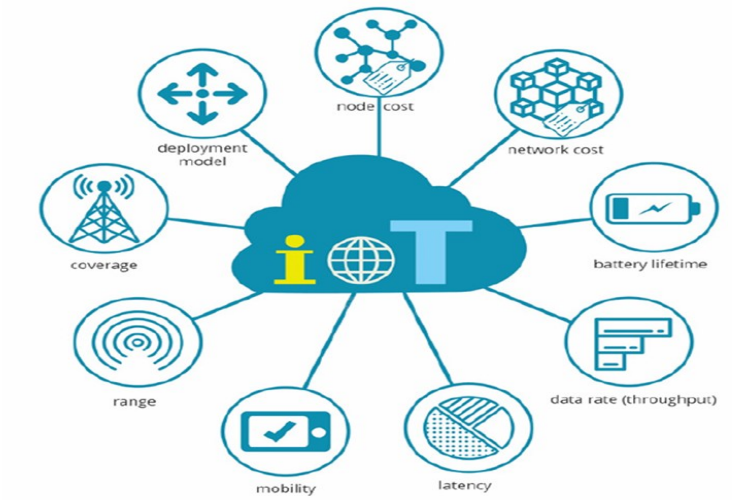

Figure 2- IoT applications challenges [89]

Lack of adequate security can lead to data loss, disrespect for privacy, and access to atomic field parameter information and other sensitive intellectual property. This can negate the competitive advantages of private farm owners who have chosen IoT solutions. The security and privacy issues of IoT have been discussed extensively in [22], [23] and [24]. On attitudes and perceptions of IoT, the security issue has a burden that can become a major obstacle in IoT deployment[22]. Heavy use of IoT devices could cause interference issues especially with IoT devices using unlicensed spectrum, such as ZigBee, Wi-Fi, Sigfox and LoRa, leading to data loss and reduced reliability of the IoT ecosystem. IoT devices that use unlicensed interference-proof spectrum are more expensive, as is using IoT devices that operate with licensed spectrum, barring

additional issues that might arise anyway.

1.2 LPWANs

It is easy to understand how one technology cannot serve all of the projected applications and volumes for IoT. Fixed and short range connections such as Wifi, Bluetooth, Zigbee, Z-Wave as well as cellular technologies have traditionally filled the gap, but cost, power and scalability concerns make these choices less appealing for the future [2].

Low Power Wide Area Network (LPWAN) communication technologies have arisen to solve this problem. Such solutions have the potential to provide a step change in the employment of cost-effective and energy efficient IoT applications. Indeed, it is expected that in 2024 more than 40% of the wide area M2M (Machine to Machine) connections will be LPWAN [8].

The LPWAN technologies are designed for sensors and applications that need to send small amounts of data over long range communications (dozens of km). The devices involved in such communications must have a low power consumption budget in order to operate several years remotely on a single battery pack, in varying environments [2] [8]. Typical application domains include smart city, metering, on street lighting control or precision agriculture [9]. Hence, in order to cover these and the new market needs that continually arise, several companies have developed different LPWAN technologies such as Long Range (LoRa), Sigfox, RPMA and Weightless [10] [11].To compare such protocols we have to bear in mind some of the most critical factors:

- Network architecture
- Communication range
- Battery lifetime or low power
- Robustness to interference
- Network capacity (maximum number of nodes in a network)

- Network security
- One-way vs two-way communication
- Variety of applications served [8]

In addition, a decisive characteristic is the spectrum use. In fact, in order to increase the communications range, a wireless device essentially needs to enhance the signal-to-noise ratio (SNR) at the receiver. Spread-Spectrum and Ultra-Narrow-Band (UNB) are two candidate technologies offering low-power long-range communication. [7] For instance, LoRa by Semtech uses Chirp Spread-Spectrum modulation, and NWave, Sigfox, Texas Instruments etc. are proposing modules based on Ultra-Narrow-Band technology [10].

Chapter 2- LoRa and LoRaWAN

2.1 Introduction

Among the several LPWAN technologies, LoRa emerges as one of the most widely deployed and is considered by a large number of industries as a base for their IoT applications [10].
The LoRa radio modulation technology was invented in 2010 by the French start-up Cycleo and subsequently acquired by the semiconductor company Semtech. Thus, a MAC layer has been included to standardize and spread the LoRa physical communication layer onto internet networks: the LoRaWAN (LoRa for Wide Area Networks) specification [2].
Along this line of thought, it is important to distinguish between LoRa and LoRaWAN in order to avoid misunderstandings. LoRaWAN is the communication protocol, open sourced and supported by the LoRa Alliance [12], a structured organization with multiple tiers of membership led by Semtech, IBM, Actility, and Microchip to name just a few [13].

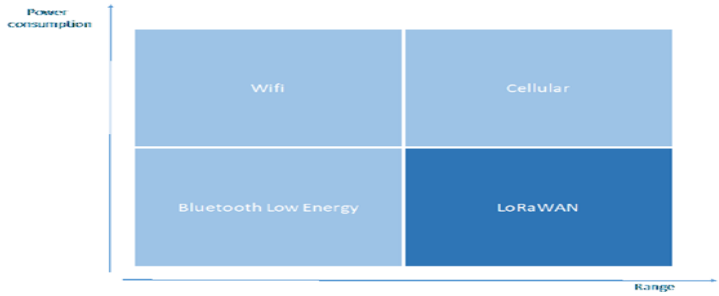

Figure 3 IoT connectivity technologies segmentation [2]

The LoRa (Long Range) is the physical layer or the wireless modulation utilized to enable the long- range communication link [8]. Hence, it is, more precisely, a proprietary spread spectrum modulation technique by Semtech. It is a derivative of Chirp Spread

Spectrum (CSS) with integrated Forward Error Correction (FEC) [10] [11].

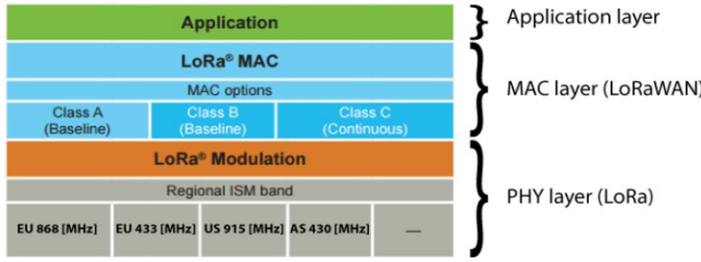

Figure 4 - LoRa protocol stack [6]

Both the protocol and the network architecture have the most influence in determining the battery lifetime of a node, the network capacity, and the quality of service, the security, and the variety of applications served by the network [6].
A LoRa receiver can decode transmissions 19.5 dB below the noise floor. Thus, very long communication distances can be bridged [11]. In fact, LoRa and LoRaWAN have a link budget greater than any other standardized communication technology. The link budget, typically given in decibels (dB), is the primary factor in determining the range in a given environment [8].
Other LoRa key properties are: high robustness, multipath resistance, Doppler resistance and low power [10]. Finally yet importantly, there is the cost. In fact, LoRa uses unlicensed spectrum below 1GHz, usually the ISM (Industrial, Scientific, Medical) bands, which come at no cost to the applications that use it. In Europe, ETSI regulates the ISM band access on the 868 MHz bands [2] [5].

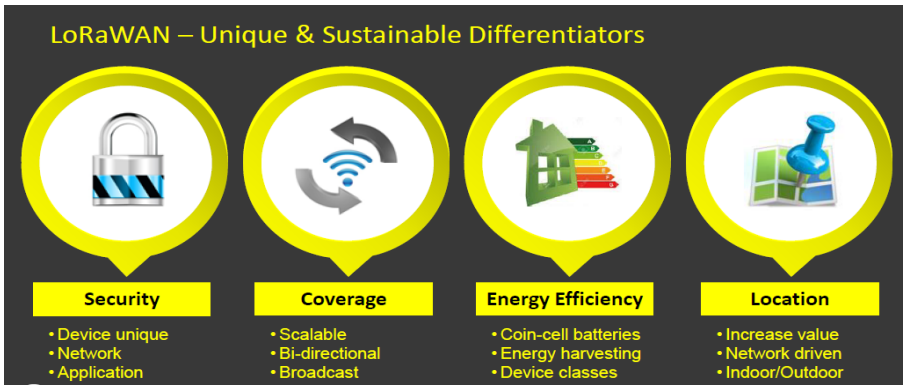

Figure 5 - LoRaWAN Differentiators [14]

However, LoRa and LoRaWAN cannot offer the same quality of service (QoS) of a time slotted cellular protocol. In fact, they are not a general-purpose solution. In terms of applications with very frequent communication and a very low latency constraint or large volumes of data, they do not represent the best option. Nevertheless, for applications that need very long battery lifetime and optimized cost, but do not need to communicate so often, LoRa configures itself as the best option. In fact, the asynchronous, ALOHA-based protocol, allows an end-device to sleep as long as the application desires. In a cellular-based synchronous protocol, the end-device must check-in with the network periodically. To that extent, an average cell phone today has to synchronize with the network every 1.5 seconds even while out of use [5].
Typical use cases are reported - depicted in the figure below.

Figure 6 - LoRaWAN application examples [2]

2.2 LoRaWAN

- **Architecture**

LoRaWAN networks are typically structured in a star-of-stars topology, in which gateway nodes transmit messages between end-devices and a central network server. End-devices send data to multiple gateways and each gateway is connected to the network server via standard IP connections. Communication is bi-directional although uplink communication from end devices to the network server is strongly favored [9]. Gateways are powerful devices with powerful radios capable to receive and decode multiple concurrent transmissions (up to 50) [11]. Many existing networks employ a mesh network architecture. In this kind of network, the different end-devices forward the information of other nodes. While this approach increases the communication's range, it also adds complexity and reduces network capacity as well as battery lifetime since nodes receive and exchange information from other nodes that are, with high probability, irrelevant for them [8].
By contrast, in LoRaWAN architecture the intelligence and complexity are moved to the network server, which controls the network filtering redundant packets, performing security checks, scheduling acknowledgements through the optimal gateway and so on. [6]. Thus, the end-devices can communicate only when they have data ready to send whether event-driven or scheduled. This type of protocol is the Aloha method. With this protocol, it is possible to avoid the periodic synchronization between nodes and network that characterizes the mesh and the synchronous networks. Exactly the frequent synchronization process consumes energy and represents the main cause of battery's lifetime reduction [8].

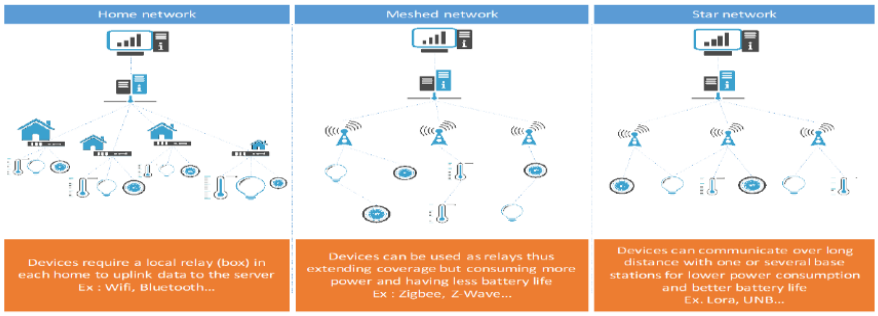

Figure 7 - other network architecture [2]

- **Device Classes**

Not all the nodes are equal. End-devices serve different applications and have different requirements. Thus, LoRaWAN distinguishes three different classes of end-devices to address the various needs of applications: Class A, Class B and Class C. Each end-device class has different behavior depending on the choice of optimization: a trade-off between downlink traffic and power consumption arises.

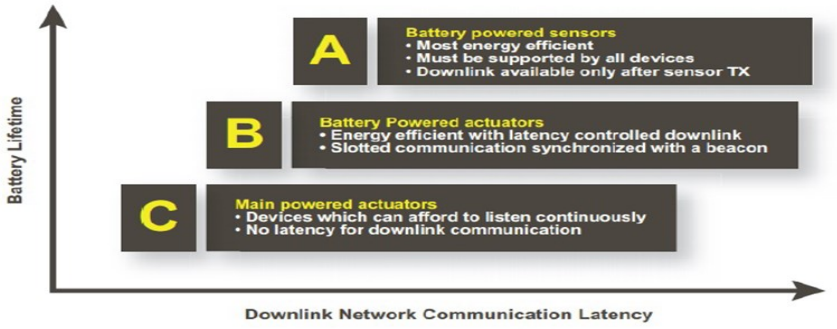

Figure 8 - other network architecture [2]

- Class A. End-devices of class A allow bi-directional

communications whereby end-devices can schedule an uplink transmission based on their own needs and each uplink transmission is followed by two short downlink receive windows. Downlink transmission from the server at any other time has to wait until the next uplink transmission occurs. Class A is the class of LoRaWAN devices with the lowest power consumption.

- Class B. The node behaves like a Class A node but opens extra receive windows at scheduled times. In order for the end-device to open its receive window at the scheduled time, it receives a time-synchronized beacon from the gateway. This allows the server to know when the end-device is listening. Class B devices are designed for applications with additional downlink traffic needs.
- Class C. End-devices of Class C have almost continuously open receive windows, only closed when transmitting. Thus, they have maximum power consumption.

The three classes can coexist in the same network and devices can switch from one class to another. However, there is not a specific message defined by LoRaWAN to inform the gateway about the class of a device and this is up to the application [8] [17] [9] [11].

- Adaptive Data Rate

In order to make a long range star network viable, the gateway must have a very high capacity to receive messages from a very high volume of nodes. The critical factors affecting capacity are the number of concurrent channels, the payload length, and the data rate (time on air). To explain this in detail, the selection of the optimized data rate is a trade-off between the communication range and the message duration. Communications using different data rates do not interfere with each other because the signals are practically orthogonal to each other, as it will be clarified, because of the spread spectrum modulation's peculiarities. LoRa data rates range from 0.3 kbps to 20 kbps. As the spreading factor changes, the effective data rate also changes. The gateway takes advantage of this property by being able to receive multiple different data rates on the same channel at the same time. Thus, in order to maximize both the battery

life of each device and the overall capacity available through the system, LoRa network infrastructures use an Adaptive Data Rate (ADR) scheme to manage the individual data rates and RF output of each connected device. By way of example, by shifting the data rate higher, the time on air is shortened opening up more potential space for other nodes to transmit [2] [8] [6].

Tabella 1LoRa parameters

Spreading Factor	Bandwidth [kHz]	Spreading Factor [chips/symbol]	Bit rate of the signal [bit/sec]	Chip rate [chips/sec]	Time per symbol [sec/symbol]
SF7	125	128	5469	125000	0,001024
SF8	125	256	3125	125000	0,002048
SF9	125	512	1758	125000	0,004096
SF10	125	1024	977	125000	0,008192
SF11	125	2048	537	125000	0,016384
SF12	125	4096	293	125000	0,032768

- **Authentication and security**

It is of paramount importance for any LPWAN to include security. LoRaWAN provides security both for the network and for the user. The network security guarantees authenticity of the end-device in the network whilst the application layer of security guarantees the network operator does not have access to the end user's application

data [6].

The LoRaWAN protocol, unlike traditional networks, separates and distinguishes between authentication and encryption, based on the AES 128 encryption scheme. In more detail, the LoRaWAN protocol prescribes two authentication methods: Activation by Personalization (ABP) and Over-The-Air Activation (OTAA). On the one hand, ABP devices are customized to interact with a unique LoRaWAN network identified by its Network ID on the other hand, the OTAA devices are not customized for a specific network but send a JOIN request to the Network of interest to receive an authorization token. The default recommendation for device makers is to use the OTAA method [2].

- **Band use**

Each network gateway listens to the same set of nine channels. According to the geographical area, the frequencies of these channels may vary [6]. In Europe, for instance, the band is estimated to be 868MHz [15]. In fact, the LoRaWAN specification varies slightly from region to region based on the different regional spectrum allocations and regulatory requirements. The LoRaWAN specification for Europe and North America are strictly defined, but the technical committee is still defining other regions, such as Asia [8].

	Europe	North America	China	Korea	Japan	India
Frequency band	867-869MHz	902-928MHz	470-510MHz	920-925MHz	920-925MHz	865-867MHz
Channels	10	64 + 8 +8	In definition by Technical Committee	In definition by Technical Committee	In definition by Technical Committee	In definition by Technical Committee
Channel BW Up	125/250kHz	125/500kHz				
Channel BW Dn	125kHz	500kHz				
TX Power Up	+14dBm	+20dBm typ (+30dBm allowed)				
TX Power Dn	+14dBm	+27dBm				
SF Up	7-12	7-10				
Data rate	250bps- 50kbps	980bps-21.9kpbs				
Link Budget Up	155dB	154dB				
Link Budget Dn	155dB	157dB				

Figure 9 - LoRaWAN regional requirements [8]

Therefore, it is correct to argue that due to these specifications, the usage of the band is submitted to limitations. The output power (EIRP) of the transmitter shall not exceed 14 dBm or 25 mW, and the duty cycle, defined as the maximum percentage of time during which an end-device can occupy a channel, imposed in Europe by ETSI, is limited to 1% (for devices) or 10% (for gateways) depending on the used sub-band [2].

Tabella 2 LoRa regional parameters

Modulation	Bandwidth [kHz]	Channel Frequency [MHz]	FSK Bitrate or LoRa DR/ Bitrate	Nb Channels	Duty cycle
LoRa	125	868.10 868.30 868.50	DR0 to DR5/ 0.3-5 kbps	3	<1%

Part II- Internet of Things for measurements

One path of my research is the upgrading of some old traditional monitoring systems and industrial activity, in terms of adoption of new technologies but also of new approaches, according to Industry 4.0 main concepts and IoT paradigm.

Chapter 3- Fire-IoT

3.1 Introduction

The goal is to describe a conceptual framework and show some preliminary results of an ICT system to be implemented to support the activities presented in the FRAC program. The aim is to provide an aid to fire risk monitoring, indicating a series of technical requirements, with a double objective, namely on one hand to monitor the forest areas at risk of fire in the so-called "Vesuvius red zone", and on the other hand to determine the Optimal Evacuation Route for Animals (OPERA from now on) in case of fire, for each of the reported animal species living in the mentioned red zone. During a fire, employees of local animal rescue organizations and/or farms work with law enforcement and firefighters to rescue as many animals as possible. These rescue operations do not turn out to be well coordinated or planned in advance, and typically depend on people unqualified in disaster management, despite the availability of government regulations such as the PETS Act of 2006 in the United States or Directive 2010/63/EU within the European Union. Collaborative and ICT technologies in emergency response have a significant impact and there is a fairly extensive literature on this.

Despite being used profitably in human rescue activities, sensor/cellular networks and decision support systems have yet to find their proper place in animal rescue. This work wants to fill this gap by proposing one of the first attempts to devise a rescue system for companion, farm and wild animals. The ICT system is concerned in the creation of a fire spread map and the definition of a compatible evacuation plan; the infrastructure that enables the implementation of the ICT system is examined, as well as the algorithms that lead to the optimization of the evacuation route. Some preliminary results are also presented, including an analysis of a study scenario.

3.2 Disaster Risk Management

Disasters have always accompanied human history. Technological advances have led to the creation of many permanent infrastructures as well as to the flourishing of studies concerning the management of catastrophic events, which includes the sum total of all activities, programs and measures that can be taken before, during and after a disaster with the aim of avoiding it, reducing its impact or recovering from its losses. The last decade of the 20th century has been devoted to promoting solutions to reduce risks from natural hazards. It started by defining some terms, for example, hazard can be defined as "a dangerous condition or event that threatens or has the potential to cause injury to life or damage to property or the environment"[25]. Vulnerability can be defined as "the extent to which a community, facility, services, or geographic area can be damaged or disrupted by the impact of a particular hazard due to its nature, construction, and proximity to hazardous terrain or a disaster-prone area." Critical importance is therefore assumed by the concept of the "Disaster Management Cycle/DMC" (Figure 10). The main phases of the DMC can be briefly described as follows [26]:

- Disaster Impact: point (in time and space) at which a disaster occurs. However, including it serves as a reminder that in

disaster management terms impact can vary between different types of disaster.

- Response: encompasses all the measures usually taken immediately prior to and following disaster impact, the latter being the most frequent application of the concept. Such measures are mainly directed toward saving life and protecting property, and to dealing with the immediate disruption, damage, and other effects caused by the disaster.
- Recovery: means the process by which communities and the nation are assisted in returning to their proper level of functioning following a disaster. The recovery process can be very protracted, taking 5–10 years, or even more.
- Development: such a segment provides the link between disaster-related activities and national development. Its inclusion is intended to ensure that the results of disaster are effectively reflected in future policies in the interest of national progress.
- Mitigation: specific programs intended to reduce the effects of disaster on a nation or community.
- Prevention: means the set of actions designed to impede the occurrence of a disaster and/or prevent such an occurrence having harmful effects on communities or key installations.
- Preparedness: usually regarded as comprising measures which enable governments, organizations, communities, and individuals to respond rapidly and effectively to disaster situations.

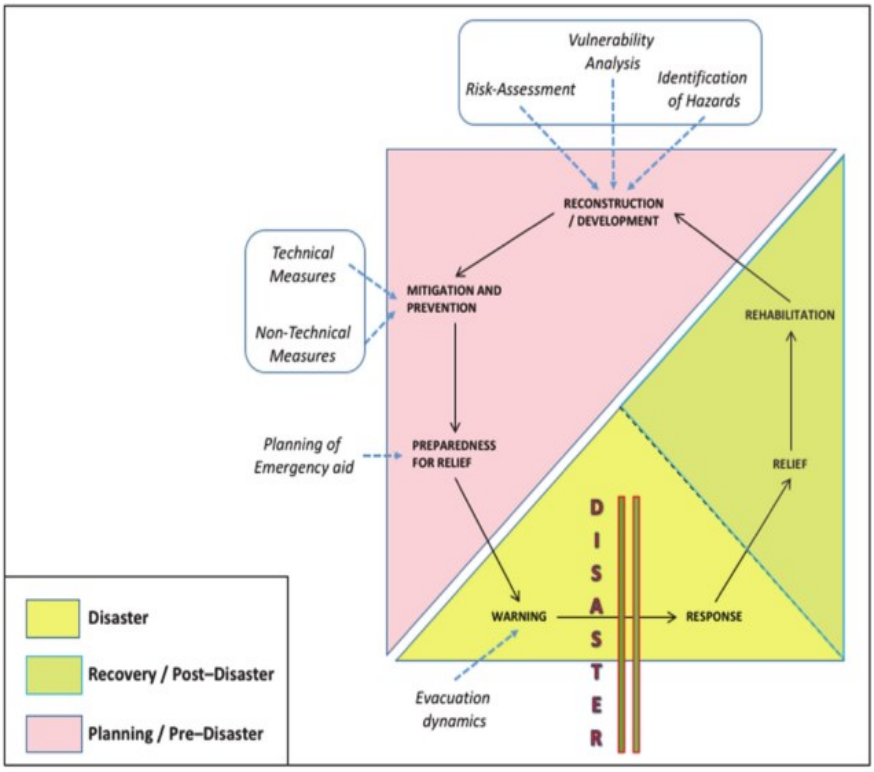

Figure 10 - DisasterManagement Cycle (elaborated from: Baird et al., 1975; Shorbi andWan Hussin, 2015).

As a dynamic entity, all phases of the DMC infer and involve action. This obviously requires a number of specialized structures and systems, usually needed to cover such things as the direction and coordination of disaster-related action, emergency operations center activities, as well as the management of warning information. Among the major contributions made to the development of the DMC, it is worth mentioning: the aforementioned "Foresight

Approach," as its importance is increasingly recognized by disaster managers and decision makers to understand long-term planning actions.

3.3 Fire Risk Monitoring

Forest fires are an unpredictable, violent, and damaging natural disaster, which is why their quantitative analysis and modeling are important to many areas of research. As a result, several types of technologies have been developed and implemented to measure key parameters for early fire detection in risk areas. In particular, the use of GIS and remote sensing technology plays an important role in forest fire detection and prediction: on the one hand, the implementation of hierarchical wireless sensor networks (WSNs) means the use of a number of sensing nodes that are able to efficiently collect information from the surrounding environment and communicate with each other to send the measured data to a base station for further processing [27][28]; on the other hand, geographic information systems (GIS) can be used to combine different factors that cause forest fires to obtain the map of forest fire risk areas. The GIS implementation allows the evaluation of a number of parameters that influence fire, such as topography and vegetation. With other land use information including population, settlements, fire towers, fire stations, intervention locations, characteristics of personnel who will intervene, and transportation; this can make it possible for example to understand the shortest route of intervention during the disaster and/or the areas to be cleared [29][30]. GPS tools methodology can be considered very accurate for small fires, it introduces errors in mapping large fires. On the other hand, remote sensing is considered to be very reliable for mapping large fires, while it is less accurate in mapping small fires. In addition, many scholars have developed general models to provide a decision-making assistant for forest fire prevention systems, and thus, provide a scientific basis for disaster prevention, mitigation, and post-disaster

loss assessment; it is e.g., the case of [[31],[32]].

3.4 ICT System Modeling

The software architecture presented in this paper aims to integrate a Distributed Sensor Network (DSN), an ad-hoc software to generate point simulations for fire risk modeling, and a GIS (Geographic Information System) for both web mapping and OPERA definition tasks. In particular, the latter step will be performed as an arborescence optimization problem to be solved, for example, through label setting correction algorithms [33]. Such a framework should overcome some of the limitations that have emerged in the description of many of the current solutions adopted in the world. In particular, there is a lack of effective integration of the individual aspects proposed as components of our system, nor do solutions appear to be available that address all DMC issues. Furthermore, the clear inclusion of animal issues within the broader dimension of emergency management strategies does not appear to be a "trending topic." While the inextricable connection between humans, animals, and the surrounding environment emerges as one of the cornerstones of the One Health concept, which is inevitably called into play when it comes to risk management (not just fire-related) [34],[35]. Figure 11 illustrates the architecture of the proposed framework [36]. At first, a set of specific information is collected to create a fire propagation map, through which the characteristics and dynamics of a fire scenario can be analyzed and evaluated (represented in the figure in the first upper rectangle). From this, an Evacuation Plan Model can be determined (the middle rectangle in the figure) by also adding anthropogenic data related to both the rate of urbanization and the development of the road system surrounding the area of interest, e.g. Vesuvius in our study. For both phases, the deployment of specific sensors is required in order to collect the necessary mentioned information about the situation and the context. Finally, the model must be enriched with the mapping of animal presence (in

terms of both type and distribution) and the clear definition of the type and size of vehicles required to rescue animal species involved in a fire episode. The determination of the OPERA for the involved rescuers (e.g., beekeepers in our study) will be analyzed as a first case scenario (in the lower rectangle of the figure), in order to show the internal logic of the system and to provide some preliminary results on its dynamics of operation.

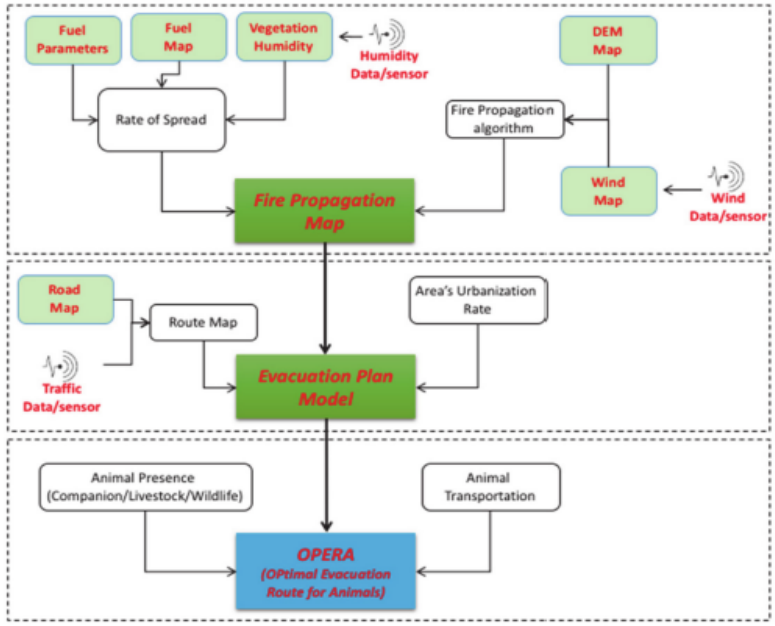

Figure 11 - Architecture of the proposed conceptual framework

3.5 DSN

DSNs have widely been investigated in the past, especially after the widespread deployment of wireless technologies, which have largely simplified and made cheap network installation and maintenance

operations [37],[38],. At present, one can say that the design of networks for a variety of applications is easily affordable. But, for severe working conditions, such as those related to the presence of fire or other kinds of harsh environments, the work of the designer becomes sensitive.

The aimed DSN is in charge of detecting critical events, monitoring their dynamics, and, eventually, signaling early warnings. Also, it is capable of tracking people and animals' activities in the area at risk, as well as informing about traffic jams along escape routes. The reliability of the aforementioned information is essential to the final goal of the overhead ICT system, devoted to real-time mapping risks and effectively implementing, on the need, the evacuation plan.

Due to the plurality of the targets demanded to the DSN the network designer has to consider several technologies and arrange solutions to let them coexist: satisfying all specifications is otherwise unfeasible. Nonetheless, he has to obey the constrains for interfacing the network with the application level of the ICT system, where the algorithms for the control of high-level operations, such as identification of optimal evacuation routes and most favorable flows scheduling, are executed. The main technical issues at design and deployment stage concern both the very purpose of the DSN and the requirements of being it a part of a multifaceted IT system.

Scrolling down the requirements of the DSN, scalability an upgradability stand as major ones. Scalability is intended as the possibility of integrating additional units in order to improve the basic network operation. Future upgradability is instead granted by conceiving the network as an open system with minimal constraints on interface requirements. In perspective, a relevant boost in DSNs performance is, in fact, expected from the utilization of the Internet of Things (IoT) devices now under testing. Thanks to the inherent granularity of IoT systems, as well as to their connectivity and integrated adaptation schemes, the DSN will definitely accomplish improved robustness and reliability with the integration of compatible IoT units.

The electricity demand of the network units should be managed with efficient strategies, also considering the presence of pre-existing infrastructures. The typical sleep/deep-sleep operative modes can be exploited, which involve that all non-critical modules are disconnected from the power supply except during their short operative slots. Nonetheless, smart power module complemented with solar, micro-wind, or piezoelectric energy harvesting systems can sustain the electricity supplies made of batteries or super-capacitors.

Concerning data communications aspects, a hybrid design approach, that merges both wireless and cable connectivity, can offer superior robustness and reliability; as for the electricity infrastructure, therefore, the presence of pre-existing cabling has to be considered. Hybrid solutions also provide additional degrees of freedom, thus offering a larger set of solutions for trading-off between number of terminal units, adopted communication means, complexity and costs of the network.

The availability of a network clock signal is necessary for synchronization purposes. To this end, gateways equipped with low-cost GPS receivers are opportune. The network can be complemented with an additional protected gateway, implementing the black-box concept, such that post–disaster analysis is made possible. The protection of the black-box gateway represents a sensitive aspect and has to be assured by physically placing, or constructing for it, (at least for the critical parts of its hardware) a safe sheltered site. In order to face issues related to harsh operating conditions, like those experienced during forest fires, the designer has to assure sufficient operating time also to other selected critical equipment, considering for them the use of superior casing structures, like IP67 anti-fire packages.

The design cannot jeopardize maintenance issues after the DSN deployment. In particular, the on-filed units of a DSN represent hot entries in maintenance programs, since most of them claim for on-site operations, such as battery replacement, which is troublesome if

the unit is installed in a harsh environment. To this end, new prognostic and diagnostic methods, based on Artificial Intelligence (AI) approaches, can offer relevant benefits, in terms of faults reduction, improved overhauls rapidity, and maintenance costs as a whole. An AI sub-system supporting the DSN maintenance program can be included at application level in the ICT system.
Conclusively, the designer has the responsibility of finding the synthesis that best satisfies the mandatory requirements and grants compliance with standards that are applicable to network topology, specific hardware and software solutions, as well as to energy supply and ancillary energy harvesting systems.

State-of-the-art technologies footing DSN

At the state-of-the-art the innovative paradigm enabling IoT applications, sketched in Figure 12, seems to offer superior advantages in both design and implementation of a candidate DSN with respect to more traditional solutions. The DSN has therefore to be conceived as a network of smart devices, or smart things, with sensing and actuating capabilities, as sketched in Figure 12.

Figure 12 - Schematic representation of a DSN for early detection and monitoring of fire in forest areas, eventually integrated with several facilities made available by IoT solutions.

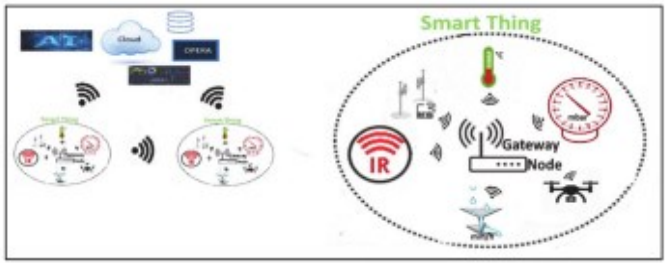

Figure 13 - Smart devices with sensing and actuating capabilities and their inter-networking

Smart devices mainly consist of sensors/actuators and gateway sections. Each sensor includes a smart power module, one or more probes, a processor, such as the one available in commercial boards hosting system-on-chips, and a communication module. The latter is often optionally included in the processor board; if not it has to be connected as an external unit to obtain connectivity.
Probes typically include an analog front-end and electronics for pre-processing the input. Most of them even provide analog to digital conversion, local data storage, and one or more standard digital interfaces. Smart detectors for smoke, relative humidity, temperature, atmosphere pressure, mono and di-oxide carbide (CO, CO2) percentages, solar irradiance, rain percentage, infrared/ultraviolet radiation intensity, volumetric water content and suction in soil, including the aforementioned characteristics, are commercially available. More recently, unmanned aerial vehicles (UAV), also known as drones, have successfully been used as sensors/actuators, thus showing the possibility of overtaking the barrier of the static concept of sensor in a DSN. Drones offer dynamic configurability and widen DSN terminal units to new kinds of operations not possible with fixed units. Furthermore, DSN units can include radio-frequency identification (RFID) options, by hosting one or more tags, and allow the intervention of personnel at the network level with the use of a hand-held reader device. The tags exchange short data

packets with the reader by exploiting the back-scattering principle, namely by radiating back a modulated version of the received signal, where the modulation is used to convey information. The reader equipment is made up of a power module, a processing machine and an RF transponder; it extracts the information from the on-field unit and makes it readable to the technician.

More in detail, RFID tags can be classed into active, passive and semi-passive. Active RFID transponders are self-powered, whereas passive ones are powered with an external electromagnetic signal. For passive tags the reader equipment transmits energy, which is temporarily stored as charge in an auxiliary capacitor complementing the tag. Further classification is based on the adopted frequency band: the low-frequency (LF) tags operate in the range 125 kHz up to 135 kHz, the high-frequency (HF) ones use the band centered at 13.56 MHz, the ultra-high-frequency (UHF) ones use the bands centered at 433 MHz, 868 MHz and 956 MHz; the very last RFIDs on the market can use the free microwave band centered at 2.4 GHz. UHF and microwave RFIDs need shorter antennas with respect to LF ones and allow reading operations at longer distances, up to 10 m. UHF frequency range is also well suited to tracking applications, where fixed readers interrogate tags associated to animals, for instance inserted in a collar, to identify them and extract further information, which can be useful during emergencies events.

Data transmitted by terminal units should match simple structures and be concise, so that traffic between terminal units and gateways can easily be upgraded to upcoming technologies and communication protocols. Concise data and low data rates cope with the low-power requirements of long–range wide-area networks and related protocols. At present LoRaWAN, a novel wide range distance communication protocol robust to noise and interference, and capable of offering a coverage radius up to 15 km, deserves particular attention since it can be implemented using ultra-low-power electronic circuits. A variety of low-cost equipment recently presented on the market support long-range data transmission and

allow rapid prototyping network solutions. For instance, there are starter packs and evaluation boards offered major manufacturers that combine powerful 32-bit microcontrollers with several different expansion boards. These can include several micro electro-mechanical sensors (MEMS) as inertial (accelerometer and gyroscope), pressure, humidity, and temperature sensors. The use of proprietary solutions that operate as serial long-range transmitters, where data are encapsulated in key-value proper structure and transmitted to the gateway, should be considered as a secondary spare.

State-of-the-art technologies footing network gateway and structured data management

Gateways collect data from the terminal units deployed on field and forward them to the core processor of the ICT system. A network can include several gateways each one connected to a subset of the terminal units. More specifically, gateways have to pre-process and merge the atomic data produced by the terminal units into structured information, and transmit it to the ICT platform. They require much more hardware in terms of processing and memory resources than terminal units.

Commercial boards, such as BeagleBone and Raspberry-pi, represent viable choices. They are very cheap single-board computers based on a renowned operative system (Linux), which can be equipped with additional modules for signal conditioning, analog-to-digital conversion, and wired/wireless standard communication interfaces. By exploiting the local storage capabilities of gateways, copies of critical data can be temporarily saved, thus avoiding information loss in case of occasional connection failure.

Gateways can communicate with the overhead ICT platform by means of either standard mobile or Ethernet protocols or message queue telemetry transport (MQTT) protocol, a publisher/subscriber application protocol fancied by IoT developers. Data refresh can be

programmed at low rate, which is sufficient for regular monitoring. The network can be designed such that data refresh is automatically increased during emergencies, eventually by complementing LoRa technology with redundant solutions. These can rely on different technologies capable of assuring wider bandwidth even at the expense of increased power requirements and shorter range coverage, and a suitable dynamic switching strategy.

Merging atomic data to produce structured information involves a distributed and hierarchical database architecture. In this scenario, each gateway plays its own role by saving data of a set of terminal units, namely those directly connected to it, and manage a portion of the whole database assembled by the overhead ICT system. Also, a subset of primary gateways of the network can be equipped with additional memory resources to store clones of the local databases hosted by adjacent gateways; this assures more robustness of the network in terms of capability to keep safe the collected data. Redis or MongoDB databases represent ideal candidates. They are recent solutions featuring innovative storage and data retrieval mechanisms, which are different from the tabular approaches used in relational databases. In particular, Redis is an open source in-memory data store, that grants high availability and fast responsiveness. It can cope with many data structures, from simple ones as strings to more complex ones as hash tables and lists. Nonetheless, its built-in replication mechanism, implemented according to a master/slave model, mostly simplifies the production of exact copies of database instances. It provides automatic partitioning, which is a way to automatically split and distribute data across different memory units. It offers a mechanism of self-diagnostic to constantly check if master and replica instances are synchronized.

Finally, the overhead ICT system can integrate cloud–computing services that simplify storage and computational tasks, and produce more consistent, accurate, and useful information than atomic systems. Cloud services also represent efficient solutions for the implementation of artificial intelligence (AI)–based approaches,

which are becoming important backings to solve very complex problems.

3.6 Mapping of the territories

Satellite data represent the primary source of information for mapping areas under risk of fire. Figure 14 reports the main results of a first extended mapping of the territories surrounding the Mount Vesuvius performed during the years 2018 and 2019 within the FRAC program. The purpose was twofold: (i) figure out a reliable map to classify the different fire risk areas, according to the Fire Risks Assessment Matrix (Figure 15) [[40]–[39]] (left side); (ii) detect and count all the farming activities concerning poultry, sheep and goats, cattle, bees, swine, and equines (right side).

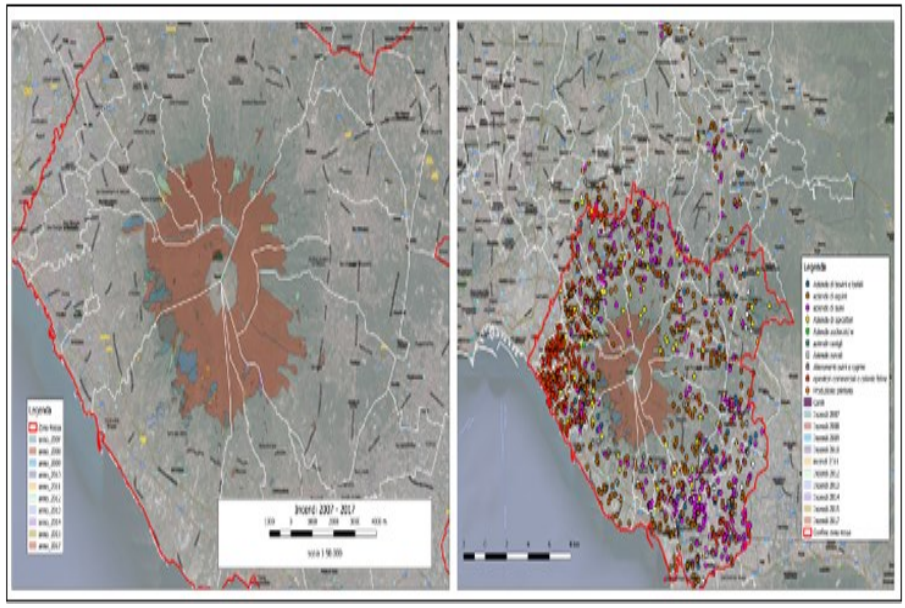

Figure 14 - Map of the territories surrounding Mount Vesuvius, reporting fire risk areas (left) and farming activities classified according to the Fire Risk Assessment Matrix (right) (Source: FRAC program)

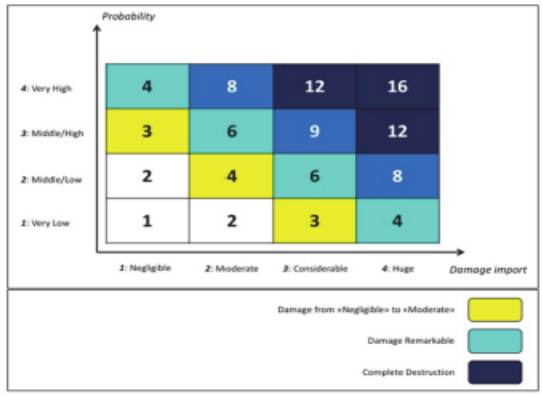

Figure 15 - Fire Risk Assessment Matrix

3.7 TIGER Simulation tool

The Fire Propagation Map is the output of the so-called TIGER simulation tool [41],[42]. In particular TIGER calculates a discrete-time spread of the fire perimeter in a 2D-landscape using two simple modules:

- the first allows calculating the rate of spread (ROS) maximum according fuel type/vegetation distribution and vegetation humidity data;
- the second performs a geometric algorithm to calculate the perimeter evolution of the fire according Digital Elevation Map (DEM) and wind data.

The effective ROS, derived by the calculation of the fire intensity / speed, is determined by :

$$ROS\_Effective = ROS\_max * WindEffect * SlopeEffect$$

where: ROS_max (m / hour) is the maximum ROS; WindEffect and SlopeEffect are the limiting factors of the wind and slope, respectively.

Moreover, each area covered by fire is described by a perimeter formed by nodes and segments. In the model, in each simulation step, the nodes move outward to form a new larger perimeter according to

the ROS_effective parameter. Consequently, the model requires the following input data:

- DEM (digital elevation map), with a horizontal grid resolution of 20-40 meters. The projection must be metric UTM WGS84;
- a fuel classification map based on the Anderson types [43];
- vegetation humidity data;
- observations and / or wind forecasts for the areas of interest (average speed and directions).

In the proposed system the vegetation humidity and wind data will be provided from the implementation of an integrated sensor net distributed on the landscape.

3.8 Preliminary Results

The first–case scenario chosen to figure out the proposed framework focuses on beekeepers as the beehives transportation is in general less problematic in terms of general set up and execution.
The geo-spatial data provided from the South Italy Experimental Zoo-prophylactic Institute (Istituto Zooprofilattico Sperimentale del Mezzogiorno, IZSM) concerning the fires occurred in the Mount Vesuvius surrounding area during the years 2007–2017, made possible to localize all the beekeepers' farms, other than collecting information as to the negative impact of the fires on their production dynamics. Since it is known that the maximum flight range of a bee swarm is of 7 km from the source point (the beehive), two buffer zones were then considered (Figure 16):

• the first (orange line; width of the buffer radius = 1 km) was meant to localize all the beekeepers' farm directly involved in fire episodes for the period 2007–2017;
• the second (yellow line; width of the buffer radius = 7 km) was meant to figure out the areas indirectly involved by the effects of the mentioned fire episodes.

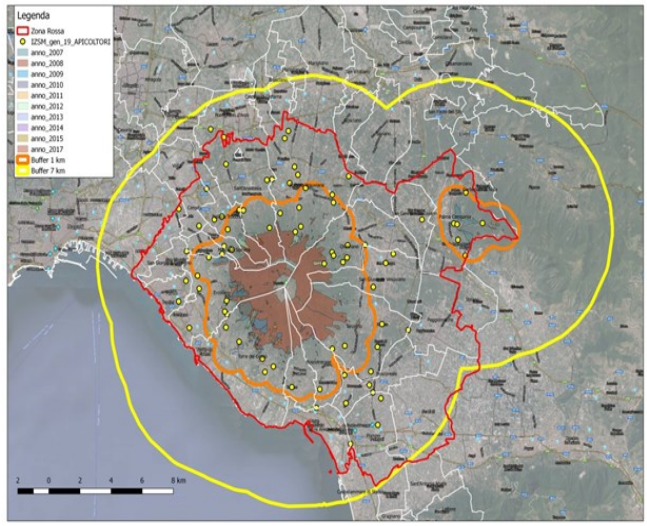

Figure 16 - Buffer zones interested by direct (inner zone) and indirect (outer zone) effects of fires on beekeepers' farms for the period 2007–2017

The mapped farms are 81, located as follows:

- 34 in the vesuvian area, and set at a distance of less than 1 km from the areas directly interested by fire episodes;
- 6 within the boundaries of the Municipality of Palma Campania, and set at a distance of less than 1 km from the areas directly interested by fire episodes;
- 41 comprised between 1 km and 7 km from the areas directly interested by fire episodes. In particular, 4 farms are outside the Vesuvius' red zone (2 in the Municipality of Pomigliano d'Arco, and 2 in the Municipality of Nola).

The results of the analysis of the data highlighted that, since all the farms are set within the radius of the external buffer, it is highly likely that all the bees have been affected by the disaster episodes occurred in the period of study.
Figure 17 reports the main working steps of the introduced ICT

systems towards the definition of the OPERA for the case of a beekeeper farm set in via Carcova (starting junction/node) on Mount Vesuvius' north-east slope, up to the safe zone located at the nearest entrance of the A30 highway (ending junction/node). The map in Figure 17a) was obtained by means of a GIS software for the purposes of the FRAC program. It shows the starting node within a white circle, along with the other beekeepers' sites standing on the territory under consideration, characterized by different fire risk areas (from yellow to red, in increasing danger level). In Figure 17b) the TIGER simulation tool is run, considering a fire source quite close to the beekeeper's site. In this case the spreading of the fire front is calculated setting up a 5-minute distance between two consecutive fire perimeters. In Figure 17c) both the simulation– and the route optimization–focused aspects have been combined as a two-layers representation on a Google Maps © chart: on the one side, the dashed yellow perimeters refer to the spreading of the fire front. In this case the simulation was run considering a 10-minutes distance between two consecutive fire perimeters; on the other side, the segmented white line was obtained by using a label setting-correcting algorithm appropriately implemented. The figure also shows the red cross meaning that that particular node, according to the simulation, would have already been reached by the fire by the time the token was supposed to get there, therefore it was necessary to calculate another path among all the available ones. The OPERA (OPtimal Evacuation Route for Animals) was eventually calculated for the case analyzed, and resulted to be the minimum path to get from the beekeeper farm in via Carcova to the A30 highway with a single vehicle to escape fire.

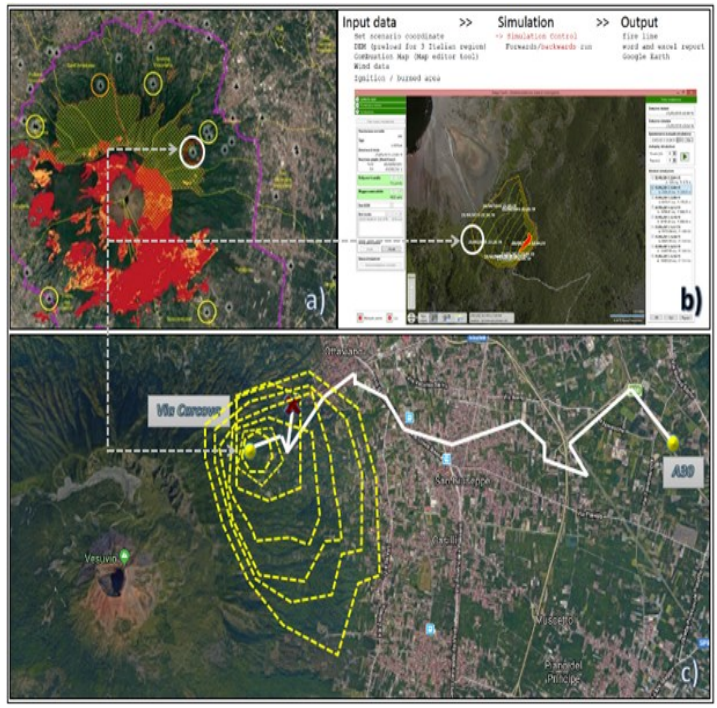

Figure 17 - (a) mapping of the beekeepers' farms in Mount Vesuvius' red zone; (b) example of the TIGER simulation tool; (c) evaluation of the OPERA for a beekeeper farm.

Chapter 4- RadIoT

4.1 Introduction

Radiological threat (i.e., the risk associated with radioactive isotopes) is usually associated with military and civil applications involving either radioactive weapons or other radiological dispersal devices (e.g., deposits in soil or water, nuclear plants and so on) [44]. In recent years, some authors evidenced that limited quantities of radioactive materials can cause heavy damages and losses if they are ingested or inhaled [45], thus providing criminal terrorists with alternative strategies for their attacks based on radioactive water sprays, as an example. Measuring and monitoring the concentration of possible nuclear pollutants turns out to be advisable or mandatory in several environmental contexts; the fast availability of an appropriate response plan allows, in fact, the consequences of radiation to be reduced or completely removed. As an example, technicians of operating or dismissed nuclear power plants continuously need to sample air, water or soil in different, strategic locations to determine if dangerous slags are leaking in the surrounding environment. To this aim, several solutions based on sensor networks, data acquisition systems and digital signal processing have recently been presented in the literature to provide real-time information about the radioactive risk [46],[48]. After investigating the potentiality of the Internet of Things (IoT) to realize an integrated platform based on a cost-effective wireless sensor network (WSN) for monitoring environmental radioactive pollution [49], it is understood that this innovative paradigm can, in fact, be adopted to design and implement a new WSN capable of taking advantage of its fascinating features, to overcome the drawback of a classic system based on a traditional WSNs [50]–[51]. In particular, scalable and flexible network infrastructure can straightforwardly be implemented; the scalability and flexibility are associated with the capacity of adding new nodes of different chemical or physical

quantities (e.g., gamma ray or alpha particles for the case study of interest) by means of minimal hardware requirements and standard software interface[52]. Moreover, cloud data management and big data processing mechanisms, typically involved in IoT platforms, can help face the other main drawbacks associated, such as the relevant computational burden needed to carry out detection algorithms (as an example, those based on Bayesian methods) [53].

4.2 Operation principle of Geiger and gamma-ray probes

Ionization detectors were the first electrical devices developed for radiation detection. Their principle of operation is based on the direct collection of ionization electrons and ions produced in a gas by the passage of radiation. During the first half of the century, three basic types of detectors were developed: the ionization chamber, the proportional counter, and the Geiger-Mailer counter. These particular devices are not widely used in modern nuclear and particle physics experiments today, unless there are specific applications. However, they are still widely used in the laboratory for radiation monitoring, given also their inexpensiveness, simplicity of use, and easy maintainability. Their implementation and basic structure, in fact, have changed little since the late 1940s, when the scintillation counter, then newly developed, began to take the place of these instruments in nuclear research. Due to the higher mobility of electrons and ions, a gas is the obvious medium for obtaining ionization collection from radiation. The three gas devices, namely the ionization chamber, the proportional counter, and the Geiger-Muller counter, serve as comprehensive examples of the application of gas ionization phenomena in this class of instruments. These detectors can be seen as the same device working in different operating scenarios, exploiting different phenomena. The simplest structure (Figure 18) consists of a container, which for simplicity we will consider a cylinder, with conductive walls and a thin terminal

window.

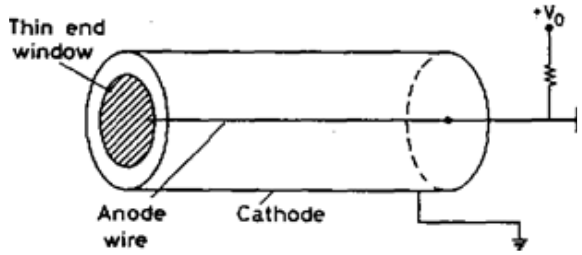

Figure 18 Basic construction of a simple ionization detector

The cylinder is filled with an appropriate gas, usually a noble gas such as argon. Along its axis is suspended a conducting wire to which is applied a positive voltage, + V0, with respect to the walls. So a radial electric field has been established. If the radiation hits the cylinder, there will be the creation of a number of electron-ion pairs. The average number of pairs created is proportional to the energy deposited in the counter. Under the action of the electric field, electrons will be accelerated toward the anode and ions toward the cathode where they are collected. The observed current signal, however, depends on the field strength. (Figure 19) depicts the trend of total charge collected as a function of applied voltage.

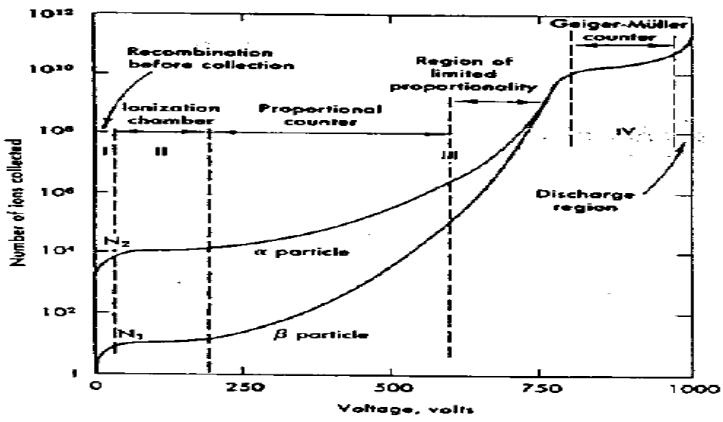

Figure 19 Number of ions collected versus applied voltage in a single wire gas chamber

At zero voltage there is no charge collected since the ion-electron pairs recombine under their mutual electrical attraction. As the voltage is increased, however, the recombination force is overcoming and the current begins to increase as more and more electron-ion pairs are collected before they can recombine. At some point, of course, all of the created pairs will be collected before they recombine and further increases in voltage show no significant change. This corresponds to the first flat region in (Figure 19). A detector working in this "region II" is known as an “ionization chamber” since it collects ionization dependent directly on the passing radiation. The signal current, in this scenario is very small. Ionization chambers are generally used to measure gamma-ray exposure and as monitoring tools for large radiation fluxes. Returning to (Figure 19), if we now increase the voltage beyond region II we find that the current again increases with voltage.

In this operating condition, the electric field is strong enough to accelerate the free electrons to such an energy that they are also capable of ionizing the gas molecules in the cylinder. The electrons freed in these secondary ionizations are also accelerated to produce even more ionization and so on, i.e., an avalanche of ionizations or cascade. Since the electric field is strongest near the anode, as seen in (Figure 19), this avalanche occurs very rapidly and almost entirely around the wire. The number of electron-ion pairs in the avalanche, however, is directly proportional to the number of electrons generated initially. The result is a proportional amplification of the current, with a gain that depends on the working voltage V. This gain can be raised to about ten million so that the output signal is much larger than that of an ionization chamber, but still proportional to the original ionization produced in the detector. This proportional gain region extends to point III and a detector operating in this operating scenario is known as a "proportional chamber". If the voltage is further increased beyond point III, the total amount of ionization created through amplification becomes large enough so that the space charge created distorts the electric field around the anode.

Proportionality thus begins to be lost. This mode of operation is known as the "limited proportionality" region. By increasing the voltage even more, the energy becomes so great that a discharge occurs in the gas. What happens physically is that instead of a single avalanche located somewhere along the anode wire (as in a proportional counter), a chain reaction of many avalanches scattered along the entire length of the anode is triggered. These secondary cascades are caused by photons emitted by de-energized molecules that travel to other areas of the counter to cause additional ionizing events. The output current thus goes into a state of complete saturation, always giving the same amplitude regardless of the energy of the initial event. To stop the discharge, a quench gas must be present in the medium to absorb the photons and drain their energy into other channels. Detectors working in this voltage region are called Geiger-Muller or breakdown counters. The Geiger voltage region, in fact, is characterized by a plateau within which the count rate varies little. The width of the plateau depends on the effectiveness of the extinguishing agent in the gas. In general, the working voltage of a Geiger counter is chosen to be in the middle of the plateau in order to minimize variations due to voltage drift. Finally, if the voltage is increased even more, a continuous breakdown occurs with or without radiation. This region, of course, is to be avoided to prevent damage to the meter.

The scintillation detector is one of the most frequently used particle detection devices in nuclear and particle physics today. Some materials, when struck by a nuclear particle or radiation, emit a small flash of light, i.e., a scintillation. If such a crystal is coupled to an amplification device such as a photomultiplier, these scintillations can be converted into electrical pulses that can then be analyzed and counted electronically to give information about the incident radiation. The basic elements of a scintillation detector are sketched in (Figure 20) and consist of a scintillating material that is optically coupled to a photomultiplier either directly or via a light guide.

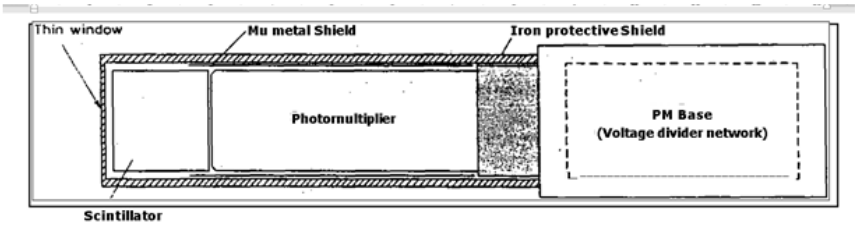

Figure 20 Schematic diagram of a scintillation counter

As radiation passes through the scintillator, it excites the atoms and molecules that make up the scintillator causing light to be emitted.This light is sent to the photomultiplier (PM or PMT for short) where there is a conversion to a weak photoelectron current which is then further amplified by an electron multiplier system. The resulting current signal is then analysed by an electronic system. In general, the scintillator signal is capable of providing a variety of information. Among its most important characteristics there is its sensitivity to energy. Above a certain minimum energy, scintillators behave almost linearly with respect to the deposited energy, i.e., the light output of a scintillator is directly proportional to the incident energy, and since the photomultiplier is also a linear device, under the appropriate operating conditions, the amplitude of the electrical output signal will be proportional to this energy. This makes the scintillator suitable as an energy spectrometer. Still scintillators present a fast time response, in fact they are fast instruments, in the sense that their response and recovery times are short compared to other types of detectors. This rapidity in response allows them to obtain temporal information, i.e., for example, the time difference between two events. This and the fast recovery time also allow scintillation detectors to withstand high count rates, since the dead time, i.e., the time lost waiting for the scintillator to recover, is reduced. With some scintillators, it is possible to recognize different types of particles by analyzing the shape of the light pulses emitted.

This is due to the different mechanisms of fluorescence by particles of different ionizing power. The technique is known as pulse shape discrimination. Scintillating materials exhibit the property known as luminescence. Luminescent materials, when exposed to certain forms of energy, e.g., light, heat, radiation, etc., absorb and re-emit energy in the form of visible light. If re-emission occurs immediately after absorption or more precisely within 10-8 s (10-8 s is approximately the time taken for atomic transitions), the process is usually called fluorescence. However, if re-emission is delayed because the excited state is metastable, the process is called phosphorescence or afterglow. In these cases, the delay time between absorption and re-emission can last anywhere from a few microseconds to hours, depending on the material. While there are many scintillating materials, not all of them can be used as detectors. In general, a good scintillation detector should meet the following requirements:
1) high efficiency for converting excitatory energy into fluorescent radiation
2) transparency to its fluorescent radiation so as to allow transmission of light
3) emission in a spectral range consistent with the spectral response of existing photomultipliers
4) a short decay constant, T.
Currently, six types of scintillator materials are in use: organic crystals, organic liquids, plastics, inorganic crystals, gases, and glasses.

4.3 Proposed ICT system

The realized platform exploits the typical solutions and protocols provided by IoT paradigm, such as a MQTT messaging strategy and LoRaWAN protocol for data transmission. Moreover, the adoption of an open-source IoT platform called ThingsBoard proves its suitability for a fast, secure and reliable implementation of the monitoring framework. The monitoring platform mainly comprises

sensor nodes, LoRaWAN communication modules, LoRaWAN Gateways and an Open-source IoT platform (Figure 21)

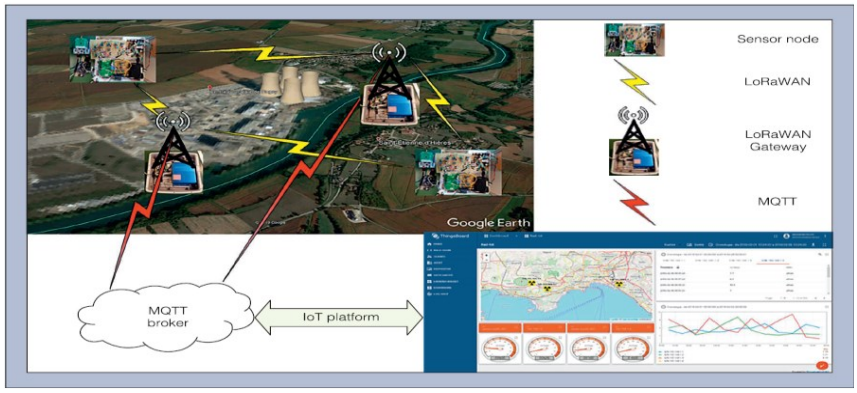

Figure 21 Principle scheme of the proposed IoT platform for radiation monitoring.

Each sensor node consists of three modules: the radiation sensor, mandated to interact with physical quantity of interest; a suitable electronic interface, needed for analog processing the signal generated by the sensor and carrying out the required measurements; and an embedded Linuxbased system, acting as node control, memory buffer and exchanging data with the communication modules, as shown in Figure 22.

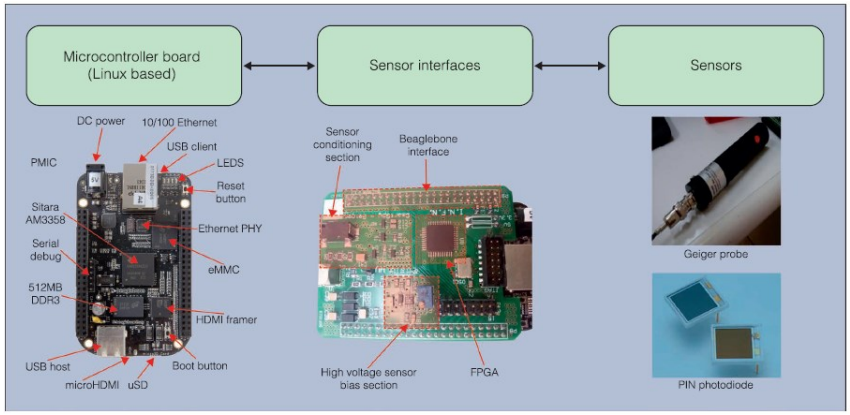

Figure 22 Hardware architecture of the realized sensor nodes

The platform enlists two possible operating states, referred to as monitoring and identification; to this aim, different sensor nodes have been designed and implemented exploiting three radiation detectors. Nodes based on a Geiger sensor are exploited to measure the radiation level during the monitoring state; in particular, the pulses per minute of the current generated by the interaction of ionizing radiation with the sensor are continuously counted and their average value is transmitted every 30 minutes to the platform. Thanks to appropriate threshold values, Geiger nodes can detect anomalous levels of radioactivity, activating the identification state and updating the measures transmission period to one minute; however, Geiger nodes cannot give indication about the pollutants. On the contrary, other two nodes, based on silicon and scintillation detectors, are exploited in the identification state to measure the energy spectrum of the detected alpha and gamma radiation, respectively[94]. Regarding the communication layer, two different ranges have to be taken into account. The first range is associated with the local wireless sensor network and is required to exchange data to and from the sensor nodes. According to the Low Power Wide Area Network infrastructure, two main requirements must be

satisfied: low power consumption and wide area coverage. Low power consumption directly descends from the need to avoid further load on power supply, since the sensor node must operate in an “always on” condition due to the specific involved measurands. From an IoT point of view, two main candidates, namely SigFox by Sigfox S.A. and LoRaWAN by LoRa Alliance, stand out. SigFox is a private data transmission service available in about 67 countries in the world. Service subscribers are allowed to transmit every day 140 uplink messages per node, each consisting of a maximum of 12 bytes, and only four downlink messages, consisting of a maximum of eight bytes. According to the procedure described above, SigFox service would be feasible in the monitoring state of Geigerbased nodes; on the contrary, if an anomalous radiation level is detected, the maximum daily number of uplink messages will be rapidly reached, thus making the service unavailable. Moreover, the dimension of data exchanged by the nodes in identification state for a single energy spectrum acquisition exceeds the 1680 bytes offered in the whole day. Because of this limitation, the authors chose to use LoRaWAN, a communication protocol characterized by the availability of either licensed/proprietary or personal network infrastructure. LoRaWAN is based on an optimization of the Chirp spread spectrum modulation that, combined with proper configuration parameters, is capable of assuring sensitivity as low as -130 dBm. It is able to grant efficient, secure and reliable transmission up to 15 km in open space and about two km in an urban environment. The local sensor network has a star topology, with individual nodes that can register themselves and communicate with one or more LoRaWAN Gateways, while remaining independent from one another. The modules for LoRaWAN communication have been realized by means of suitable devices provided by STMicroelectronics, namely a STM32 Nucleo F401RE board equipped with a Semtech SX1272 LoRa Shield. The module has been programmed through the integrated development environment (IDE) Mbed in such a way to act as a serial LoRa

modem for the sensor node[93]. In particular, a traditional asynchronous receiver/transmitter bus was adopted to transfer data from the node to the communication module and configure commands from the module to the node. Data received from the sensor are encapsulated in a proper structure according to the so-called “key-value” paradigm and transmitted to the LoRa Gateway. Configuration and monitoring
messages, exchanged between nodes and the IoT platform through the Gateway, present a simple structure and a frequency of repetition (tens of minutes during regular monitoring operation) which does not require ad hoc solutions.
In regards to long range communication, a MultiConnect® ConduitTM by MultiTech was adopted; the considered LoRa Gateway exchanges data with network nodes through LoRaWAN protocol and communicates with the open-source IoT platform by means of either mobile or Ethernet connection. In particular, a publisher/subscriber model is exploited for data transmission to and reception from the platform thanks to a Message Queue Telemetry Transport (MQTT, also known as ISO/IEC PRF 20922) broker. MQTT is a lightweight application protocol that allows devices to communicate effectively and asynchronously. The broker is a messaging server that matches interests between subscribers and publishers with subsequent messages dispatching. In other words, a publisher sends messages on a specific topic to the broker. A subscriber (i.e., a consumer who subscribes to messages posted on the same topic) receives them from the broker when available. This communication model greatly simplifies the protocol and turns out to be one of the main application layer protocols for IoT applications. More specifically, data exchanged with sensor nodes are published on a topic whose structure is “lora/device_lora_address/packet_recv” and the payload of the message contains the encrypted measured values. Once decrypted, the data are sent to the MQTT broker built in the IoT platform with a dedicated topic. A similar approach is followed when configurations are sent from the platform; the

messages are dispatched to the device whose LoRa address corresponds to that of the received MQTT topic. Finally, the open-source IoT platform, namely Things-Board, was adopted to store and visualize monitoring data. ThingsBoard allows straightforward set up of an IoT platform, thanks to offering the possibility of adding nodes whose security is assured by a specific token required to exchange data with the platform; profiling user access to limit the visibility of the results according to their identity; and providing a suitable set of gauges and graphs for the visualization of the measurement results. This way, it is possible to:

- view the node status (active, inactive, or alarmed)
- view historical trends of measurements carried out by the active sensors
- update name and physical location of nodes
- update acquisition parameters (e.g., characteristic times, storage frequency), and update calibration parameters (e.g., conversion factors, threshold limits).

4.4 Inside the Sensor Node

The sensor node which is equipped with a Geiger probe is used to point out anomalous radiation conditions, making the platform move from monitoring to identification states. To suitably detect the specific radioactive pollutant, the network is equipped with other two different sensor nodes that are able to carry out energy-resolved measurements of gamma ray and alpha particles. The nodes, currently are in the stage of laboratory prototypes. A cost-effective windowless silicon (Si) diode (namely, S3590 Si PIN photodiode by Hamamatsu) was used to develop the alpha particles spectrometer, while a NaI(Tl) scintillation radiation detector (namely, 905-3 by Ortec, 2 by 2 inches Crystal) was exploited for gamma ray spectrometry. With specific regard to the case of alpha particles, the node exploiting the silicon sensor is equipped with a flushing system able to concentrate atmospheric particulate on a millipore filter

positioned at 1 cm in front of the detector, as shown in Figure 23.

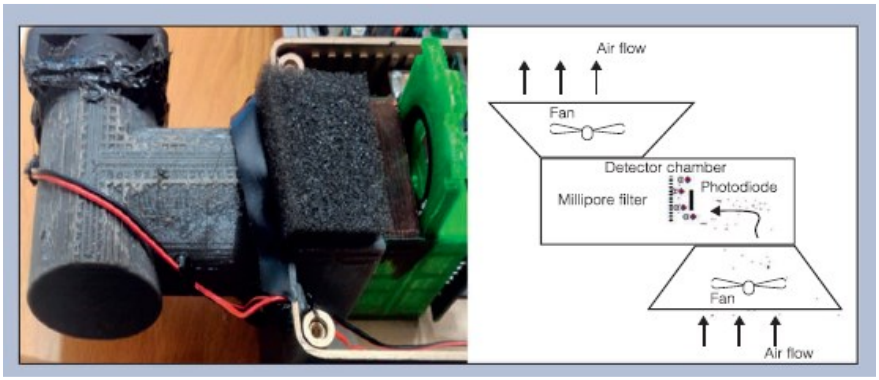

Figure 23 Air pumping system realized for sensor nodes based on a silicon detector;

This way, the energy loss by the particles along the path through the air is minimized, thus enhancing the node sensitivity. One critical issue is the light sensitivity of the silicon photodiode; the drawback has been overcome thanks to the geometry of the air pumping system implemented in 3D print technology. The sensor interface is mandated to carry out the radiation measurements; in particular, spectrometric measurements are provided as energy levels histogram of particles or rays impinging on the detector surface. The sensor interface comprises a sensor conditioning section, mandated to convert the current pulses provided by the sensors into voltage signals compliant with the successive microcontroller ADC module; Figure 24 shows the actual prototype currently realized, while Figure 25 reports the functional block diagram of the conditioning section.

Figure 24 Sensor node based on a silicon detector.

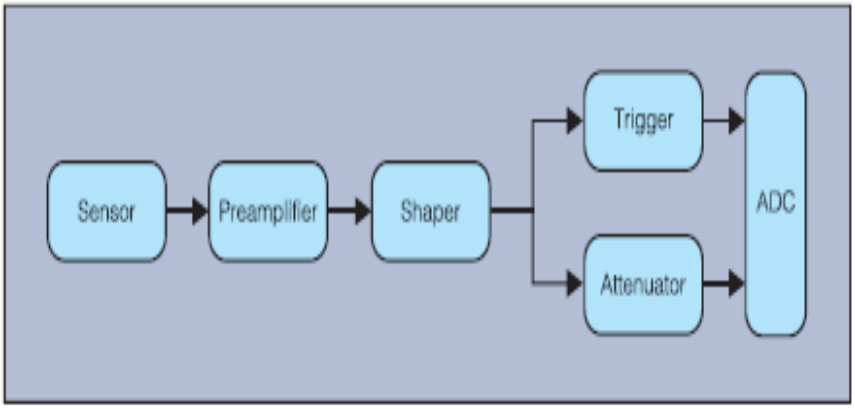

Figure 25 Block diagram of the conditioning section for spectrometer nodes.

The preamplifier is a low-noise hybrid charge amplifier that carries out the very first conversion of current into a voltage pulse. It is worth noting that ORTEC 905-3 is equipped with its own preamplifier section and a voltage divider network for external adjustment of photomultiplier grid potential to increase performance of scintillation detector Figure 26.

Figure 26 Sensor node based on a scintillation detector.

The successive block is mandated to shape the received voltage into semi-Gaussian pulses and grant that the output baseline is no longer dependent on pulses counting rate. To this aim, an ad-hoc filtering section, based on the cascade of a high-pass filtering stage (with pole-zero cancellation), low pass filtering stage, amplification, a further low filtering stage and a final baseline restorer, has been realized. The obtained signal is then given as input to a peak detector (to generate a trigger signal for the ADC when the semi-Gaussian pulse reaches its peak value) and an attenuator (to adapt the pulse amplitude to the input ADC range). A microcontroller (STM32F303VCT6) with built-in ADC module is mandated to carry out the energy spectrum estimation along with its transmission to the embedded system. Regarding the measurement algorithm, voltage provided by the conditioning section is digitized with nominal

sampling rate and vertical resolution equal respectively to 5.1 MHz and 12 bits. To reduce latency and computational burden of the microcontroller, acquired samples are transferred by means of a direct memory access (DMA) channel from ADC data register into 30 memory locations managed according to a circular buffer strategy. When a trigger signal is generated from the conditioning section, the maximum of the last 30 values provides the code associated with energy of the detected event (particle or ray); the code is exploited as index to update the histogram of absolute occurrence. Since the resolution of the ADC is 12 bits, the node is nominally capable of resolving 4096 levels of event energy, and the number of times that a certain ADC code is digitized directly corresponds to the occurrences of an event with that specific energy level. The whole histogram is periodically transferred via serial universal synchronous/asynchronous receiver transmitter to the embedded system. To prevent artifacts due to the harmful interference with sampling and updating operations, the memory size dedicated to histogram values is twice its dimension, in such a way as to allow a double buffer configuration; when one half of the buffer is involved in the histogram update, the other one is sent to the embedded system, and vice-versa. The embedded system accumulates the received histograms, thus providing the desired energy spectrum that is finally sent to the IoT platform for storage and visualization.

With regards to power supply issues, actual consumptions have not been a key issue, due to the specific considered measurand. In fact, nodes based on Geiger sensors to continuously measure counts associated with the environmental radiation; this way, they are designed to be main powered or equipped with battery packs locally recharged by photovoltaic panels. On the contrary, spectrometer nodes are in sleep condition for most of their operating life, being activated only when Geiger nodes detect an anomalous counts value; this way, spectrometers are battery powered and battery size (22000 mAh, typically adopted for quadcopter power source) was chosen in such a way as to grant an active interval sufficient to identify the

radioactive material.

4.5 Preliminary Results

The performance of the IoT platform was assessed by means of a number of tests. Specifically, sensor nodes were first verified in the laboratory through known radioactive sources. In [49], measurement results collected during preliminary tests on a hybrid platform showed the reliability of the Geiger nodes.
Further tests were carried out on the spectrometer nodes; in Figure 27, the measured energy spectrum of the gamma detector is shown. Energy peaks related to a cobalt isotope (60Co, located at 1100 and 1400 keV) can be straightforwardly detected and recognized.

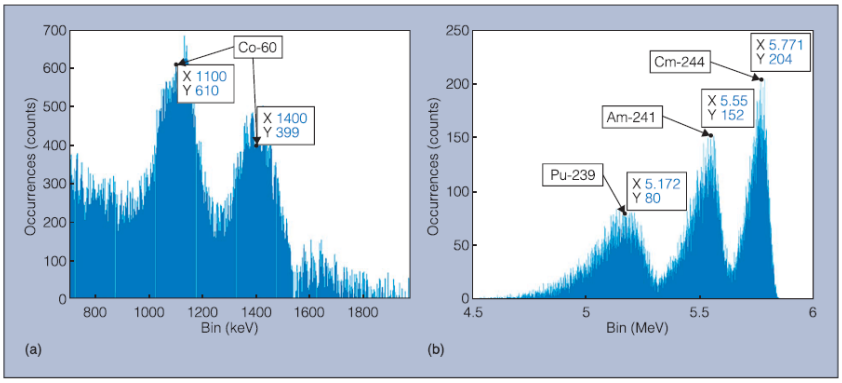

Figure 27 Energy spectra obtained by the realized wireless sensors for reference (a) gamma and (b) alpha ray sources.

With regards to the most relevant metrological specifications, the full-scale range of the spectrometer is equal to 2 MeV with an energy resolution (evaluated as full width at half maximum) of 100 keV. In regards to the alpha detector, its performance was preliminarily assessed by putting a radioactive source (made of three isotopes

Plutonium-239, Americium-241, Curium-244) into the detector chamber. As shown in Figure 27b, three peaks of emission can be seen, one associated with Plutonium-239 centered at 5.17 MeV, another with Americium-241 centered at 5.55 MeV, and the last one associated with Curium-244 centered at 5.77 MeV.
Finally, the whole platform was implemented, and a screenshot of all three detectors working together can be seen in Figure 28, where the Node-Red flow implemented on the LoRa gateway to send the measurement results to the IoT platform is shown.

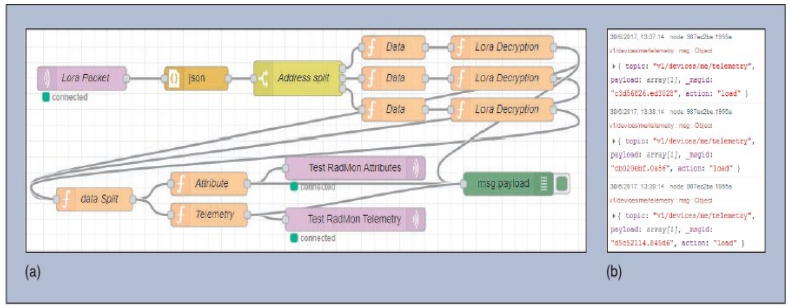

Figure 28 (a) Node-red flow implemented in the LoRaWAN Gateway for testing the IoT monitoring platform. (b) Example of messages sent to the dashboard of final IoT platform.

As it can be appreciated, data are differently decrypted according to the specific LoRa address of the sensor node; each message contains both general information (referred to as "Attributes" and including node ID and operating status) and measurement results (referred to as "Telemetry"). Required information are encapsulated in a message whose topic is equal for all of the nodes ("v1/devices/me/telemetry," Figure 28b), and the association with the specific node is granted by the token (i.e., a password unique for each node) adopted to open the connection with the ThingsBoard platform. As an example, a monitoring platform consisting of nodes based on Geiger sensors and monitoring the environmental radiation in three buildings of

University of Naples Federico II located in different geographical areas is shown in Figure 29; all of the sensors are georeferenced and their position can be appreciated on a suitable map Figure 29. The counts associated with each sensor are represented in terms of either instantaneous values by means of gauges and in tabular form or evolution versus time; since the measures are saved in a proper database, the platform user can select a specific time interval to be plotted.

Figure 29 Example of dashboard exploited in ThingsBoard for radiation monitoring.

It is worth noting that the measured counts are fully compliant with the natural ground radiation.

Part III-Measurements for Internet of Things

The other path of my research is finding methods for the estimation of parameters that can be useful in order to analyze an IoT system, and new approaches that allow optimization of hardware resources.

Chapter 5 - Problem statement

5.1 LoRa Modulation Basics

It is worthwhile stating that LoRa is a spread spectrum modulation scheme that uses wideband linear frequency modulated pulses whose frequency increases or decreases over a certain amount of time to encode information. The main advantages of this approach are twofold: a substantial increase in receiver sensitivity, due to the processing gain of the spread spectrum technique, and a high tolerance to frequency misalignment between receiver and transmitter. Thus, this allows the modulation to be immune to the Doppler effect whilst the receiver can decode transmissions 19.5 dB below the noise floor [59], [58],[56].

- **Parameters of the Physical Layer**

Several parameters are available for the customization of the LoRa modulation. The selection of these parameters determines energy consumption, transmission range and resilience to noise [60].

- **Transmission Power (TP)**. TP on a LoRa radio can be adjusted from −4 dBm to 20 dBm, in 1 dB steps, however, because of hardware implementation's limits, the range is often limited to 2 dBm to 20 dBm. Additionally, because of hardware limitations, power levels higher than 17 dBm can only be used on a 1% duty cycle. TP has both a direct influence on energy consumption and on the signal's range [61] [56].

- **Carrier Frequency (CF).** CF is the centre frequency that can be programmed in steps of 61Hz between 137MHz to 1020MHz. Depending on the particular LoRa chip, this range may be limited to 860MHz to 1020MHz [56].

- **Spreading Factor (SF).** The spread spectrum LoRa modulation is performed by representing each bit of payload information by multiple chips of information. The rate at which the spread information is sent is referred to as the symbol rate (Rs), where the ratio between the nominal symbol rate and chip rate is the spreading factor, which represents the number of symbols sent per bit of information. If on the one hand, a higher spreading factor increases the Signal to Noise Ratio (SNR), and thus, both sensitivity and range, on the other hand, increases the airtime of the packet. The number of chips per symbol is calculated as 2^{SF}. For instance, with an SF of 12 (SF12) 4096 chips/symbol are used. Each increases in SF halves the transmission rate and, hence, doubles the transmission duration and ultimately energy consumption. Spreading factor can be selected from 6 to 12. SF6, is a special case and requires special operations. Radio communications with different SF are orthogonal to each other and therefore using different SF network separation is possible.

SF (RegModemConfig2)	SF (Chips/symbol)	LoRa Demodulator SNR
6	64	-5 dB
7	128	-7.5 dB
8	256	-10 dB
9	512	-12.5 dB
10	1024	-15 dB
11	2048	-17.5 dB
12	4096	-20 dB

Figure 30 Range of Spreading Factors [62]

Let us cast a spotlight upon the resulting signal to noise ratio (SNR) required at the receiver input. It is clear that the negative SNR allows the receiver to increase its own sensitivity, thus link budget and range [62] [56][60].

- **Bandwidth (BW).** BW is the width of frequencies in the transmission band. Higher BW gives a higher data rate (thus shorter time on air), but a lower sensitivity (because of integration of additional noise). Data are send out at a chip rate equal to the bandwidth. Therefore, a bandwidth of 125 kHz corresponds to a chip rate of 125 kcps. BW can be set from 7.8kHz up to 500kHz. However, in a typical LoRa deployment, only 125kHz, 250kHz and 500kHz are considered. Moreover, the LoRa modem bandwidth refers to the double sideband bandwidth (or total channel bandwidth) as opposed to the FSK modem, which is described in terms of the

single sideband bandwidth [62] [56] [61]

Bandwidth [kHz]	Spreading Factor	Coding Rate	Nominal Rb [bps]	Sensitivity [dBm]
125	12	4/5	293	-136
250	12	4/5	586	-133
500	12	4/5	1172	-130

Figure 31- The effect of the BW on Rb and Sensitivity [62]

- **Coding Rate (CR).** CR is the amount of Forward Error Correction (FEC) that is applied to the message to protect it against burst of interference and can be set to either 4/5, 4/6, 4/7 or 4/8. A higher CR makes the message longer, introducing a transmission overhead, and therefore, increases the time on air. Radios with different CR (and same CF, SF and BW) and operating in 'explicit header mode', can still communicate with each other, as the CR is encoded in the header [56] [61].

CodingRate (RegModemConfig1)	Cyclic Coding Rate	Overhead Ratio
1	4/5	1.25
2	4/6	1.5
3	4/7	1.75

4	4/8	2

Figure 32- Cyclic Coding Overhead [62]

- **Shannon– Hartley Theorem**

It is impossible to complete a discussion on spread spectrum techniques without a brief recap of the Shannon– Hartley Theorem.
In terms of information theory, the Shannon-Hartley theorem states the maximum rate at which information can be transmitted over a communications channel of a specified bandwidth in the presence of noise.
The theorem establishes Shannon's channel capacity for a communication link and defines the maximum data rate that can be transmitted within a specified bandwidth in the presence of noise interference:

$$C = BW * \log_2\left(1 + \frac{S}{N}\right) \quad \textbf{Eq.1}$$

C = channel capacity [bps].

BW = channel bandwidth [Hz].

S = average received signal power [W].

N = average noise or interference power [W].

S/N = Signal-to-Noise Ratio (SNR) expressed as a linear power ratio

[dB].

By rearranging Equation 1 from log base 2 to the natural log base e, and by noting that ln=loge it is therefore possible to manipulate the equation as follows:

$$\frac{C}{BW} = 1.433 * \frac{S}{N} \quad \textbf{Eq.2}$$

For spread spectrum applications, the signal to noise ratio is small,

since the signal's power is often below the noise floor. Assuming a noise level such that S/N << 1, Equation 2 can be re-written as:

$$\frac{C}{BW} \approx \frac{S}{N} \quad \textbf{Eq.3}$$

Or:

$$\frac{N}{S} \approx \frac{BW}{C} \quad \textbf{Eq. 4}$$

Hence, Equation 4 demonstrates that to transmit error free information in a channel of fixed noise-to signal ratio, only the transmitted signal bandwidth needs to be increased. This characteristic is the basic principle of the Spread Spectrum Techniques as will be shown in the following sections [63] [64].

- **Direct Sequence Spread Spectrum**

Thus, by increasing the bandwidth of the signal we can compensate the degradation of the Signal-to-Noise Ratio of a radio channel.
Spread Spectrum techniques are methods by which a signal generated with a particular bandwidth is deliberately spread in the frequency domain, resulting in a signal with a wider bandwidth [64].
In Direct Sequence Spread Spectrum (DSSS) systems, the carrier phase of the transmitter varies according to a code sequence. This method is usually realised by multiplying the data signal with a spreading code: the chip sequence. Such sequence occurs at a much faster rate than the data signal and thus spreads the signal bandwidth. The term chip is used to distinguish the shorter coded bits from the longer un-coded bits of the information signal.

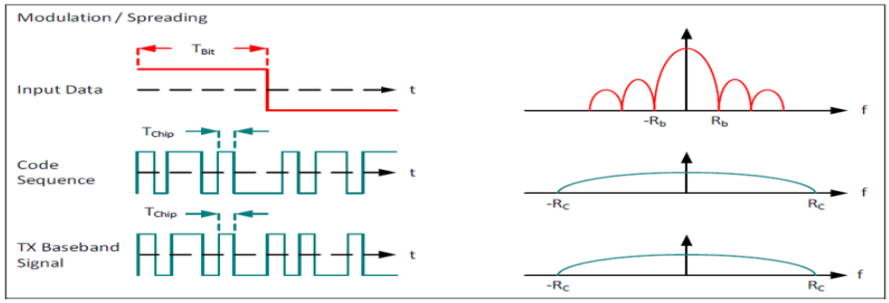

Figure 33 - DSSS Modulation [63]

Regarding the receiver, the data signal is multiplied with a locally generated replica of the chip sequence. Accordingly, the signal, previously spread, is compressed back to its original un-spread form and reconstructed [63].

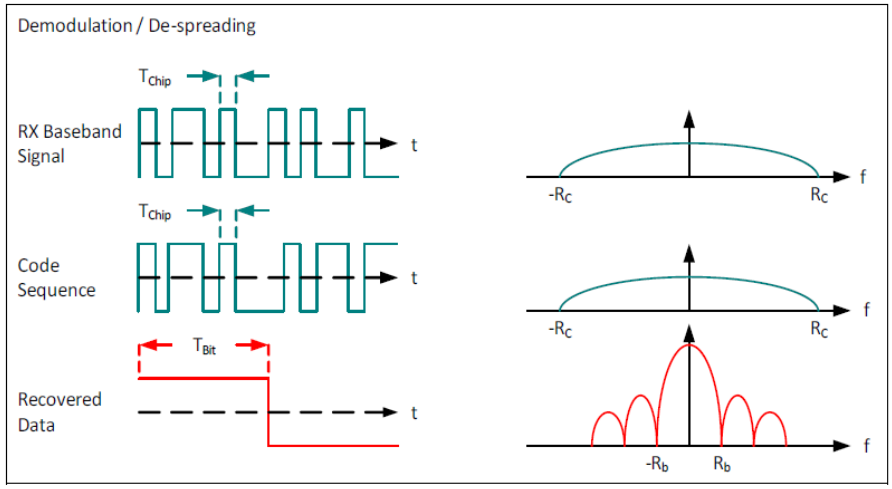

Figure 34 - DSSS Demodulation [63]

However, challenges exist for low-cost or power-constrained devices

and networks. Oftentimes, the system described above, needs a highly accurate and expensive reference clock source. In fact, the longer the spreading code or the sequence is, the longer is the time required by the receiver to perform a correlation over the entire length of the code sequence [65].

- **The Chirp Spread Spectrum core: the chirp pulse**

The chirp spread spectrum modulation technique has been used in military and space communication for decades due to the long communication distances that can be achieved and robustness to interference, but LoRa™ is the first low cost implementation for commercial usage [63].
In LoRa modulation, the spreading of the spectrum is achieved by generating a signal that continuously varies in frequency: "the chirp". Chirp stands for '**C**ompressed **H**igh **I**ntensity **R**adar **P**ulse' because its first use was in Radar applications [66] however, the term "chirp" comes from the onomatopoeic sound which resembles the bird chirp or the cricket sound; a short pulse, high pitched sound. This pulse is called a chirped pulse. However, the term chirp, within the signal frame refers more properly to a wave whose instantaneous frequency varies over time. Chirps come in many frequency sweep forms: linear chirp, quadratic chirp, logarithmic-chirp, etc. A linear chirp is a function whose frequency changes linearly with time. For instance, whilst a wave function of the form exp ($j\omega_0 t$) has constant frequency ω_0, the complex chirp exp ($j(\omega_0 t + \gamma_0 t^2)$) has an instantaneous frequency $\omega_0 + 2\gamma_0 t$ at time $t \in R$ [67].
A chirp waveform can be written as

$$s(t) = a(t)\cos[\theta(t)] \quad \textbf{Eq.5}$$

$\theta(t)$ is the phase, and a(t) is the envelope of the chirp signal which is zero outside a time interval of length T: the period. The instantaneous frequency is defined as

$$f_M(t) = \frac{1}{2\pi}\frac{d\theta}{dt} \qquad \textbf{Eq.6}$$

Within T the frequency changes in a monotonic manner from a lower value to a higher one ("Up-Chirp") or reverse ("Down-Chirp"). The difference between these two frequencies is a good approximation for the bandwidth B of the chirp pulse, which exactly is

$$B = |\mu|T \qquad \textbf{Eq.7}$$

μ is the chirp rate, defined by

$$\mu(t) = \frac{df_M}{dt} = \frac{1}{2\pi}\frac{d^2\theta}{dt^2} \qquad \textbf{Eq.8}$$

and represents the rate of change of the instantaneous frequency. Hence, the waveforms with $\mu(t) > 0$ are up-chirps and those with $\mu(t) < 0$ are down-chirps. For a linear chirp $\mu(t)$ is constant, and thus $f_M(t)$ is a linear function of t, and $\theta(t)$ is a quadratic function [68].

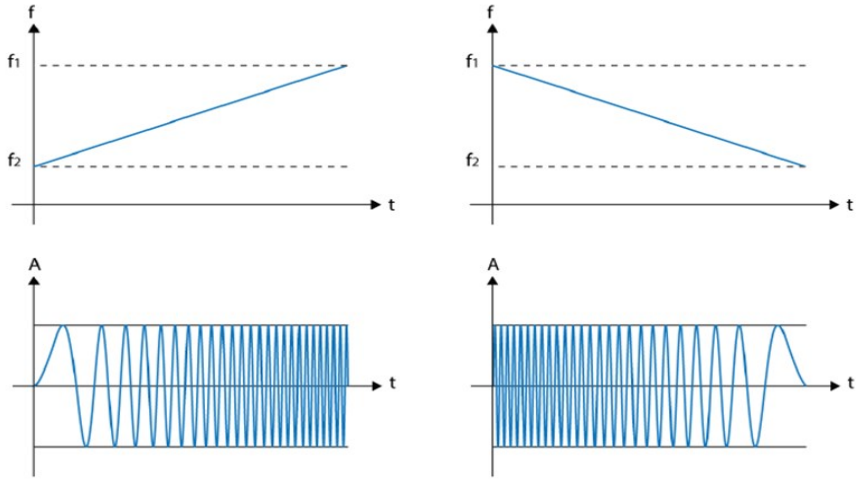

Figure 35 - - Up and Down chirps [6]

The spectrum of the chirp can be reached using the Fourier transform, and with some mathematical manipulations it can be expressed in terms of the Fresnel integral as follows:

$$S(f) = \frac{1}{\sqrt{\mu}} e^{j\frac{\pi}{\mu}f^2} \left[F_S\left(\frac{f}{\sqrt{\mu}} + \sqrt{\mu}\frac{T}{2}\right) - F_S\left(\frac{f}{\sqrt{\mu}} - \sqrt{\mu}\frac{T}{2}\right)\right] \quad \textbf{Eq.9}$$

$F_S\ (x)$ is the complex Fresnel integral, defined as

$$F_S(x) = \int_0^x e^{-j\pi t^2} dt \quad \textbf{Eq.10}$$

[69]

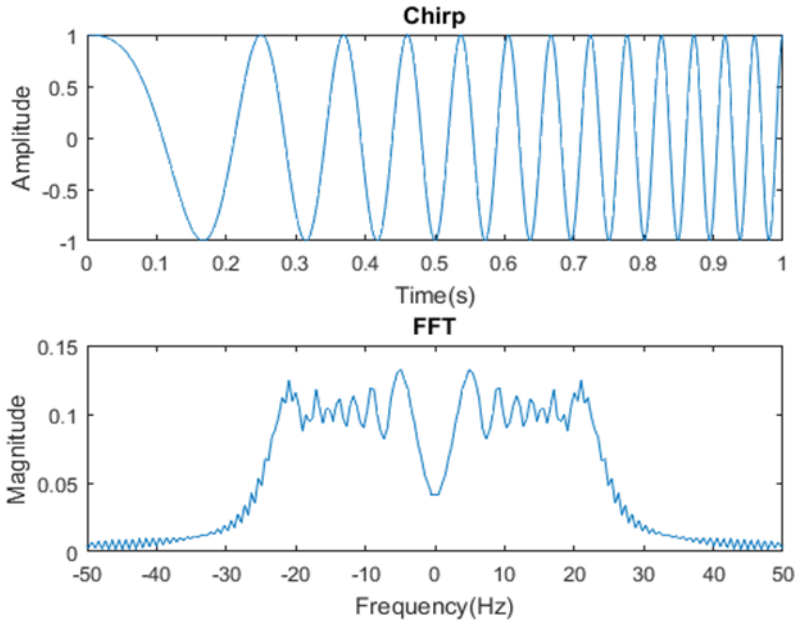

Figure 36 - A chirp and its Fourier Transform

- **LoRa chirp spread spectrum modulation**

LoRa modulation, derivative of Chirp Spread Spectrum (CSS), works by chirping, breaking the chirps in different places in terms of time and frequency in order to encode a symbol [64]. A LoRa symbol is composed of 2^{SF} chirps, which cover the entire frequency band. In fact, the frequency bandwidth of this chirp is equivalent to the spectral bandwidth of the signal. When the maximum frequency of the band is reached, the frequency wraps around, and the frequency's growth starts again from the minimum. The position of this discontinuity in frequency is what encodes the information transmitted. Since there are 2^{SF} chirps in a symbol, a symbol can effectively encode SF bits of information.

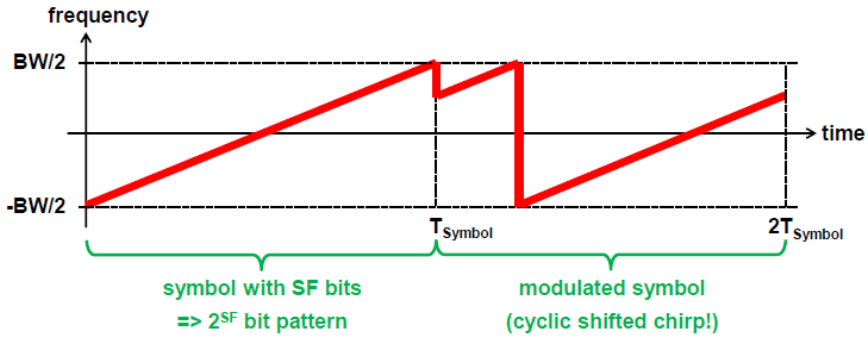

Figure 37 - A frame of the LoRa signal: the information is encoded in the frequency discontinuity between two chirps [70]

In LoRa, the chirp rate depends only on the bandwidth: the chirp rate is equal to the bandwidth (one chirp per second per Hertz of bandwidth). This has several consequences on the modulation. A chirp with a spreading factor 8 takes exactly twice the time and half the frequency of the same chirp with a spreading factor 7. A chirp with a spreading factor 9 takes exactly twice the time and half the frequency of the same chirp with a spreading factor 8 and so on (as

2^{SF} chirps cover the whole bandwidth). Consequently, the higher the spreading factor, the higher the OAT and the lower the Data Rate are. However, an increase of one of the spreading factor will not divide the bit rate by two, as one more bit will be transmitted in each symbol. Indeed, the LoRa transmission is not just simply binary but it has a lot of information that can be conveyed (high symbol depth) [56] [66].

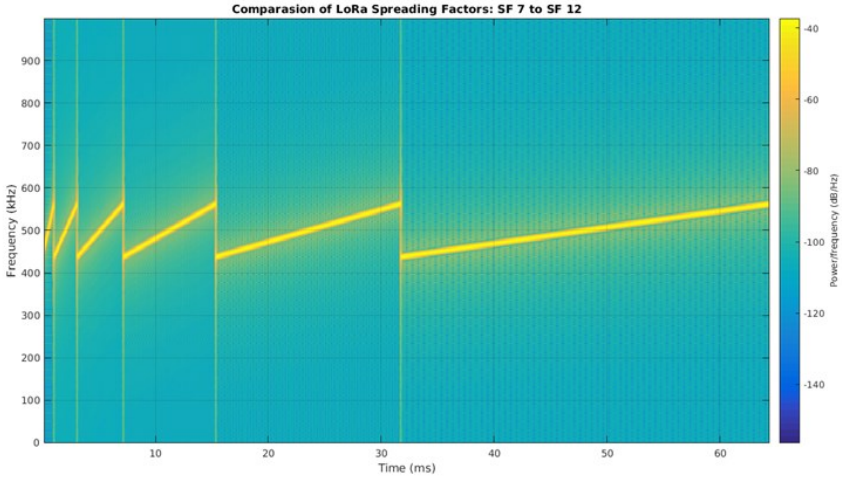

Figure 38 Spectrogram of the LoRa chirps vaying the SF [22]

A LoRa modulation peculiarity is the employing of a form of Forward Error Correction (FEC) that permits the recovery of bits of information lost due to corruption by interference. This requires a small overhead of additional encoding of the data in the transmitted packet, measured by the coding rate. The most important performance's gain of FEC lies in the presence of bursts of

interference. If the radio link is likely to be subject to such interference, the usage of FEC should be evaluated [59].
The FEC, the high BT product (BT >> 1) and the asynchronous nature, make the LoRa signal very resistant to both in-band and out-of-band interference mechanisms. Additionally, the usage of the chirp pulse, which is relatively broadband, makes LoRa immune to multipath and fading, making it ideal for urban and suburban environments, where both mechanisms dominate [63].

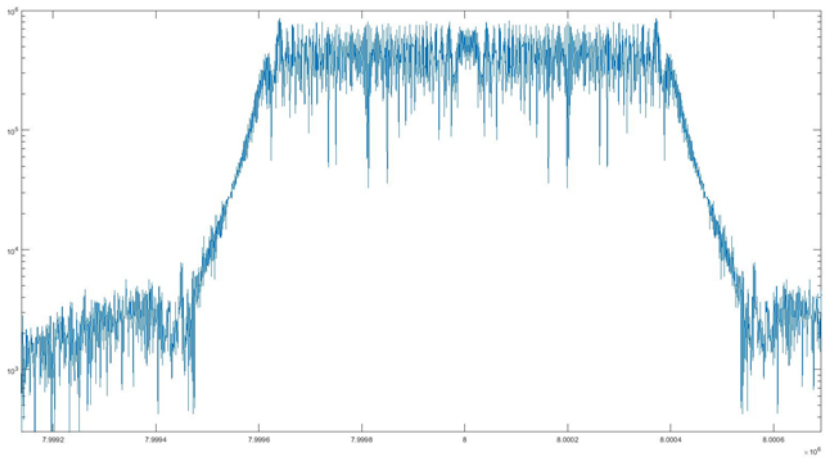

Figure 39 The spreading effect on the LoRa signal's Spectrum

- **LoRa Transmission parameters relationship**

This can be translated in the equations that relate the wanted data bit rate, symbol rate and chip rate for LoRa modulation. The modulation bit rate Rb is

$$R_b = SF * \frac{1}{\left(\frac{2^{SF}}{BW}\right)} \quad [bits/s] \qquad \textbf{Eq.11}$$

SF = spreading factor (7, ... ,12)

BW = modulation bandwidth (Hz)

The symbol period T_s is

$$T_S = \frac{2^{SF}}{BW} \quad [s] \qquad \textbf{Eq.12}$$

SF/BW	125 kHz	250 kHz	500 kHz
7	1.0240 ms	0.5120 ms	0.2560 ms
8	2.0480 ms	1.0240 ms	0.5120 ms
9	4.0960 ms	2.0480 ms	1.0240 ms
10	8.1920 ms	4.0960 ms	2.0480 ms
11	16.3840 ms	8.1920 ms	4.0960 ms
12	32.7680 ms	16.3840 ms	8.1920 ms

Figure 40- The Time Symbol computed for each combination of SF and BW.

At the same BW, the Time Symbol doubles when SF increases. At the same SF, the Time Symbol is halved when BW increases. The biggest value is reached for BW125kHz and SF12, the smallest one

for BW500kHz and SF7. The same values are highlighted with the same colour.

Considering that the chirp period is

$$T_{chirp} = \frac{1}{BW} \quad [s] \qquad \textbf{Eq.13}$$

Ts is equal to

$$T_S = 2^{SF} * T_{chirp} \quad [s] \qquad \textbf{Eq.14}$$

Thus, 2^{SF} represents the *Spreading Gain*, which describes how much the spectrum is spreaded. In fact

$$BW * T_S = 2^{SF} \gg 1 \qquad \textbf{Eq.15}$$

The symbol rate, R_S, is the reciprocal of T_S:

$$R_S = \frac{1}{T_S} = \frac{BW}{2^{SF}} \quad [symbols/s] \qquad \textbf{Eq. 16}$$

And the chip rate, R_C, is

$$R_C = R_S * 2^{SF} \; [chips/s] \qquad \textbf{Eq. 17}$$

And substituting Rs with its expression

$$R_C = \frac{BW}{2^{SF}} * 2^{SF} = BW \; [chips/s] \qquad \textbf{Eq. 18}$$

This relation clarify the chip definition: *"…one chip is sent per second per Hz of bandwidth…" [62]*. Therefore, a LoRa bandwidth of 125 kHz corresponds to a chip rate of 125 kcps.
Finally, we can express the Chirp Rate as

$$R_{Chirp} = \frac{BW}{T_S} = BW * \frac{BW}{2^{SF}} \ [Hz/s] \qquad \textbf{Eq. 19}$$

As said, LoRa modulation also includes a variable error correction scheme (the FEC) that improves the robustness of the transmitted signal at the expense of redundancy, inserting an additional overhead indicated by the Coding Rate (CR).
Thus, the nominal bit rate of the data signal can be rewritten as

$$R_b = SF * \frac{\left(\frac{4}{4+CR}\right)}{\left(\frac{2^{SF}}{BW}\right)} \ [bits/s] \qquad \textbf{Eq. 20}$$

[63]

- **The orthogonality**

Because the LoRa signal has a very distinct pattern, the LoRa receiver can detect quieter chirps, for example below the noise floor. This feature allows to demodulate many signals with different Spreading Factors at the same time taking advantage of his orthogonality [64].

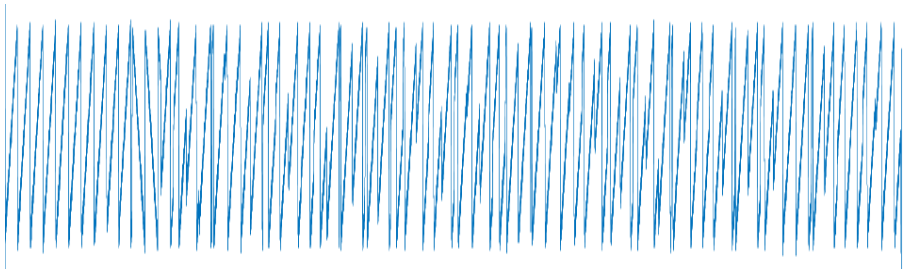

Figure 41 - LoRa frequency variation over time pattern

In fact, signals, which are transmitted with different chirp rate, are

always orthogonal. In such a manner, LoRa symbols can be simultaneously transmitted and received on a same channel without interference. However, it is important noting that not all the combinations of spreading factor and bandwidth are orthogonal. By way of example, it is possible to calculate the chirp rate for the cases:

1. SF=7, BW=125 kHz

2. SF=9, BW=250 kHz

R_{chirp1}= 122.07 kHz/sec

R_{chirp2}= 122.07 kHz/sec

It is worth noting that the results achieved are the same. Therefore, both the combinations are not orthogonal and cannot be used on a same channel.

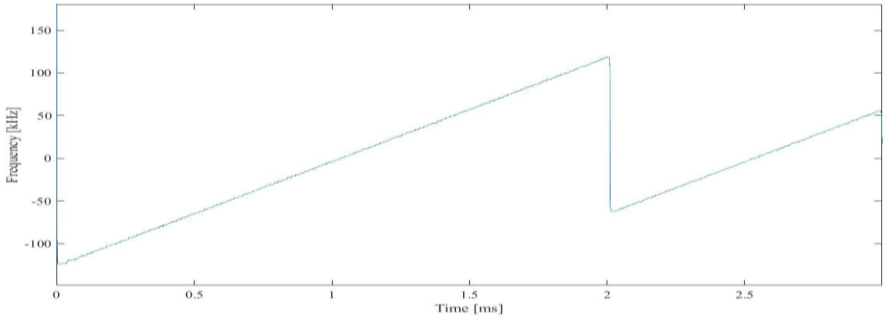

Figure 42 - LoRa chirps for BW 250 kHz SF 9 and BW 125 kHz SF 7: the slopes, and thus the chirp rates, are evidently the same

Bearing in mind the chirp's rate definition (Equation 8), it is possible to argue that the slope of the lines represents the orthogonality. In fact, the same chirp rate means the same chirp's slope, hence, two

chirps with the same slope are not orthogonal [66].

SF		07	08	09	10	11	12	07	08	09	10	11	12	07	08	09	10	11	12
	BW	125	125	125	125	125	125	250	250	250	250	250	250	500	500	500	500	500	500
07	125	x								x								x	
08	125		x								x								x
09	125			x								x							
10	125				x								x						
11	125					x													
12	125						x												
07	250							x								x			
08	250								x								x		
09	250	x								x								x	
10	250		x								x								x
11	250			x								x							
12	250				x								x						
07	500													x					
08	500														x				
09	500							x								x			
10	500								x								x		
11	500	x								x								x	
12	500		x								x								x

Figure 43 - non-orthogonal ('X') combinations of LoRa channels characterized by spreading factor (SF) and bandwidth (BW) in kHz [71]

- **LoRa packet's structure**

Although the LoRa modulation can be used to transmit arbitrary frames, a physical frame format is specified and implemented in Semtech's transmitters and receivers. The bandwidth and spreading factors are constant for a frame.
To observe it in more detail, the LoRaTM modem employs two types of packet format, explicit and implicit.
In both cases, a LoRa frame begins with a preamble used to synchronize receiver with the incoming data flow. The preamble starts with a sequence of constant up-chirps that cover the whole frequency band. The last two up-chirps encode the sync word. The sync word is a one-byte value that is used to differentiate LoRa networks that use the same frequency bands. The sync word is followed by two and a quarter down-chirps, for a duration of 2.25 symbols. By default, the packet is configured with a 12,25 symbols long sequence (8 configurable symbols + 4.25 default symbols). This is a programmable variable so that the total duration of this preamble can be configured between 10.25 and 65,539.25 symbols.

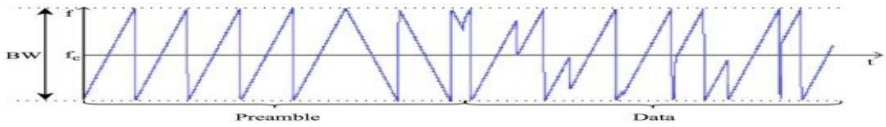

Figure 44 - LoRa frequency variation over time pattern. The preamble consists of 4 up-chirps and 2.25 down-chirps [54]

Thereafter, depending upon the chosen mode of operation, explicit or implicit, two possibilities are available.
If on the one hand, in the explicit mode the packet includes a short header that indicates the size of the payload (in bytes), the code rate used for the end of the transmission and whether or not a 16-bit CRC (Cyclic Redundancy Check) for the payload is present at the end of the frame. This header is transmitted with a coding rate of 4/8.
On the other hand, in the implicit mode the header is not present. This choice may be advantageous to reduce transmission time when the payload length, coding rate and CRC presence are known in advance.
The header is followed by the payload, and at the end of the frame there is the optional CRC. The packet payload is a variable-length field that contains the actual data.
For a given combination of spreading factor, coding rate and signal bandwidth the total on-the-air transmission time of a LoRa packet can be calculated.
The preamble duration is

$$T_{preamble} = (N_{preamble} + 4.25)T_S \qquad \textbf{Eq.21}$$

Npreamble is the programmed preamble length.
The payload duration depends upon the header mode that is enabled and can be expressed as

$$T_{payload} = N_{payload} * T_S \qquad \textbf{Eq.22}$$

$N_{payload}$ is the number of symbols required to transmit the payload and it is a function of all of these parameters.

$$N_{payload} = 8 + max\left(ceil\left[\frac{(8PL-4SF+28+16CRC-20IH)}{4(SF-2DE)}\right](CR+4), 0\right)$$

Eq.23

PL is the payload size in bytes, CRC is 16 if the CRC is enabled and zero otherwise, H is 20 when the header is enabled and zero otherwise and DE is two when the low data rate optimization is enabled and zero otherwise.
Finally, the addition of the preamble and payload durations gives the total packet time on air.

$$T_{packet} = T_{payload} + T_{preamble} \qquad \textbf{Eq.24}$$

[58] [62]

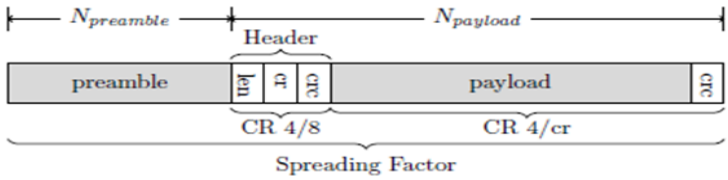

Figure 45 - - LoRa packet structure. Grey shaded areas are required, white shaded areas are optional [59].

- **Demodulating LoRa**

Finally, attention must be posed on the process of demodulation of a

LoRa signal. The most common strategy adopted consists in multiplying the waveform by the conjugate chirp.
In fact, whilst encoding the LoRa symbols, the modulator cyclically shifts the frequency of the LoRa signal. Therefore, multiplying the received 'frequency shifted LoRa chirp' with the 'inverse chirp' turns each modulated symbol into regions of constant frequency. Besides that, the FFT of each region is computed. The location of the peak bin in the FFT represents the transmitted symbol, even in the presence of very high noise. This is how 2SF FFT bins are transformed back into SF bits which compose the index of the FFT bin [66],[72].

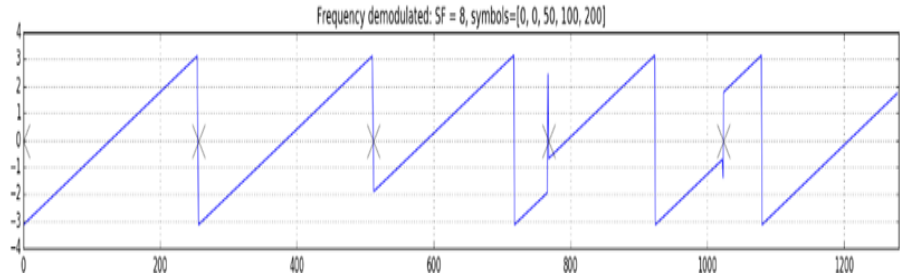

a.

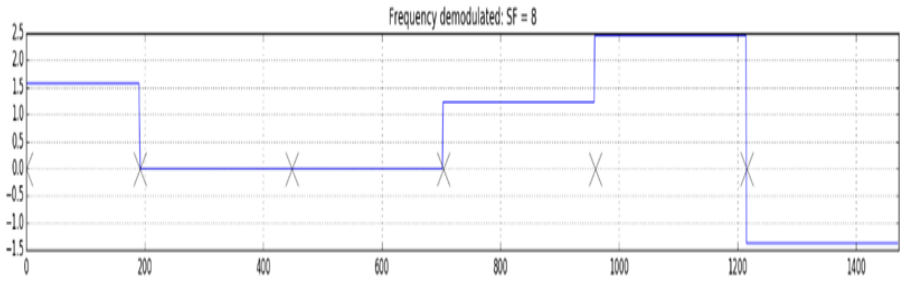

b.

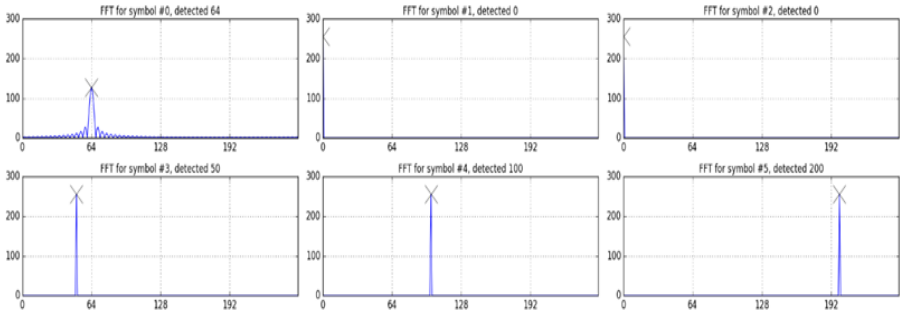

c.

Figure 46 - - - a. Frequency demodulation shows the shifted chirps as simple ramping waveforms with 5 symbols encoded. b. The constant regions arose from the multiplication with the conjugate chirps. An intentional partial chirp was inserted in order to test the technique of synchronizing. c. The symbols encoded as the peak indexes in the FFT [72].

5.2 LoRa Classification Algorithm

Test and measurement are fundamental issues of the lifecycle (development, deployment and maintenance) of new technologies. Leader manufacturers of measurement solutions, which are also members of the LoRa Alliance, have already distributed their own proprietary hardware and software suites to test LoRa devices [73],[74]. These suites include expensive instruments like high performance digital oscilloscopes, spectrum analyzers and signals generators. Therefore, assessing the performance of LoRa devices is, at present, a costly task. Costs of the afore mentioned suites are basically related to the core hardware components, namely the digitizer and its complementing acquisition memory and processor, adopted to digitize, record and process the input signal. As a matter of fact, in digital signal processing, the conventional paradigm for sampling and exactly reconstructing signals or images from measured data follows the well celebrated Shannon's theorem: when uniformly sampling a finite bandwidth signal, the sampling rate must be at least two time faster than its bandwidth, the so-called Nyquist rate. In fact, this principle underlies nearly all signal acquisition protocols used in consumer audio, visual electronics, medical imaging devices, radio receivers, and so on. This approach guarantees the preservation of the information embodied in the sampled signal. However, the resulting Nyquist's rate can be so high that it ends up with far too many samples to be handled with. That said, it may often be too expensive, or even physically impossible, to build devices capable of acquiring samples at the necessary rate. Designing cost-effective LoRa test solutions essentially requires skills related to sampling strategies and Digital Signal Processing (DSP). In particular, the sampling strategy should grant a significant reduction of instrument memory requirements, which have a large impact on the hardware costs. The digital processing stage should be characterized by low computational burden and fast responsiveness. Even though LoRa signals are characterized by values of bandwidth

never greater than 500 kHz, traditional solutions based on signal downsampling, either analog or digital, prove to be inefficient; analog approaches, in fact, require the exploitation of further electronic circuitries for baseband translation (as an example [75]-[76]), while digital methods, such as those presented in [77]-[78] suffer from unsuitable reduction of the signal-to-noise ratio if improperly used. To better understand the issue in an operative scenario, it could be fine verifying the possibility of successfully performing classification tasks, i.e. automatically determining configuration parameters of the reconstructed LoRa signal. To this end, a suitable classification algorithm operating on time-domain reconstructed signals has been defined, implemented, and tested. The need of an automatic LoRa modulation classification arises from the characteristics of both LoRaWAN protocol and LoRa signal modulation/demodulation process. The LoRaWAN, as previously said, is thought to operate in the ISM bands and to use licence-free spectrum. Hence, a shared use of radio spectrum with other users is expected and consequently interferences arise with a high degree of probability. In such scenario, both the spectrum's knowledge and the physical parameters information are crucial to adapt the user's transmissions in order to avoid harmful interferences. At same time, the LoRa demodulation rests upon the multiplication between the signal and its conjugate. In order to provide a correct result, the opposite signal needs to present the same characteristics (the Bandwidth, the Spreading Factor and the Coding Rate) of the original one. Thus, the Physical layer parameters must be known in advance on both transmit and receive sides of the link. In particular, the prior knowledge of the Spreading Factor is crucial as LoRa signals with different spreading factors could be orthogonal to each other. Therefore, in accordance with the frame so depicted, an algorithm that can automatically detect the properties of an unknown LoRa signal would be extremely useful either to enhance the demodulator's performances, generating a proper conjugate signal, or to guarantee an optimal band use. The algorithm proposed is thought

to have as input the LoRa signal in the time's domain. It can be the entire waveform or simply a frame; it is only necessary to take at least few preamble chirps. These chirps are essential in the detection process. In fact, they present, in the time-frequency plane, an extremely regular shape and cover the whole frequency band. By contrast, the payload chirps, broken in different positions to encode the symbols, exhibit an irregular trend, which makes them unsuitable for the classification. Thus, it is easy to understand how obtaining a representation in the time-frequency plane will be crucial to perform a correct classification. Other inputs are the signal's frequency and the sampling frequency. This is not a restrictive condition either because the signal's frequency is limited in EU to few possible channels, around 868 MHz, or because the sampling frequency is known in advance.
The outputs are the Bandwidth and the Spreading Factor of the unknown signal.

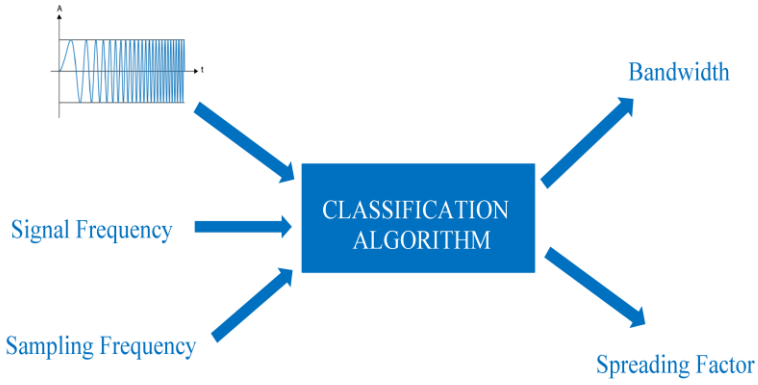

Figure 47 Classification at black box level: inputs and outputs are shown.

The algorithm operates executing three main steps.

- *Step 1:* Frequency over time representation. As said, to perform the classification, the signal in the time domain has firstly to be represented by means of the instantaneous frequency. Such instantaneous frequency is computed from the phase through Eq.6.

$$f_M(t) = \frac{1}{2\pi}\frac{d\theta}{dt}$$

The phase information is achieved by way of the I-Q demodulation. Thus, in the signal written in Eq. 5, reported below

$$s(t) = a(t)\cos\left[\theta(t)\right]$$

The carrier is removed to isolate the information a(t) using this scheme:

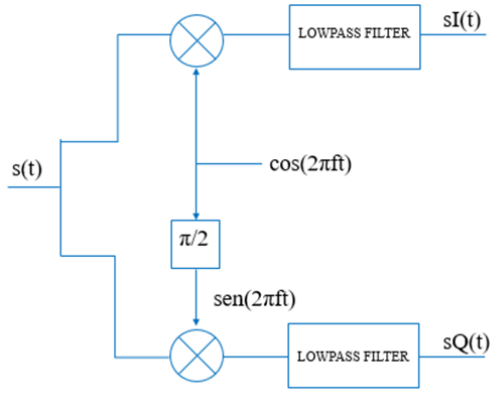

Figure 48 I and Q demodulation scheme

The signal is multiplied with the carrier and the 90-degree phase shifted carrier to obtain the in-phase (I) and quadrature (Q) components. Thereafter, both components are filtered

with a low-pass filter so as to reject the high frequency parts of the signal. Accordingly, the signal can be written through a complex representation:

$$s(t) = s_I(t) + js_Q(t) \qquad \textbf{Eq. 25}$$

The instantaneous phase is hence simply

$$\langle s(t) = \tan^{-1}\left(\frac{s_I(t)}{s_Q(t)}\right) \qquad \textbf{Eq. 26}$$

Finally, the phase is unwrapped with the aim of making them a continuous function of the argument *t* [79] **[**80**]**.

- *Step 2: Bandwidth detection.* In order to find the Bandwidth the first step is to filter the frequency over the time signal. In fact, undesired outliers, that can alter the detection process, are common. The filtering is performed only on the first 50% of the signal. In fact, at least in principle, only one preamble chirp is necessary to find the bandwidth. By contrast, using the entire payload, signal's frames, corrupted by the noise, may be involved in the BW measurement. The chosen filter is the median filter. Such a filter substitutes every point of a signal by the median of that point and a stated number of neighboring points. Consequently, median filtering rejects points that differ significantly from their surroundings. If x is the signal to filter and y is the filtered signal, k the current index and n the filter order, or otherwise the number of neighboring points, the value y(k) is the median of

$x(k-(n-1)/2 : k+(n-1)/2)$ when n is odd

$x(k-n/2 : k+(n/2)-1)$ when n is even

a

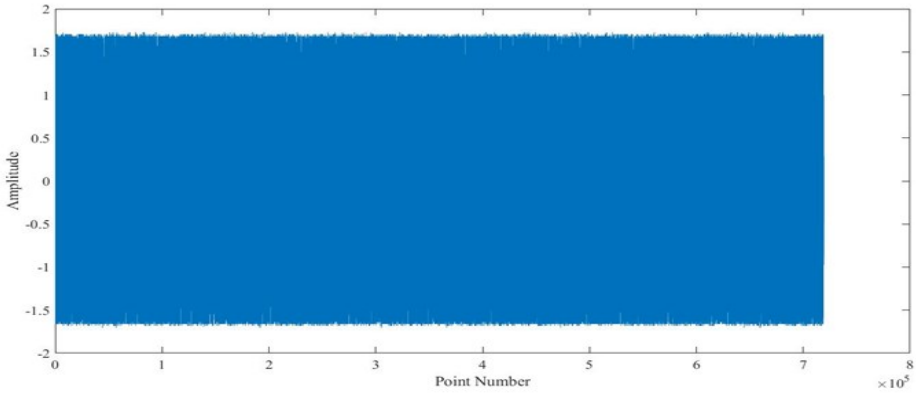

b

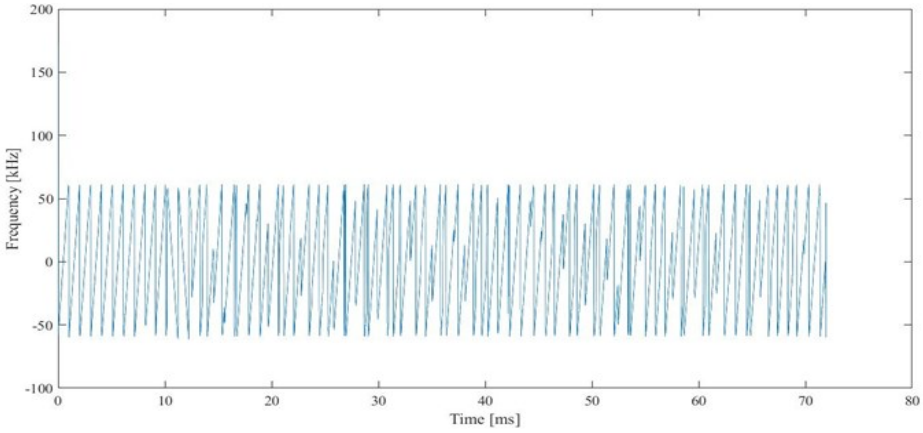

Figure 49 a. the input signal, b. the frequency over time representation

Hence, the filter order is a key parameter: if too high, the filter

will cut off useful signal portions, however, if too low, the filter will not remove all the outliers causing a bandwidth overestimation. In order to properly choose the filter's order a mechanism of outliers' detection is established. Infact, outliers appear as spikes overlapped on the useful signal. Therefore, they constitute peaks that stand out in a very isolated manner and, thus, easy to spot. For this purpose, a peaks detection mechanism is implemented. A local peak is seen as a data sample that is either larger than its two neighboring samples or is equal to Infinite. Hence, an appropriate threshold is set. In this way, only the peaks whose prominence exceeds the threshold are identified. The prominence of a peak measures how much the peak stands out given its intrinsic height and its location relative to other peaks. A low isolated peak can be more prominent than one that is higher, however, it is at the same time an unremarkable member of a tall range. If the threshold is correctly chosen, the identified peaks correspond to the tops of the useful signal and exactly to the outliers. Therefore, by making the difference between the maximum peak (which with high probability will be associated with the maximum outlier) and the minimum peak (which with high probability will be associated with one of the useful signal tops) it is possible to provide an estimation of the outliers' level on the signal. Finally, depending on the calculated value, a higher or lower filter order is chosen among three possible options. Once the signal has been filtered, the peak research's algorithm is applied again, however, this time, without threshold. Therefore, it is possible to find both the "positive" and the "negative" peaks. The difference between the maximum positive and the minimum negative peak values represents a Bandwidth estimation. Finally, the differences between the founded value and the three allowed Bandwidth (125 kHz, 250 kHz and 500 kHz) are computed. The

permitted Bandwidth, which presents the minimum difference with the estimated value, is chosen.

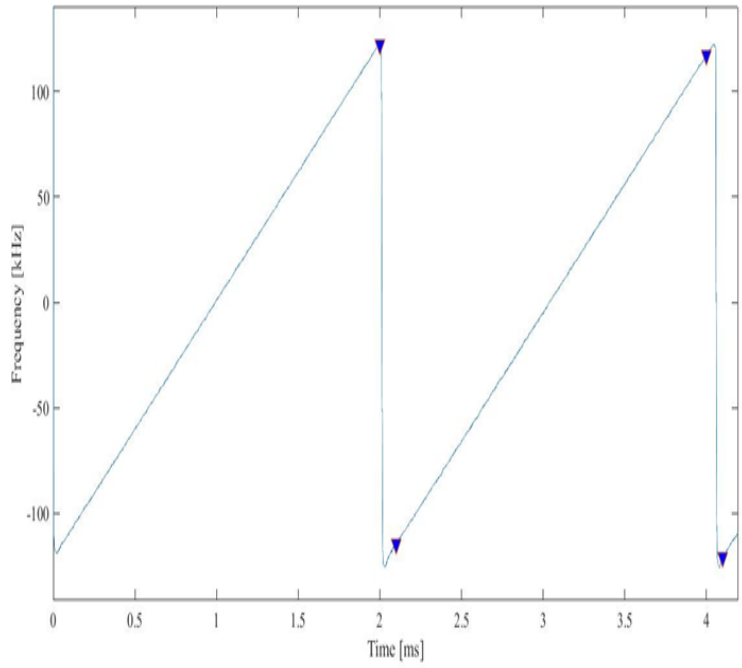

Figure 50 the positive and negative peaks founded on a signal frame.

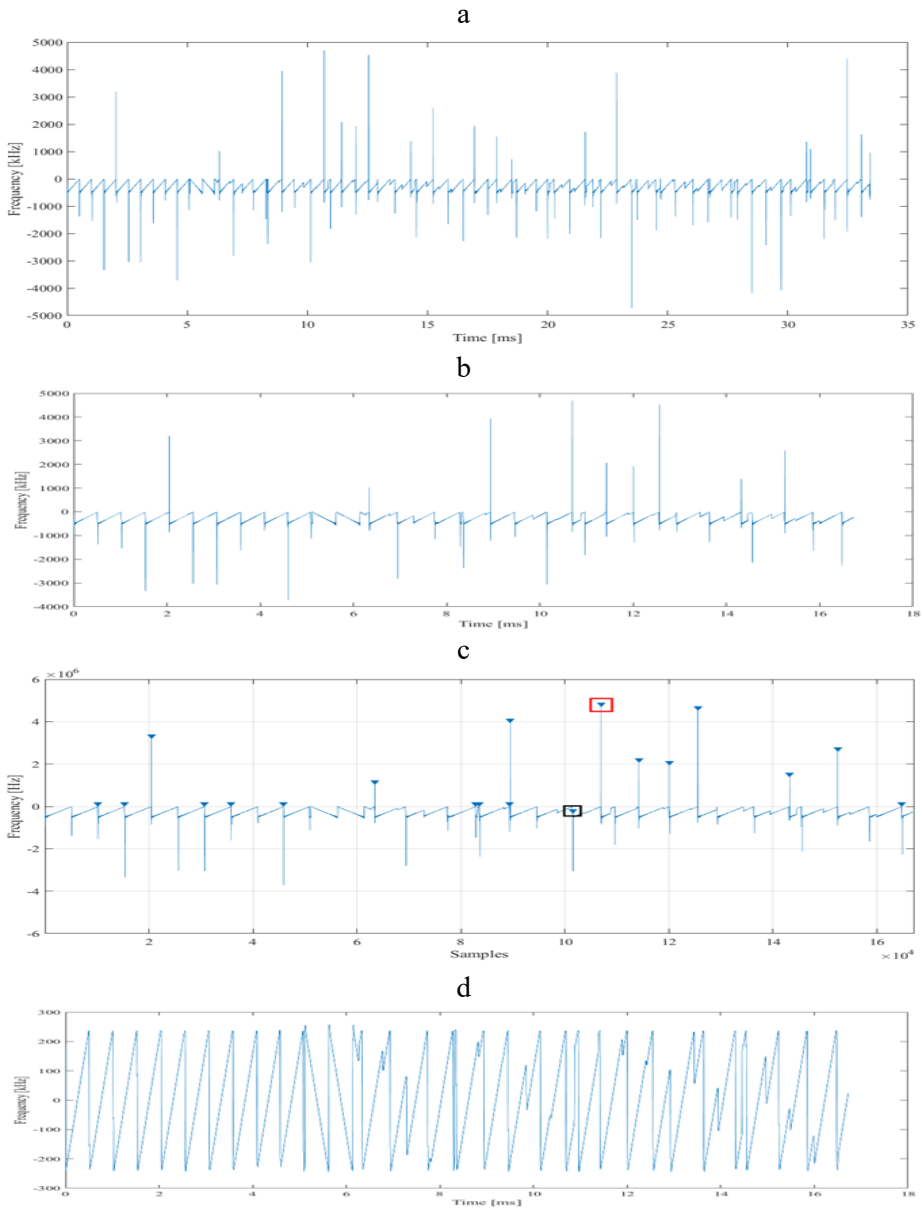

*Figure 51 the filtering process: **a.** the original signal, **b.** the half signal, **c.** the result of the peaks detection algorithm: in black the minimum peak, in red the maximum one, **d.** the filtered signal*

- *Step 3: Spreading Factor detection.* Having identified the Bandwidth, in order to find the Spreading Factor:

$$T_S = \frac{2^{SF}}{BW} \quad [s]$$

$$SF = \log_2(T_S * BW) \qquad \textbf{Eq. 27}$$

It is thus essential to calculate the Time Symbol. The Time Symbol can be seen as the temporal distance between two preamble peaks in the time-frequency plane. Therefore, to estimate it, it is possible to use again the peaks detection algorithm with the aim of evaluating the peaks' position on the time's axis rather than their amplitude, as in the previous case. Once again, in order to ensure that the detected ones are useful signal peaks and not outliers, a median filtering is performed. An order equal to the 0.05% of the signal length is set. This very high value will probably eliminate both the outliers and a useful portion of the signal. However, this does not represent a serious damage as only the position of the peaks and not their amplitude values are of interest. Once the signal is filtered, the detection algorithm of the peaks is applied on the whole signal, with a threshold equal to the bandwidth previously identified. If, on the one hand, the peaks founded are at least six (as six are the up-chirps that make up the preamble), the distance between the first five positions identified is calculated and then the mean is computed. If, on the other hand, the peaks identified are less than six, then only the distance between the first two positions is used as an estimate of the Time Symbol. Finally, the SF is evaluated by means of the Equation 27 rounded to the nearest integer. The possibility taken into account, to find less than six peaks, is not linked to errors in the algorithm. In fact, it must be kept in mind that the algorithm is designed to work with an input consisting of either a complete signal trace or its unspecified portion.

To calculate the Bandwidth it is clear that only the preamble of one symbol is sufficient, or rather two, since only half of the input signal is involved in the measurement's process. In order to calculate the Time Symbol, just two symbols are sufficient to calculate the distance between the peaks. Therefore, the algorithm is able to work perfectly with a very small trace at the input, at least, constituted by only two preamble's up-chirp. This is the deeply rooted reason why the number of peaks identified can be less than six.

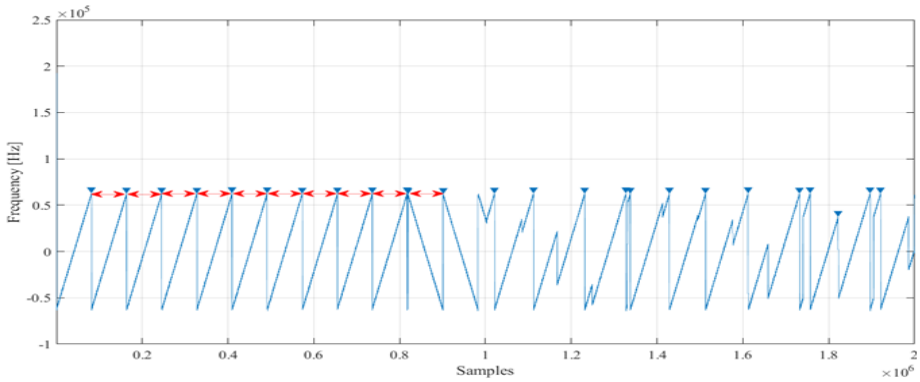

Figure 52 the peaks founded on a frame: the distance between the preamble's peaks (the red arrows) estimate the Ts

The issue will arise soon in the Spreading Factor evaluation as well described in the figure below:

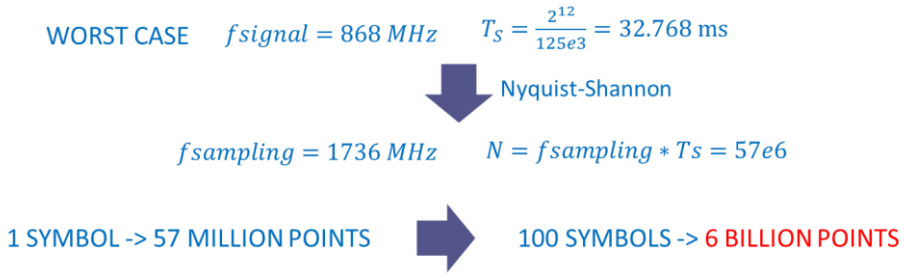

Figure 53 Nyquist's rate must be so high that it ends up with far too many samples to be handled with

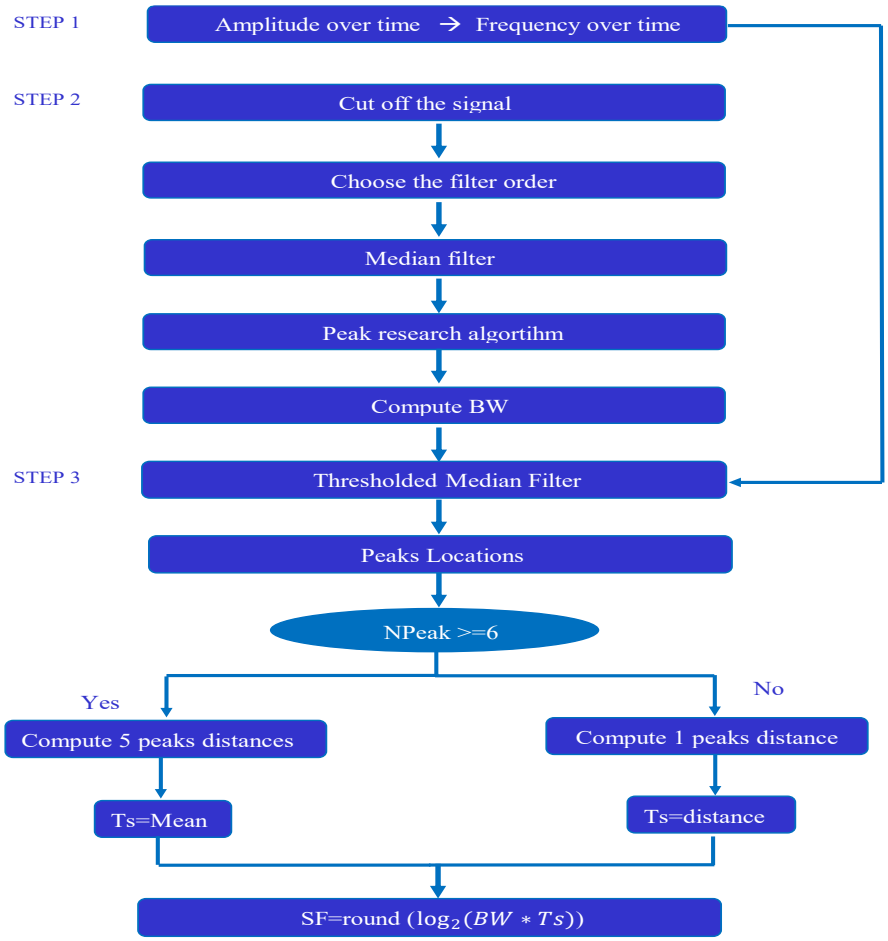

Figure 54 the classification algorithm flowchart

DCT representation of LoRa signal and compressive sampling seems a promising solution path as described in Chapter 6.

Chapter 6 - DCT representation of LoRa signal

6.1 Compressive sampling (CS)

Compressive sampling is a promising alternative approach to standard sampling paradigms [81]. CS theory asserts that a reliable reconstruction of the signal of interest can be achieved from far fewer samples and measurements than traditional methods with no reduction of actual sampling rate. Accordingly, the CS, in the last years, has attracted considerable attention in signal processing, statistics and computer science, as well as the broader scientific community [82][83][84]. From a mathematical point of view, time-domain sampling of discrete signals can be expressed as

$$y[N] = \Phi[NxN] \cdot x[N] \qquad \textbf{Eq. 28}$$

y $\in R^N$ is the vector of measurements, x $\in R^N$ is the unknown input signal, Φ is an NxN sampling matrix [85].
The possibility to reduce the number of measurements required to completely describe a signal, often depends on compression, which aims to find the most concise representation of a signal that is able to achieve a target level of acceptable distortion. The most popular techniques for signal compression typically rely on finding a basis or frame that provides *sparse* or *compressible* representations for signals in a class of interest.
Sparsity expresses either the idea that the "information rate" of a continuous time signal may be largely smaller than what is suggested by its bandwidth, or that a discrete-time signal depends on a number of degrees of freedom which is comparably much smaller than its (finite) length [82][83].
Mathematically speaking, it is possible to express a signal in R^N in terms of a orthonormal basis of Nx1 vectors $\Psi = [\Psi_1,\ldots,\Psi_N]$ as

$$x = \sum_{i=1}^{N} s_i \Psi_i \qquad \textbf{Eq. 29}$$

Or

$$x[N] = \Psi[NxN] \cdot s[N] \qquad \textbf{Eq. 30}$$

Ψ is the NxN matrix with $\Psi_1,\ldots,\Psi_N$ as columns and s is a vector of size Nx1 [86].

Therefore, it comes without saying that *x* and *s* are equivalent representations of the same signal, with *x* in the time domain and *s* in the Ψ domain. The signal *x* is *K*-sparse in the basis Ψ if there are only few coefficients, K<<N, whose value is significantly different from zero.
The implication of sparsity is, thus, clear: a *K*-sparse signal is well approximated by only *k* coefficients and, hence, it can be represented without much perceptual loss by discarding the small coefficients and preserving only the values and locations of the largest coefficients [84].

In other words, since Ψ is an orthonormal basis (or "orthobasis"),

$$\|s - s_S\|_{l2} = \|x - x_S\|_{l2} \qquad \textbf{Eq. 31}$$

and if *x* is sparse or compressible in the sense that the sorted magnitudes of the (x_i) decay quickly, then *x* is well approximated by x_S and, therefore, the error $\|s - s_S\|_{l2}$is small [82].
The typical example is the sinusoidal signal. In the time domain it presents an endless evolution while in the Fourier domain it contains the same information in only two non-zero coefficients. Thus, the traditional approach consists of sampling the whole signal in the time-domain according to the Nyquist-Shannon theorem; then the acquired sequence is properly transformed in a K-sparse signal in order to drop the zero or negligible (N-K) values. Finally, the original signal is reconstructed by inverse transforming the *K* most significative

coefficients [85].
The performance of the compression process can be measured by the signal to noise ratio *SNR* and the compression ratio *Cr*:

$$SNR = 10\log\left(\frac{\sigma_x^2}{\sigma_e^2}\right) \quad \textbf{Eq. 32}$$

$$C_r = \frac{length\ of\ original\ signal}{length\ of\ compressed\ signal} \quad \textbf{Eq. 33}$$

σ_x^2 is the variance of the original signal and σ_e^2 the variance of the difference between original and reconstructed signals [86].

The Compressive Sampling

The traditional process, described above, of massive data's acquisition, followed by compression, is, evidently, extremely unworthy. It forces the acquisition system to spend a considerable effort collecting all the data and then computing all of the transforming coefficients, when it is already known that most of them will be discarded.
The Compressive Sampling arises to exceed this limit. It allows to sense the data directly in a compressed form, or to acquire at a sampling rate lower than the Nyquist one, without throwing away anything.
In other words, it is possible to acquire M<<N samples through the inner product between the signal and the sensing matrix Φ

$$y[M] = \Phi[MxN] \cdot x[N] \quad \textbf{Eq. 34}$$

By combining Eq. 34 and Eq. 30

$$y[M] = \Phi[MxN] \cdot \Psi[NxN] \cdot s[N] \qquad \textbf{Eq. 35}$$

It is possible to introduce a new MxN matrix Θ

$$\Theta[MxN] = \Phi[MxN] \cdot \Psi[NxN] \qquad \textbf{Eq.36}$$

Thus, the system becomes

$$y[M] = \Theta[MxN] \cdot s[N] \qquad \textbf{Eq. 37}$$

[85]

This measurement process is non-adaptive; that is, Ψ not dependant in any way on the signal *x*.

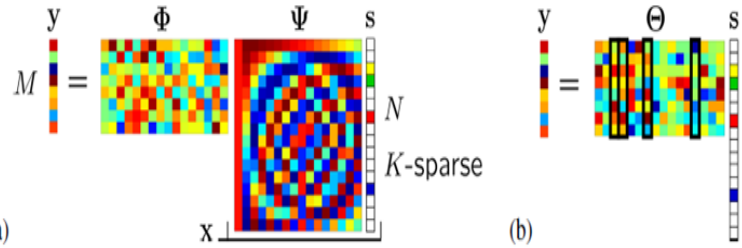

Figure 55 CS measurement with random measurement matrix Φ and DCT matrix Ψ, the s vector is 4-sparse. b) Measurement through Θ= ΦΨ, with the four columns corresponding to the non-unneglectable elements highlighted [37].

To make sure that a correct reconstruction of the signal from only M<<N measurements is allowed, CS theory relies upon two principles: the aforementioned sparsity and the incoherence. In fact, a

certain level of incoherence between the sensing matrix Φ and the representation basis Ψ is required: the greater the incoherence of the measurement/sparsity pair (Φ, Ψ), the smaller the number of measurement needed.
The coherence between Φ and Ψ is defined as

$$\mu(\Phi, \Psi) = \sqrt{N} \cdot max_{1 \le k,j \le N} \left| \langle \Phi_k, \Psi_j \rangle \right| \quad \textbf{Eq. 38}$$

Strictly speaking, the coherence measures the largest correlation between any two elements of Φ and Ψ. If Φ and Ψ contain correlated elements, the coherence is large. Otherwise, it is small. From linear algebra, it follows that

$$\mu(\Phi, \Psi) \in [1, \sqrt{N}] \quad \textbf{Eq. 39}$$

[82]

In the Fourier example, Φ consist of a discrete spikes basis

$$\delta_{m,k} = \delta[m-k] = \begin{cases} 1 & m = k \\ 0 & m \neq k \end{cases} \quad \textbf{Eq. 40}$$

And Ψ of the Fourier basis

$$\Psi_{n,k} = \frac{1}{\sqrt{N}} e^{j\frac{2\pi}{N}nk} \quad \textbf{Eq. 41}$$

In such case, there is the maximal incoherence

$$\mu(\Phi, \Psi) = 1 \quad \textbf{Eq. 42}$$

[85]

Solving the Equation 37 for *s* given *y* is a linear algebra problem, however, with M<N there are fewer equations than unknowns are.
Through the *K*-sparsity of *s,* it is possible to state that *y* is just a linear combination of *K* columns of Θ and thus it is possible to form an *MxK* system of linear equations with a number *M* of equations equal or greater than the *K* number of unknowns. For *K*-sparse signals, it is possible to demonstrate that a sufficient condition to make sure that the system is well conditioned is that Θ should satisfy, for an arbitrary *3K*-sparse vector *v*

$$1 - \varepsilon \leq \frac{\|\Theta v\|_2}{\|v\|_2} \leq 1 + \varepsilon \qquad \textbf{Eq. 43}$$

That is the so-called Restricted Isometry Property (RIP).

In alternative, it is worth considering the theorem, which states that the problem is well-conditioned if the following position upon the coherence holds

$$M \geq C * \mu^2(\Phi, \Psi) * S * \log(N) \qquad \textbf{Eq. 44}$$

M is the number of measurements, *C* a constant, *S* the sparsity of *s*. [84]
If the coherence is very close to one, or the incoherence between Φ and Ψ is very high, only *S*log(N)* samples are needed. This confirms that the highest the incoherence is and the fewer samples are requested.
It is demonstrable that it is possible, with high probability, to sidestep, for a given sparsifying basis Ψ, a high degree of incoherence, by choosing Φ as a proper random matrix. [84][85]

Signal recovery algorithms

Once the reconstruction of the original signal has been theoretically guaranteed, it is important to consider how to perform the recovery step. The goal is to regenerate the *N*-length signal *x*, or equivalently

its sparse coefficients' vector *s* from the measurements *y* and the Φ and Ψ matrices. On the face of it, Equation 37 presents an infinite number of solutions *s'*. The first aim is to find a useful signal's sparse coefficients vector *s*.
Having defined the *lp* norm of the vector **s** as

$$\left(\|s\|_p\right)^p = \sum_{i=1}^{N} |s_i|^p \qquad \textbf{Eq. 45}$$

The minimization of the l_2 norm (the *lp* norm for *p=2*), corresponding to the usual least square minimization, constitutes the most simple approach. However, the provided solution is almost never sparse, and consequently incorrect.
By contrast, the minimization of the l_0 norm, that considers only the number of coefficients of the solution, would be the optimal approach. Unfortunately, the solution of Equation 45 for *p=0* is numerically unstable.
Thus, the l_1 norm minimization represents the only possible solution. The provided results are close to those guaranteed by the l_0 norm and the computational burden is still acceptable also in presence of very long sequences.
The process of resolution of the Equation 45 for *p=1*, represents a convex optimization problem that reduces to a linear programming known as basis pursuit[84][85].

$$\hat{s} = argmin\|s'\|_1 \quad such\ that\ \Theta s' = y \qquad \textbf{Eq. 46}$$

Although there are many powerful recovery algorithms based on convex optimization techniques the one used in the following applications, for solving such problem, is a greedy/iterative method. This kind of algorithm relies on an iterative calculation of signals' coefficients and offers similar results to those awarded by the norm l_1, even if based on different approach.
Among the diverse kind of possible greedy algorithm implementations, the one used here is the Orthogonal Matching Pursuit (OMP).

The OMP begins by finding the column of Θ most correlated with measurements. This step is repeated by correlating the columns with the residual 'signal until either a limit on the number of iterations is reached or until a requirement, that $y = \Theta\hat{x}$ is satisfied [83].

6.2 CS and LoRa

As previously said the LoRa sequences may be very long depending on the information encoded in the payload and, consequently, the number of acquired points may become quickly too high to handle. The worst case is represented by a LoRa signal with BW 125 kHz and SF12, for which, bearing in mind Eq.12, the Time Symbol is the greatest possible

$$T_S = \frac{2^{12}}{125e3} = 32.768\, ms \qquad \textbf{Eq. 47}$$

Considering that, in EU the carrier of the LoRa signal is usually located about 868 MHz, respecting the Nyquist-Shannon criterion, the minimum sampling frequency requested to acquire the signal is 1736 MHz.
Thus, in the worst-case scenario, to acquire only one symbol of the signal about 57 million points would be necessary, whilst in order to acquire a preamble of 8 symbols, 455 million points would be necessary and so on, also considering that 5 billion points will be needed to acquire a payload of 100 symbols!
Hence, the CS could drastically reduce the record's length and so it represents the ideal solution to win the computational challenge posed by such a large number of points. Furthermore, the sparsity and incoherence allow to correctly reconstructing the original signal

without assuming any knowledge about this. For this reason, the CS represents an ideal modelling tool which permits every kind of signal processing: accurate statistical estimation, efficient data compression and, above all, classification [84].

The first challenge that arises when one tries to apply the CS paradigm to LoRa signals is the proper choice of the sparsyfing basis Ψ. Stationary signals, such as sinusoids or quasi-periodic speech segments, can be made sparse in the frequency domain through the classical Discrete Fourier Transform (DFT) or the Discrete Cosine Transform (DCT). In these cases, the Fast Fourier Transform (FFT) algorithm provides a very efficient way to obtain a sparse signal representation. On the contrary, basis functions involving chirplet or polynomial chirplet can be suitably tailored to LoRa signals [82][84], but involve an unacceptable computational burden. The proposed CS approach consists in dividing the LoRa signal in short time segments, each of which characterized by signal portion exhibiting an almost stationary frequency behavior. In particular, the whole observation interval is partitioned into sufficiently small intervals (referred to as acquired segments in the following) in which the instantaneous frequency swing is sufficiently low to reliably approximate the input signal by a sine wave of the same amplitude. The corresponding portions of the LoRa signal are acquired exploiting a compressive sampling approach that uses discrete cosine basis functions. A discrete signal x can be represented in terms of discrete cosine basis functions according to:

$$X(k) = \begin{cases} \sqrt{\frac{1}{N}} \sum_{n=0}^{N-1} x(n) \;\; for\; k = 0 \\ \sqrt{\frac{1}{N}} \sum_{n=0}^{N-1} x(n) \cos\left(\left[\frac{\pi(2n+1)k}{2N}\right] \; for\; k = 1, .., N-1 \right. \end{cases} \quad \textbf{Eq. 48}$$

where x(n) with n = 0, ...N-1 are the components of discrete-time array x, i.e. the samples of the input signal. Eq. 48 expresses a real transformation, named Discrete Cosine Transform (DCT), that offers higher computational efficiency with respect to classical Discrete Fourier Transform (DFT), since it does not involve complex-valued calculation. The time duration of each acquired segment must be defined according to the chirp rate signal. Let T_w be the duration of an acquired segment; the corresponding increment of the instantaneous frequency of the LoRa signal is given by:

$$\Delta f = \frac{BW}{T_s} T_w = \frac{BW^2}{2^{SF} 2\Delta f_w} \quad \boldsymbol{Eq.49}$$

where Δf_w is the frequency resolution featuring the representation in the DCT domain, which is inversely proportional to T_w i.e. $\Delta f_w = 1/(2T_w)$. Therefore, DCT coefficients have significant values only in a neighborhood centered in the corresponding average frequency of the signal and wide around Δf. In actual operating conditions, the worst case in terms of chirp frequency slope is associated with LoRa signals characterized by BW=500 kHz and SF=7 and equal to about 2 MHz/s. To assure a sparse representation of chirp signal in the observation interval, let the frequency variation Δf assumed to be equal to at most 10 times the frequency resolution Δf_w. If this is the case, solving Eq.49 for Δf_w,signal segmentation requires a time duration T_W equal to 50 μs. As an example, the DCT coefficients corresponding to the worst-case Lora signal acquired at 10 MSamples/s in the considered observation interval are shown in Figure 56. It is worth noting that only few tens of coefficients (represent less than the 5% of the whole set) are significantly different form zero. Hence, the signal can be considered locally sparse in the DCT domain and recovered through a compressive sampling approach. To achieve the sparse representation of the signal

of interest from its random samples, two main reconstruction approaches can be followed, referred to as basis pursuit and matching pursuit. With regard to reconstruction performance, BP approaches turned out be better than those based on MP; on the contrary, they are characterized by a heavier computational burden. With specific regard to the considered proposal, to solve the considered recovery problem and closely approximate the sparse coefficients of the signal of interest, a greedy approach has been deployed. The algorithm adopted approximates an OMP with a directional optimization scheme based on conjugate gradient. The CG is a quite popular procedure which approximates the burdensome orthogonal projection stage in a number of steps equal to the dimension of the problem.

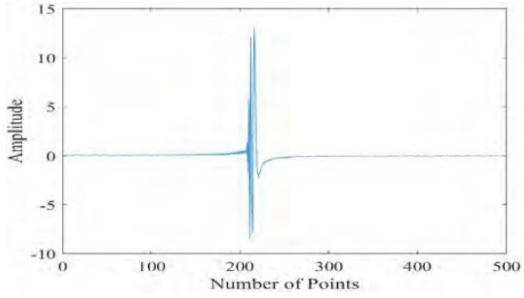

Figure 56 DCT representation of LoRa signal characterized by SF = 7 and BW=500 kHz, within a time interval not exceeding 50 μs

The CGP is faster than classical OMP methods [87] with lower storage costs, making it more suitable to problems with larger sizes while keeping a good accuracy level, especially in compressed sensing applications. In detail, the proposed approach can be implemented throughout the following steps:
random acquisition of M samples of the LoRa signal according to a quasi-random sampling scheme; segmentation of the acquired record in different subset of M_i successive samples, related to short intervals with duration not exceeding 50 μs; computation of N_i samples by processing the M_i samples through the adopted greedy algorithm

[83]; recovery of a long record characterized by N samples by linking the reconstructed frames. For the sake of clarity, the main steps of the proposed method are also elucidated by means of a flow diagram given in Fig. 58. Acquired signal can be classified using an algorithm exploiting classical signal processing tools using a lower number of points. This way, the CS approach allows the possibility to reduce the algorithm computational cost.

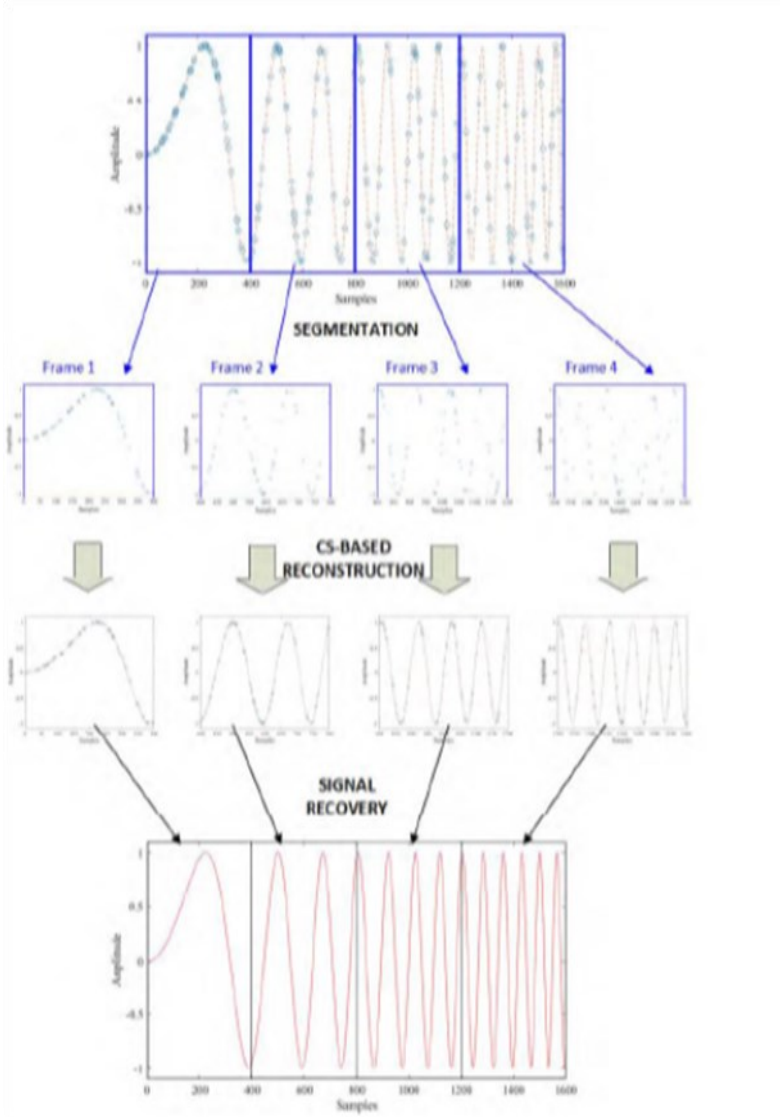

Figure 57 DCT representation of LoRa signal characterized by SF = 7 and BW=500 kHz, within a time interval not exceeding 50 μs

a

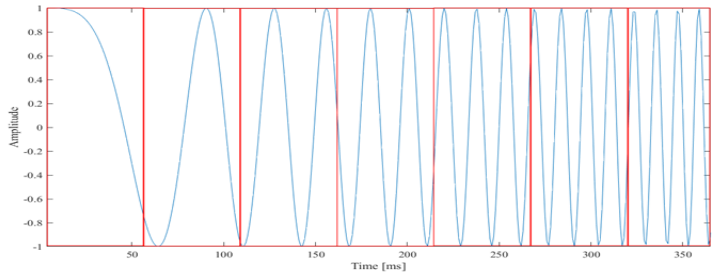

b

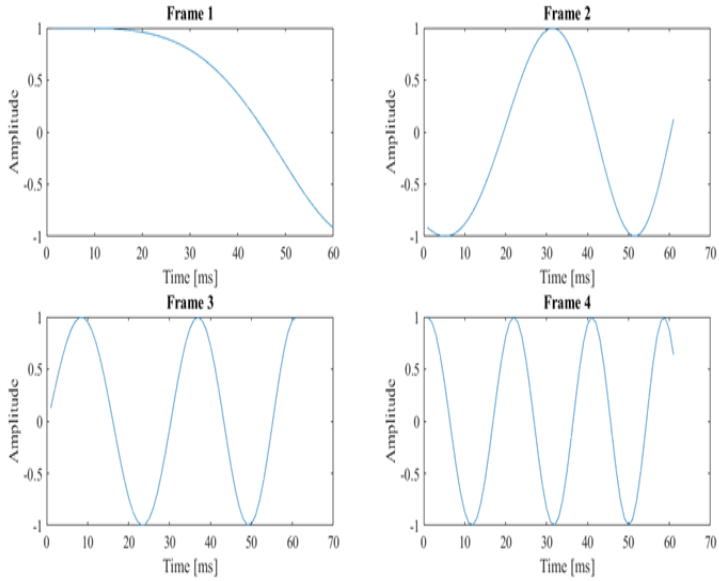

Figure 58 a) A chirp in the time domain divided in frames of 60 ms b) The first four frames of the chirp; let us note they are sinusoids with different frequencies.

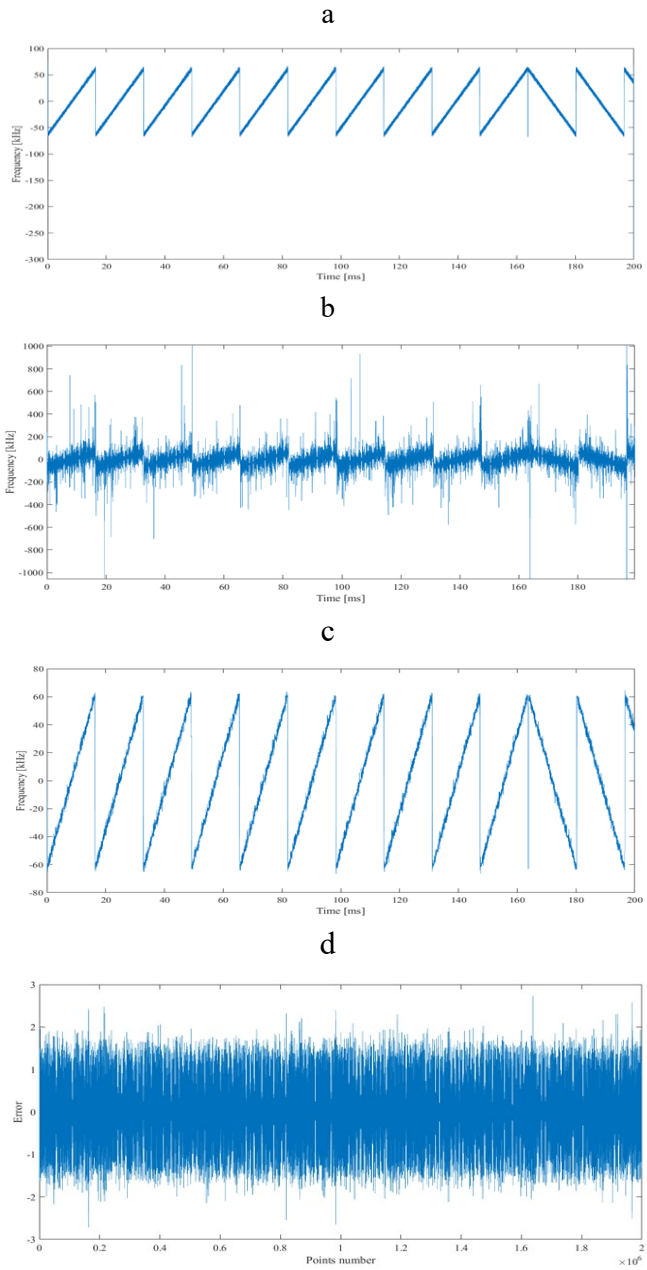

Figure 59 An example of compressed recovery of a LoRa signal with the approach proposed. a) The original signal in the time-frequency plane. b) The reconstructed signal with 15% of the samples in the time-frequency plane. c) The filtered reconstructed signal. d) The error between the original and the unfiltered reconstructed signal in the time domain.

6.3 Preliminary results

A proper experimental setup, shown in Figure 60, has been arranged to validate the proposed CS approach for Lora signal reconstruction and classification. LoRa signals have been generated by means of a 32-bits ARM STMicroelectronics Nucleo L152RE Mbed board and a Semtech SX 1272 LoRa shield. The LoRa shield has been connected to the Nucleo board in order to create a node of the LoRaWAN network. The node has been configured and controlled via USB interface by means of a Personal Computer running the web-based ARM Mbedplatform. A software routine programmed in C language has been edited, compiled and downloaded on the platform, thus enabling the configuration on the node of the LoRa parameters (bandwidth, spreading factor, coding rate, number of preamble symbols, bit rate, explicit or implicit header, CRC, carrier frequency, transmission power, etc.)

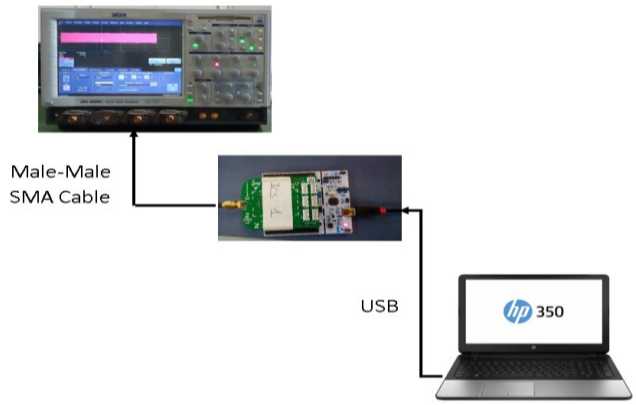

Figure 60 Experimental set-up for both the generation

The antenna connector of the node has been linked to a LeCroy

SDA6000A digital oscilloscope via a male SMA connector in order to acquire the generated LoRa signal. The tests have considered 36 LoRa signals realizations, that represent all the possible combinations of BW and SF for either lowest, 4/5, or highest, 4/8, coding rate.

SF/BW (CR4/5 and CR4/8)	125 kHz	250 kHz	500 kHz
7	BW125SF7	BW250SF7	BW500SF7
8	BW125SF8	BW250SF8	BW500SF8
9	BW125SF9	BW250SF9	BW500SF9
10	BW125SF10	BW250SF10	BW500SF10
11	BW125SF11	BW250SF11	BW500SF11
12	BW125SF12	BW250SF12	BW500SF12

Figure 61 The signals generated

The other signals parameters are set as:
Carrier Frequency: 868 MHz;
Transmission Power: 14 dBm;
Preamble Length: 8;
CRC: enabled;
Implicit header: off.
The oscilloscope is configured with the following

parameters for all the acquisitions:
Vertical volts/division scale: 500 mV/div;
Horizontal time/division scale: 20 ms/div;
Trigger mode: auto;
Sampling Frequency: 10 MSamples/s.

The selected configuration allows the acquisition of a time window of 200 ms. Some settings of Lora parameters result in signals exhibiting duration lower than 200 ms (BW125SF7, BW500SF10, BW250SF8), others characterized by higher SF and lower BW have a duration longer than 200 ms (for instance BW125SF10, BW250SF11, and BW500SF12). In the first scenario the irrelevant, additional samples are removed during a signal preprocessing step on the PC, in the second samples are partially acquired, these signals will be used for testing the algorithms' performances when the input data are incomplete.

Being fc equal to 868 MHz, the information of the LoRa signal is retrieved by observing its alias centered at 2 MHz. The chosen sampling frequency is lower than that required by the Shannon Nyquist criterion, granting many cheap available commercial board.

Specifically, pseudo-random noisy sequences have been generated according to values of SNR varying within the range from 50 dB to -20 dB with a -5 dB step and added to the input signal. The obtained results are given in Figure 62, where the percentage of correct classifications, for the signals with CR=4/5, are highlighted using a color map. The results are given as a function of the SNR and SF values. For each SNR SF couple, six percentage values are given; each SF is, in fact, associated with two rows: the upper one relates with the percentage of correct identification of BW; the lower one with the percentage of correct identification of SF. Moreover, results are given in three columns, corresponding to the three different BW values. By inspecting the provided color map, it is worth noting that

the blue region, where the percentage of correct classification is close to 100%, extends up to SNR 0.

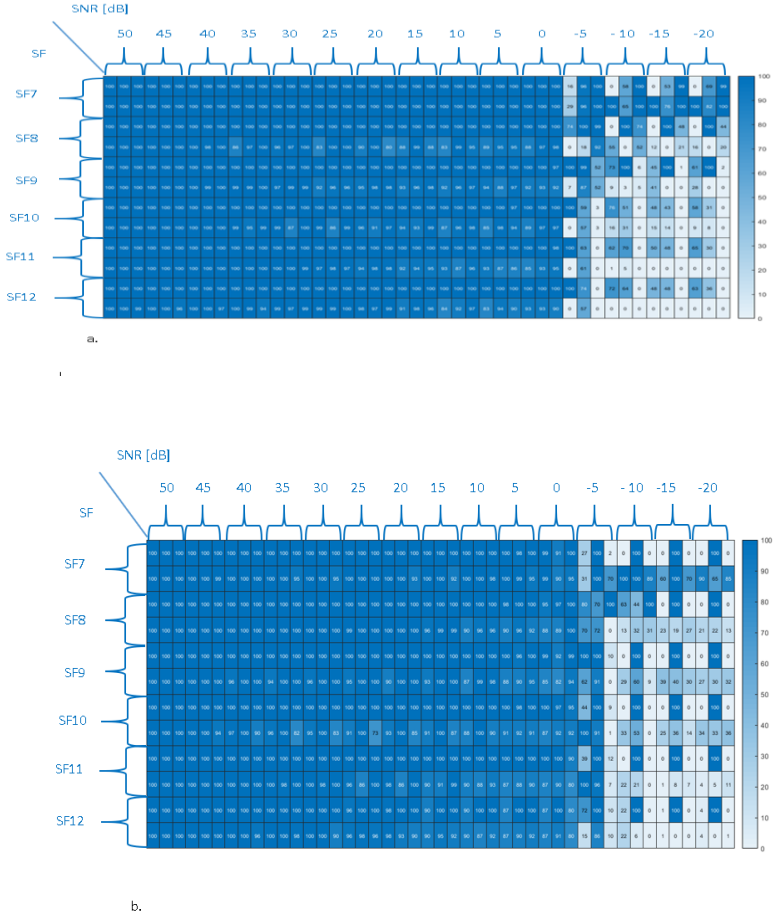

Figure 62 The tables indicate, in colour scale, the percentage of correct classifying BW and SF as the SNR varies, a) for the signals with CR=4/5 and b) for the signals with CR=4/8.

As the SNR decreases, the percentage of correct classification drastically gets worse. It is also interesting to observe that for negative SNR values the algorithm tends to underestimate the SF and the blue colored part for SF=7 extends up to -20 dB. In addition, for negative SNR values and SF up to 9, the percentage of correct classification is higher for the configuration with BW equal to 250 kHz and 500 kHz than for 125 kHz; on the contrary, for SF ranging within 10 and 12, the percentage of correct classification is better for the case BW equal to 125 kHz. The most interesting result, however, relates to the computational burden and execution time. In fact, the given results have been obtained with a number of samples equal to 15% of those requested by an approach based on a conventional sampling paradigm.

Chapter 7 - Estimation of interfering instantaneous frequency (IF)

7.1 Interfering instantaneous frequency (IF)

Non-stationary signals, in particular, do not lend themselves well to being decomposed into sinusoidal components. For these types of signals, the classical notion of frequency does not adequately describe the characteristics of the signal, and hence the need arises to introduce a parameter that describes the time-varying nature of the process. This need has led to the development of the concept of instantaneous frequency. The instantaneous frequency (IF) of a signal, in many applications, significantly describes the events that led to the genesis of the signal itself, allowing to obtain useful information about the physical phenomena related to it. Non-stationary signals are also used for estimating Doppler frequency shifts in radar, for tracking narrowband components in sonar, and for studying bat echo-location systems. For all these signals, the instantaneous frequency is an important feature: it is a time-varying parameter that defines the position of the spectral peak of the signal as a function of time. Conceptually, it can be interpreted as the frequency of a sine wave that locally fits the signal under analysis. Physically, it has meaning only for single-component signals, for which there is only one frequency or a small range of frequencies that changes position as time passes. For multicomponent signals, this concept loses its meaning and the analysis of individual frequency components becomes necessary. Van der Pol arrived at the definition of instantaneous frequency: $f_i(t) = \frac{1}{2\pi}\frac{d\phi(t)}{dt}$. Time-frequency representations were introduced to describe signals with time-varying frequency content, for which both time and frequency domain representations are inadequate. The advantage of these representations lies in the fact that all information regarding t-f laws is present in a single representation, from which the instantaneous

frequency law can be easily derived, using techniques for finding maxima. One expects a representation of the signal centered around the instantaneous frequency, with a width dependent on the Fourier transform of the signal envelope. The distribution is centered around the time-varying IF with the amplitude information distributed over time and frequency. Since the instantaneous frequency can be considered as the average of the frequencies present at a given instant of time, it seems reasonable to investigate the standard deviation, or more generally the spread, at that particular instant. This spread can be interpreted as the instantaneous band (IB), which is related to the instantaneous frequency in the same way that band and frequency are related in their common meanings. Within the framework of TFR theory, the concept of elementary cells specifying the signal concentration is also introduced, the size of the cells depending on the FM law of the signal and the BT product (Figure 63).

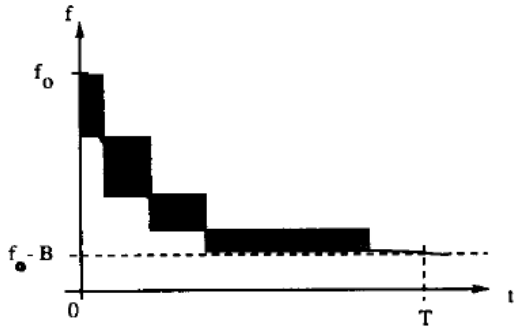

Figure 63 Elementary cells in the time-frequency plane

TFRs also allow easier study of multicomponent signals by direct observation of the time-frequency plane. It is possible to determine whether a signal is single-component or multicomponent by

observing whether the energy distribution at a particular instant of time is present around a single frequency or there is a clear separation of energy between two or more frequencies. It would be useful a methodology for maintenance and troubleshooting of LoRa networks sharing the same operating frequency interval. In this context the estimation of instantaneous frequency (IF) of signals characterized by interfering IF trajectories, can be very useful, for example to analyse transmission system quality. Both chirplet and warblet methodologies are excellent for the analysis of all those single-component and multicomponent signals composed of IF trajectories occupying distinct sectors of the TF plane. Due to their structure, however, they are inadequate for the study of multicomponent signals that present intersections. Infact for each of these methods we start from the assumption that after the calculation of the 'rough' TFR (the one calculated neglecting the various parameters characterizing the various atoms), applying the peak-location algorithm we have an estimate of the IF trajectories of the signal under examination. This, unfortunately, is not true for those signals which in the TF plane present an intersection. The limitations of the previous proposals will be illustrated in the following by referring to a significant example for the case of the optimized chirplet transform. Suppose we want to analyze a signal s(t) whose components have IF trajectories characterized by linear and intersecting paths. Figure 64 shows the imposed paths of the IF trajectories. The first step in the processing of such a signal is to perform an STFT transform (spectrogram) to verify the trend in the joint time-frequency domain of the signal components. It is important to note that an optimal choice of the effective window duration did not, however, yield better results, in terms of resolution in the TF plane, than those shown in Figure 65. At this point, the optimized chirplet method requires that the chirp parameters can be evaluated by analyzing the trajectories identified by the application of a peak location algorithm.

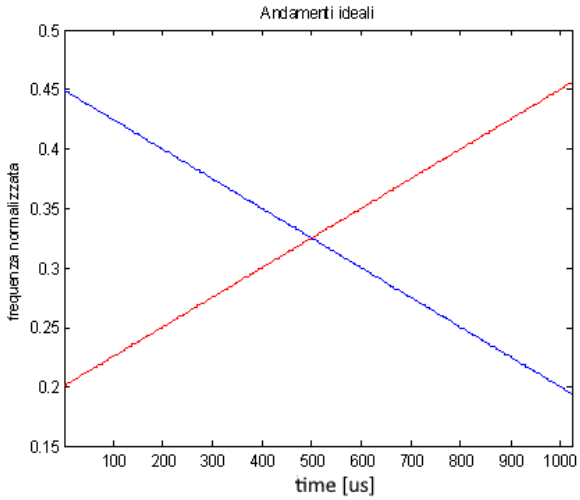

Figure 64 IF of s(t)

In the case under consideration, since the representations of the trajectories overlap in the TF plane, this algorithm gives rise to erroneous results: infact the situations shown in Figure 65, are possible depending on the relative value of the STFT coefficients.

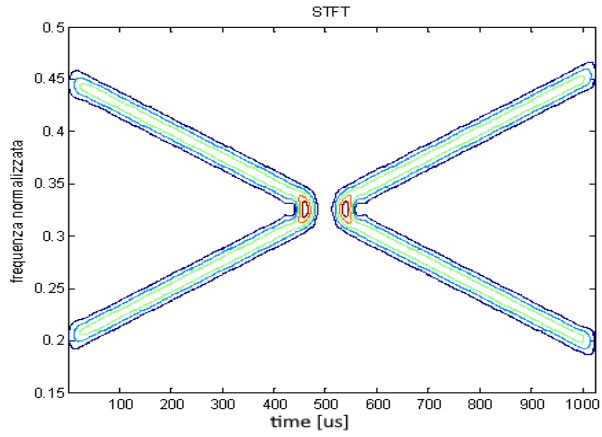

Figure 65 STFT of s(t)

From such trajectories it is therefore not possible to obtain a correct estimate of the values of the parameters characterizing the chirplet atom, consequently making it impractical to perform the optimized version developed in previous works[54],[55].

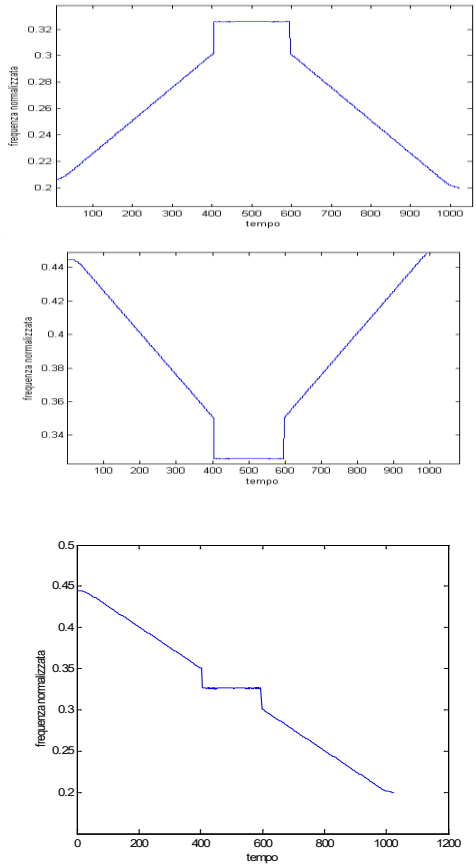

Figure 66 STFT of s(t)

7.2 Proposed method

In order to estimate the instantaneous frequency (IF) of signal with interfering IF, in this thesis work, a method based on numerical

signal processing is presented. The signal is first digitized and then processed through a proper algorithm in order to set the optimum value of the parameters of the mother chirplet (chirp rate, scale and curvature) according to its local features on each cell of TF plane. Starting from the same rough estimation obtained by STFT, allows to obtain the correct reconstruction of the IF trajectories in case they present intersection zones.

The proposed method consists of the following steps:

- Preliminary transformation of the signal in the TF domain by STFT.
- Optimization of the peak location algorithm for situations where no information is available on the portion of the TF plane occupied by the signal components under analysis.
- Localization in the TF plane of the intersections between trajectories.
- Identification of the parts of IF trajectories contained between two successive intersections.
- Aggregation of the IF trajectory sections identified on the basis of the analysis of suitable classifiers.
- Use of appropriate interpolation techniques to reconstruct the IF trajectory around the intersection.

The first step is to apply the STFT to the signal under test in order to derive the TFR matrix. The STFT is computed through a traditional algorithm based on moving window Fast Fourier Transform (FFT); the obtained results, taken in modulus and squared, provide the so-called spectrogram [56]. Let us suppose to analyze the signal s(t) shown in Figure 67 :

$s(t) = x(t) + y(t)$

x(t) and y(t) are expressed by

$x(t) = \cos [\, 2\pi(-125t^2 + 4.5 \cdot 10^5\, t)]$

$y(t) = \cos [\, 2\pi(125t^2 + 2 \cdot 10^5\, t)]$

$0<t<1024\ \mu s$

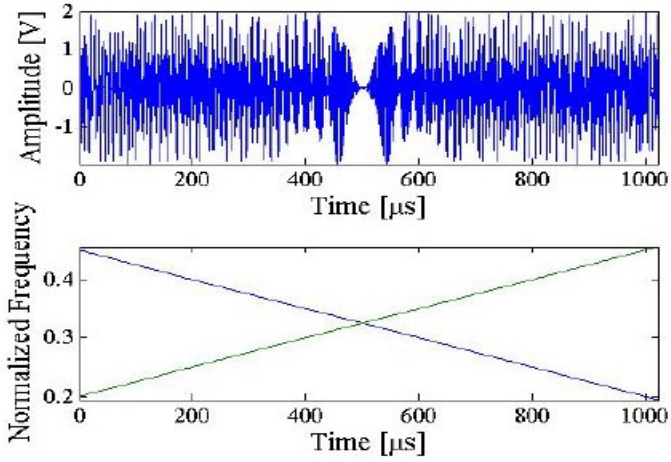

Figure 67 a) Signal involving two components with linear IF trajectories interfering with one another. b) Evaluation of the instantaneous frequency trajectories on the TF plane; the vertical axis of the time-frequency representation is normalized to the adopted sample rate (1 MS/s).

The signal spectrogram (Figure 68) is organized in a matrix. Each column of this matrix provides information about the frequency content of the signal at the time considered corresponding to the row index. Each column of the TFR is in fact the FFT of the signal multiplied by an appropriate Gaussian window. The choice of the duration of the window affects the resolution of the TF plane. A window of short duration will result in a good resolution in time but a poor resolution in frequency, vice versa you will have a very good resolution in frequency and a poor resolution in time for windows of long duration. For the choice of the optimal parameter, we must make a compromise between the good resolution in time and that in frequency; The length of the window is, in particular, chosen equal to 1.25‰ of the observation interval for achieving the desired resolution throughout the TF plane.

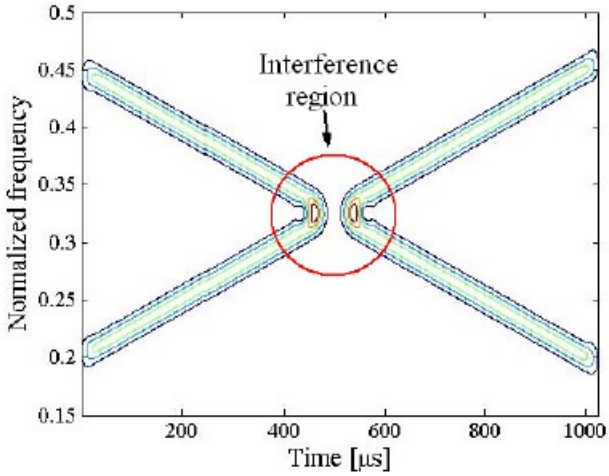

Figure 68 Contour plot of the spectrogram of the signal under test

A standard peak location algorithm is applied to each column of the matrix to roughly estimate the involved IF trajectories. Outside the interference region, the algorithm correctly points out the presence of two different IF trajectories (Figure 69);

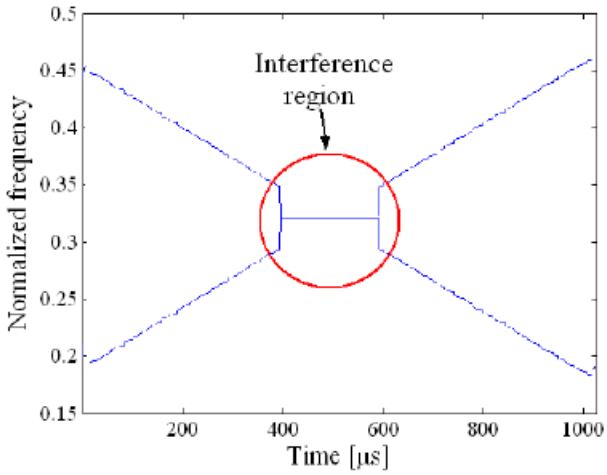

Figure 69 Results provided by the peak location algorithm when applied to the spectrogram values.

To gain the desired result the measurement procedure provides for the application of chirplet transform (CT) to the digitized signal; The parameters for the mother chirplet have, in particular, to be optimized according to the local features of the IF trajectories roughly estimated in the previous step. No optimization of the mother chirplet is possible in the interference region. Moreover, outside the interference region, the specific strategy adopted for CT calculation does not allow both IF trajectories to be evaluated in an optimized

way at the same time, that is for each sampling time, the parameters of the mother chirplet can be optimized according only to one IF trajectory. More applications of the CT are needed if an accurate reconstruction of all IF trajectories has to be pursued. The proposed solutions mainly concern the second and third steps of the measurement procedure (Figure 70).

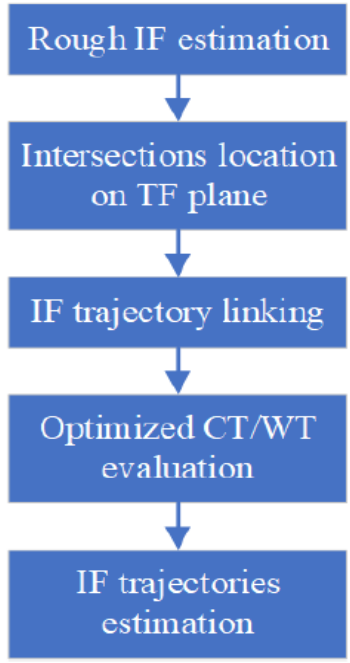

Figure 70 Block diagram of the proposed method.

Rough IF estimation

In the first step of the proposed method, the following actions are

carried out for each sampling time nT (n=1,..,N):

1. selection of the n-th column of the matrix containing spectrogram results

2. determination of all the local maxima included in the considered column

3. association of the IF frequency value to the detected local maxima,

As for the considered example, Figure 71 shows the spectral content related to the first column of the spectrogram matrix; two components are identified, and the values of the corresponding local maxima are collected respectively in record_1 and record_2.

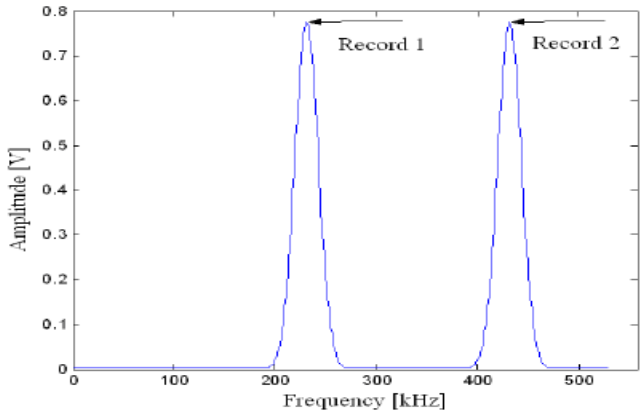

Figure 71 Content of the first column of the spectrogram matrix. The arrows single out the two local maxima collected in record 1 and 2.

Location on TF plane of the intersection and IF trajectories linking

In the presence of interfering IF trajectories, the number of detected local maxima could not match the number of components because the standard peak location algorithm isn't able to single out more than one local maximum in the interference region. So, the content referred to the interference region is eliminated from the records arranged in the previous step. The remaining portions of the records correspond to different segments of the measured IF trajectories; it is necessary to assess which segments belong to the same IF trajectory. To this aim, a suitable set of parameters, such as mean values of local maxima and derivatives of each segment in the neighborhood of the intersection, are enlisted. In the considered example, four portions, referred respectively to as segment_1, segment_2, segment_3, and segment_4 survive (Figure 72). Even though both IF trajectories are characterized by the same amplitude, the analysis of the first derivative allows to properly link segment 1 to segment 4 and segment 3 with segment 2 by means of straight lines. The application of traditional polynomial regression algorithms to the obtained IF

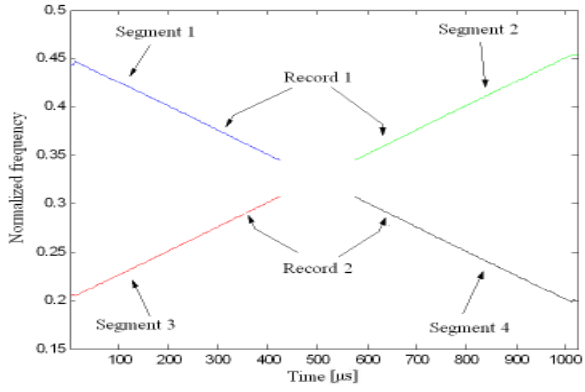

Figure 72 Four portions of IF trajectories, referred respectively to assegment 1,..,4, are identified by the proposed methods. The use of a suitable set of parameters allows to correctly link segments with one another.

trajectories finally allows to set the values of optimizing parameters of the CT mothers. It is worth noting that the number of involved mothers is equal to that of separate maxima singled out by the peak detection stage. The availability of records containing time-frequency location of IF trajectories allows to locally evaluate the optimized chirplet transform.

7.3 Preliminary results

Obtained results are reported in Figure 73; to suitably appreciate the method performance, the root mean square, expressed in dB, of the difference (RMSD) between nominal and estimated IF trajectories has been evaluated; values of -29.9 and -29.8 dB, respectively have been experienced for the signals involved in the application example.

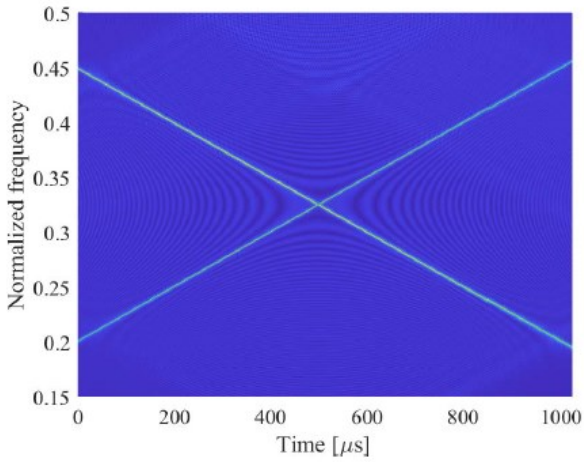

Figure 73 IF Trajectories estimated by means of the proposed method.

The performance of the method has been assessed by setting up a suitable measurement station capable of emulating and acquiring monocomponent and multicomponent signals, numerically generated and assumed as reference. It includes (i) a processing and control unit, (ii) an arbitrary waveform generator, and (iii) an 8-bit data acquisition system. All these instruments are interconnected by means of an IEEE-488 interface bus.

As another example, let us consider a two-components test signal, each of which exhibiting a sinusoidal IF trajectory:

$s(t) = x(t) + y(t)$

x(t) and y(t) are expressed by

$x(t) = \cos [\ 2\pi f_c t+(8.53\sin(2\pi \cdot 5859t)]$

$y(t) = \cos [\ 2\pi fct+(34.13\sin(2\pi \cdot 5859t)]$

f_c=250 kHz and f_s=1 MS/s.

Results of the rough time-frequency representation carried out by means of STFT are given in Figure 74, while IF trajectories provided by proposed method are plotted in Figure 75a. As it can appreciated, STFT results are characterized by inadequate readability, making it difficult the estimation of IF trajectories. On the contrary, a high-resolution representation is attained through the proposed method also in all the interference zones. Moreover, the adopted strategy for (WT) warblet transform evaluation (i.e. local optimal evaluation in the neighborhood of rough IF trajectory estimate) also allows each IF trajectory to be singled out (Figure 75b and c). Corresponding values of obtained RMSE were equal respectively to -27.4 and -27.2 dB [91],[92].

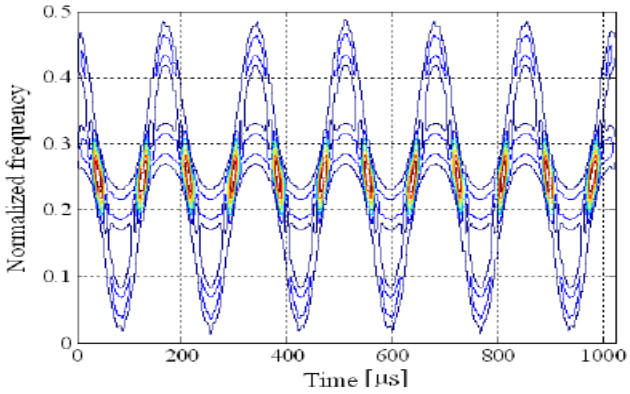

Figure 74 Results obtained through STFT

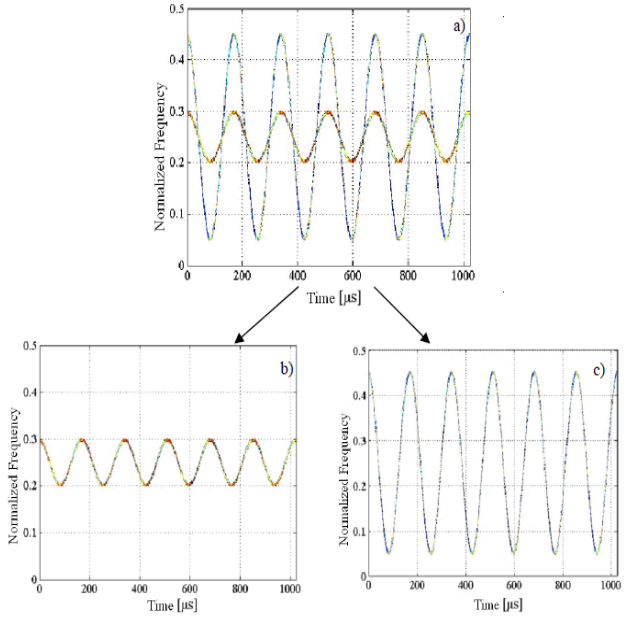

Figure 75 Contour plot on the time frequency plane of the results, taken in modulus and squared, obtained from the application of the proposed to the signal under test (a); the values on the vertical axis are normalized to the adopted sample rate (1 MS/s). The adopted strategy for WT evaluation also allows each IF trajectory to be singled out.

Conclusion

The research activities carried out during the Ph.D. have been mainly focused on the definition of innovative methods and strategies, tailored for the implementation of IoT platforms for the measurement and carrying out performance assessment on IoT communication protocol. In particular, a first research activity has deeply investigated a conceptual IoT framework that best suits the issues related to fire Propagation Map simulation and Evacuation Plan Model of animals, OPERA (OPtimal Evacuation Route for Animals), to support the activities of the Regional Veterinary referral Center for non-epidemic emergencies (CeRVEnE) in the Campania Region. The main issue but also the innovation is the integration of Distributed Sensor Network (DSN), an ad-hoc software to generate timely simulations for fire risk modeling, and a GIS (Geographic Information System) for all the activities. Guaranteeing the prevention of systematic failure in disaster risk management is the main goal of the system which use a "Foresight approach" perspective to grant it. A strong criticality is that the considered scenario, the Mount Vesuvius, hosts a unique combination of both animal and anthropic elements within a delicate natural ecosystem. IoT approaches are used with efficiency in human rescue activities, but this is not the case for animal rescue. Filling this gap by proposing one of the first attempts of IoT-enforced rescue system for companion, farm and wild animals well suits my research course.

Measuring and monitoring the concentration of possible nuclear pollutants turns out to be advisable or mandatory in several environmental contexts; the fast availability of an appropriate response plan allows, in fact, the consequences of radiation to be reduced or completely removed. So, the research activities also focused on the use of Internet of Things (IoT) to realize an integrated platform based on a cost-effective wireless sensor network (WSN) for monitoring environmental radioactive pollution. This solution has

fascinating features like scalability and flexibility to overcome the drawback of a classic monitoring system. Moreover, cloud data management and big data processing mechanisms, can face the relevant computational burden needed to carry out detection algorithms (as an example, those based on Bayesian methods). The monitoring platform mainly comprises sensor nodes, LoRaWAN communication modules, LoRaWAN Gateways and an Open-source IoT platform. Each sensor node consists of three modules: the radiation sensor, mandated to interact with physical quantity of interest; a suitable electronic interface, needed for analog processing the signal generated by the sensor and carrying out the required measurements; and an embedded Linux-based system, acting as node control, memory buffer and exchanging data with the communication modules. Different sensor nodes have been designed and implemented exploiting three radiation detectors. Nodes based on a Geiger sensor are exploited to measure the radiation level during the monitoring state and if anomalous levels of radioactivity are detected, Geiger nodes activate the identification state and other two type of nodes, based on silicon and scintillation detectors, wake up to measure the energy spectrum of alpha and gamma radiation, respectively. Network sensor nodes are connected by means of LoRaWAN protocol and use the “key-value” paradigm, which grants wide area coverage with reduced power consumption, to a proper Gateway, which exchanges measurement data and node information with a suitable platform implemented with the open-source platform ThingsBoard. With specific regard to the nodes, reference radioactive source with known energy spectrum has been adopted to assess the capability of the realized conditioning section and digital processing to carry out spectrometry and transmit the results to the IoT platform for the visualization.

On the other hand, the second path of research during the Ph.D can be addressed as “measurements for IoT”. Internet of Things paradigm requires even more reliable and long-distance communication systems. In this scenario, LoRa technology, based on

an efficient Chirp Spread Spectrum modulation can grant both long range distance and low energy consumption in the communication link. Also the challenge of acquiring and processing LoRa signals to extract valuable parameters like “Bandwidth and Spreading factor” has been addressed. Assessing the performance of LoRa devices is, at present, a costly task even if leader manufacturers of measurement solutions, which are also members of the LoRa Alliance, have already distributed their own proprietary hardware and software. Costs are basically related to the digitizer and its complementing acquisition memory and processor, adopted to digitize, save and process the input signal. In particular, the sampling strategy should grant a significant reduction of instrument memory requirements, which have a large impact on the hardware costs. So, an alternative approach to standard sampling paradigms, referred to as compressive sampling (CS), has been addressed. CS-based test solutions have been proposed and assessed to support classification tasks of signals exploiting common frequency modulation schemes, but LoRa relies on new challenging modulation schemes. So, during Ph.D activities a novel measurement instrument has been deeply investigated. It is based on digital signal processing strategies associated with low-cost acquisition hardware, for the reconstruction and classification of LoRa signals. The RF front-end of the instrument can be arranged using off-the-shelf modules and on CS paradigm that exploits the possibility of representing LoRa signals as locally sparse signals in terms of Discrete Cosine base functions. CS-based approach and a classification algorithm, designed to operate on the acquired signal is considered in order to highlight, throughout classification tests, the reliability at estimating the characteristic parameters of LoRa signals, bandwidth, spreading factor and symbol time of transmitted data, for given carrier frequency and sampling rate. The proposed CS approach consists in dividing the LoRa signal in short time segments, each of which characterized by signal portion exhibiting an almost stationary frequency behavior to reliably approximate the input signal by a sine wave of the same amplitude. The corresponding

portions of the LoRa signal are acquired exploiting a compressive sampling approach that uses discrete cosine basis functions. The proposed approach enlists the following operating steps: Random acquisition of M samples of the LoRa signal according to a quasi-random sampling scheme; segmentation of the acquired record in different subset of Mi successive samples, related to short intervals with duration not exceeding 50 μs; computation of Ni samples by processing the Mi samples through a greedy algorithm; recovery of a long record characterized by N samples by linking the reconstructed frames.

It also would be useful a methodology for maintenance and troubleshooting of LoRa networks sharing the same operating frequency interval. This context requires the estimation of instantaneous frequency (IF) of signals characterized by interfering IF trajectories. Two digital signal processing methods have been adopted, the first one based on chirplet transform that addresses IF trajectories whose evolution versus time can roughly be modelled by polynomial law. The second one exploiting the warblet transform (WT), addresses signals with IF trajectories, which exhibit a certain periodicity in the time domain. They decompose the signal under analysis into a set of oscillating, time-limited functions, all obtained by modifying an original window function, respectively called mother chirplet or warblet. They overcome some limits affecting traditional solutions, such as low time-frequency resolution or appearance of IF artifacts, while showing good accuracy (within 1%) along with remarkable resolving capability. Optimized versions also grant promising results where two or more IF trajectories interference with one another.

Bibliography

[1] Nolan, Keith & Guibene, Wael & Kelly, Mark. (2016). An Evaluation Of Low Power Wide Area Network Technologies For The Internet Of Things. 10.1109/IWCMC.2016.7577098.

[2] LoRa Device Developer Guide-Orange connected objects & partnerships. Available online: https://partner.orange.com/wp-content/uploads/2017/11/LoRa-Device-Developer-Guide-Orange.pdf

[3] A. Zanella, N. Bui, A. Castellani, L. Vangelista, and M. Zorzi, "Internetof Things for smart cities,"IEEE Internet Things J., vol. 1, no. 1,pp. 22–32, Feb. 201

[4] L. Sanchezet al., "Smartsantander: IoT experimentation over a smartcity testbed,"Comput. Netw., vol. 61, pp. 217–238, Mar. 201

[5] E. Park, Y. Cho, J. Han, and S. J. Kwon, "Comprehensive approachesto user acceptance of Internet of Things in a smart home environment,"IEEE Internet Things J., vol. 4, no. 6, pp. 2342–2350, Dec. 201

[6] E. Husniet al., "Applied Internet of Things (IoT): Car monitoring system using IBM BlueMix," inProc. Int. Seminar Intell. Technol.Appl. (ISITIA), Jul. 2016, pp. 417–42

[7] C. Brewster, I. Roussaki, N. Kalatzis, K. Doolin, and K. Ellis,"IoT in agriculture: Designing a Europe-wide large-scale pilot,"IEEECommun. Mag., vol. 55, no. 9, pp. 26–33, Sep. 201

[8] N. P. Sastra and D. M. Wiharta, "Environmental monitoring as an IoT application in building smart campus of Universitas Udayana," inProc.Int. Conf. Smart Green Technol. Elect. Inf. Syst. (ICSGTEIS), Oct. 2016,pp. 85–88.

[9] S. M. R. Islam, D. Kwak, M. H. Kabir, M. Hossain, and K.-S. Kwak,"The Internet of Things for health care: A comprehensive survey,"IEEE Access, vol. 3, pp. 678–708, 2015

[10] L. Li, "Application of the Internet of Thing in green agricultural products supply chain management," inProc. IEEE Int. Conf. Intell.Comput. Technol. Autom. (ICICTA), vol. 1. Shenzhen, China, 2011,pp. 1022–1025.

[11] IERC. (Mar. 2015).European Research Cluster on the Internet of Things-Outlook of IoT Activities in Europe. Accessed: Sep. 20, 2017.[Online].Available:http://www.internet-of-things-research.eu/pdf/IERC_Position_Paper_IoT_Semantic_Interoperability_Final.pdf

[12] N. Dlodlo and J. Kalezhi, “The Internet of Things in agriculture forsustainable rural development,” inProc. Int. Conf. Emerg. Trends Netw.Comput. Commun. (ETNCC), May 2015, pp. 13–18
[13] S. Wolfert, L. Ge, C. Verdouw, and M.-J. Bogaardt, “Big data in smartfarming—A review,”Agricult. Syst., vol. 153, pp. 69–80, May 2017
[14] O. Elijah, I. Orikumhi, T. A. Rahman, S. A. Babale, and S. I. Orakwue,“Enabling smart agriculture in Nigeria: Application of IoT and dataanalytics,” inProc. IEEE 3rd Int. Conf. Electro Technol. Nat. Develop.(NIGERCON), Owerri, Nigeria, Nov. 2017, pp. 762–7
[15] R. Nukalaet al., “Internet of things: A review from ‘farm to fork,”’ inProc. 27th Irish Signals Syst. Conf. (ISSC), Jun. 2016, pp. 1–6
[16] Y. D. Beyeneet al., “NB-IoT technology overview and experience fromcloud-RAN implementation,”IEEE Wireless Commun., vol. 24, no. 3,pp. 26–32, Jun. 2017
[17] U. Raza, P. Kulkarni, and M. Sooriyabandara, “Low power wide areanetworks: An overview,”IEEE Commun. Surveys Tuts., vol. 19, no. 2,pp. 855–873, 2nd Quart., 201
[18] R. S. Sinha, Y. Wei, and S.-H. Hwang, “A survey on LPWA technology:LoRa and NB-IoT,”ICT Exp., vol. 3, no. 1, pp. 14–21, 2017.[27]Machina.Accessed:Oct.1,2017.[Online].Available:https://machinaresearch.com/reports
[19] Locke, Dave. "Mq telemetry transport (mqtt) v3. 1 protocol specification." IBM developerWorks Technical Library (2010).
[20] X. Chen, Q. Shi, L. Yang, and J. Xu, “ThriftyEdge: Resource-efficientedge computing for intelligent IoT applications,”IEEE Netw., vol. 32,no. 1, pp. 61–65, Jan./Feb. 2018.
[21] G. Premsankar, M. D. Francesco, and T. Taleb, “Edge computing forthe Internet of Things: A case study,”IEEE Internet Things J.,vol.5,no. 2, pp. 1275–1284, Apr. 2018
[22] M. Asplund and S. Nadjm-Tehrani, “Attitudes and perceptions ofIoT security in critical societal services,”IEEE Access,vol.4,pp. 2130–2138, 201
[23] L. Chenet al., “Robustness, security and privacy in location-basedservices for future IoT: A survey,”IEEE Access, vol. 5, pp. 8956–8977,2017
[24] P. Varga, S. Plosz, G. Soos, and C. Hegedus, “Security threats andissues in automation IoT,” inProc. IEEE 13th Int. Workshop FactoryCommun. Syst. (WFCS), May 2017, pp. 1–6
[25] Khan, H.; Vasilescu, L.G.; Khan, A. Disaster management cycle. A theoretical approach. J. Manag. Mark 2008,6, 43–50.
[26] Carter,W.N. DisasterManagement: A DisasterManager’s Handbook;

Asian Development Bank: Manila, Philippines,2008.
[27] Bayo, N.; Antolín, D.; Medrano, N.; Calvo, B.; Celma, S. Early detection and monitoring of forest fire witha wireless sensor network system. Procedia Eng. 2010, 5, 248–251.
[28] Molina-Pico, F.; Cuesta-Frau, D.; Araujo, A.; Alejandre, J.; Rozas, A. Forest monitoring and wildland early fire detection by a hierarchical wireless sensor network. J. Sens. 2016, 1–8.
[29] Erten, E.; Kurgun, V.; Musaoglu, N. Forest fire risk zone mapping from satellite imagery and GIS: A case study. In Proceedings of the XXth Congress of the International Society for Photogrammetry and Remote Sensing, Istanbul, Turkey, 12–23 July 2004; pp. 222–230.
[30] Negi, M.S.; Kumar, A. Assessment of increasing threat of forest fires in Uttarakhand, Using Remote Sensing and Gis Techniques. Glob. J. Adv. Res. 2016, 3, 457–468.
[31] Voigt, S.; Tonolo, F.G.; Lyons, J.; Kuˇcera, J.; Jones, B.; Schneiderhan, T.; Platzeck, G.; Kaku, K.; Manzul Kumar Hazarika, M.K.; Czaran, L.; et al. Global trends in satellite-based emergency mapping. Science 2016, 353, 247–252.
[32] Qiao, C.; Wu, L.; Chen, T.; Huang, Q.; Li, Z. Study On Forest Fire Spreading Model Based On Remote Sensing And GIS. In Earth an Environmental Science (IOP Conference Series); IOP Publishing: Bristol, UK, 2018; Volume 199, p. 022017.
[33] Ziliaskopoulos, A.; Wardell, W. An intermodal optimum path algorithm for multimodal networks with dynamic arc travel times and switching delays. Eur. J. Oper. Res. 2000, 125, 486–502.
[34] Coburn, H.L.; Snary, E.L.; Kelly, L.A.;Wooldridge, M. Qualitative risk assessment of the hazards and risks from wild games. Vet Rec. 2005, 157, 321–322.
[35] OIE Bulletin. The ‘One Health’ Concept: The OIE Approach; WHO Outbreak communication guidelines; WHO/CDS: Geneva, Switzerland, 2005.
[36] Luzi, D.; Pecoraro, F.; Tamburis, O. Appraising Healthcare Delivery Provision: A Framework to Model Business Processes. Stud. Health Technol. Inform. 2017, 235, 511–515.
[37] Bayo, N; Antolín, D.; Medrano, N.; Calvo, B.; Celma, S. Early detection and monitoring of forest fire with a wireless sensor network system. Procedia Engineering 2010, 5, pp. 248-251.
[38] Molina-Pico, F.; Cuesta-Frau, D.; Araujo, A.; Alejandre, J.; Rozas, A. Forest monitoring and wildland early fire detection by a hierarchical wireless sensor network. Journal of Sensors 2016.
[39] Watts, J.M. Criteria for fire risk ranking. Fire Safety Science 1991, 3, pp.

457-466
[40] Marotta, N.; Maffei, P.L. L'analisi del valore nella valutazione del rischio incendio. Ambiente & sicurezza, Il Sole - 24 Ore Pirola, N. 23, 2000.
[41] Giannino, F.; Ascoli, D.; Sirignano, M.; Mazzoleni, S.; Russo, L.; Rego, F. A combustion model of vegetation burning in "tiger" fire propagation tool. In Proceedings of AIP Conference Proceedings, 1906, art. no. 100007, 2017.
[42] Giannino, F.; Russo, L.; Sirignano, M.; Di Fonzo, M.; Rego, F. A minimal model for the vegetation combustion in wildfire simulators. Chemical Engineering Transactions 2018, 67, pp. 19-24.
[43] Anderson, H.E. Aids to determining fuel models for estimating fire behavior (Vol. 122). US Department of Agriculture, Forest Service, Intermountain Forest and Range Experiment Station, 1981.
[44] C. D. Ferguson and M. M. Smith, "Assessing radiological weapons: attack methods and estimated effects," Defence Against Terrorism Review, vol. 2, no. 2, pp. 15-34, Fall 2009.
[45] J. Acton, B. Rogers, and P. Zimmerman, "Beyond the dirty bomb: re-thinking radiological terror," Survival, vol. 49, no. 3, pp.151-168, Jul. 2007.
[46] F. Ding, G. Song, K. Yin, J. Li, and A. Song, "A GPS-enabled wireless sensor network for monitoring radioactive materials,"Sens. Actuat. A Phys., vol. 155, pp. 210-215, 2009.
[47] D. Magalotti, P. Placidi, M. Paolucci, A. Scorzoni and L. Servoli,"Experimental characterization of a wireless personal sensor node for the dosimetry during interventional radiology procedures," IEEE Trans. Instrum. Meas., vol. 65, no. 5, pp. 1070-1078, May 2016.
[48] S. Corbellini et al., "Modified POF sensor for gaseous hydrogen fluoride monitoring in the presence of ionizing radiations," IEEE Trans. Instrum. Meas., vol. 61, no. 5, pp. 1201-1208, May 2012.
[49] A. Tocchi, V. Roca, L. Angrisani, F. Bonavolontà, and R. Schiano Lo Moriello, "First step towards an IoT implementation of a wireless sensors network for environmental radiation monitoring," in Proc. 2017 IEEE Int. Instrum. Meas. Technol. Conf. (I2MTC), pp. 588-593, 2017.
[50] B. Ooi, Z. Kong, W. Lee, S. Liew and S. Shirmohammadi, "A collaborative IoT-gateway architecture for reliable and cost effective measurements," IEEE Instrum. Meas. Mag., vol. 22, no. 6,pp. 11-17, Dec. 2019.
[51] C. Scuro, P. F. Sciammarella, F. Lamonaca, R. S. Olivito and D. L. Carni, "IoT for structural health monitoring," IEEE Instrum. Meas. Mag., vol. 21, no. 6, pp. 4-14, Dec. 2018.
[52] F. Abate, M. Carratù, C. Liguori, M. Ferro and V. Paciello, "Smartmeter

for the IoT," in Proc. 2018 IEEE Int. Instrum. Meas. Technol. Conf. (I2MTC), pp. 1-6, 2018.
[53] G. Betta, G. Cerro, M. Ferdinandi, L. Ferrigno and M. Molinara,"Contaminants detection and classification through a customized IoT-based platform: a case study," IEEE Instrum. Meas. Mag., vol. 22, no. 6, pp. 35-44, Dec. 2019.
[54] L. Angrisani and M. D'Arco, "A Measurement Method Based on a Modified Version of the Chirplet Transform for Instantaneous Frequency Estimation," IEEE Trans. on Instr. and Meas., vol. 51, no. 4,pp. 704-712, August 2002.
[55] L. Angrisani, M. D'Arco, R. Schiano Lo Moriello, M. Vadursi, "On the use of the warblet transform for instantaneous frequency estimation," IEEE Trans. on Instr. and Meas., vol. 54, no. 4, pp. 1374-1380, April 2004.
[56] Carratù, M., Ferro, M., Pietrosanto, A., & Sommella, P. (2017). Adopting smart metering RF networks for particulate matter distributed measurements. Paper presented at the 7th IMEKO TC19 Symposium on Environmental Instrumentation and Measurements, EnvIMEKO 2017, 2017-August 50-55.
[57] Bor, Martin & Roedig, Utz & Voigt, Thiemo & M Alonso, Juan. (2016). Do LoRa Low-Power Wide-Area Networks Scale?.10.1145/2988287.2989163.
[58] Augustin, A.; Yi, J.; Clausen, T.; Townsley, W.M. A Study of LoRa: Long Range & Low Power Networks for the Internet of Things. Sensors 2016, 16, 1466.
[59] SX1272/3/6/7/8: LoRa Modem Designer's Guide. Available online: https://www.semtech.com/images/datasheet/LoraDesignGuide_STD.pdf
[60] Bor, Martin & Vidler, John & Roedig, Utz. (2016). LoRa for the Internet of Things. EWSN. 361-366.
[61] Thiemo Voigt, Martin Bor, Utz Roedig, and Juan Alonso. 2017. Mitigating Inter-network Interference in LoRa Networks. In Proceedings of the 2017 International Conference on Embedded Wireless Systems and Networks (EWSN '17). Junction Publishing, USA, 323-328.
[62]]Semtech SX1272/73. Available online:http://www.semtech.com/images/datasheet/sx1272.pdf
[63] AN1200.22.LoRa™ Modulation Basics. Available online: https://www.semtech.com/images/datasheet/an1200.22.pdf
[64] E. Ruano, "LoRaTM protocol Evaluations, limitations and practical test", May 11 2016
[65] LoRaWAN™. What is it? Available online: https://www.lora-alliance.org/what-is-lora

[66] All about LoRa and LoRaWAN. Available online: http://www.sghoslya.com/
[67] Osama A. S. Alkishriwo. THE DISCRETE LINEAR CHIRP TRANSFORM AND ITS APPLICATIONS. PhD dissertation. University of Pittsburg. 2013
[68] Springer, Andreas & Gugler, Wolfgang & Huemer, Mario & Reindl, Leo & Ruppel, Clemens & Weigel, R. (2000). Spread spectrum communications using chirp signals. EuroComm Conference. 166 - 170. 10.1109/EURCOM.2000.874794.
[69] Ouyang, Xing & Dobre, Octavia & Guan, Yong & Zhao, Jian. (2017). Chirp Spread Spectrum towards the Nyquist Signaling Rate - Orthogonality Condition and Applications. IEEE Signal Processing Letters. PP. 1-1. 10.1109/LSP.2017.2737596.
[70] LoRa CSS-Modulation. Available online: https://home.zhaw.ch/~rumc/wcom2/unterlagen/wcom2chap3CSS.pdf
[71] Nicolas Sornin, Ludovic Champion. Patent. Signal concentrator device. US 20160020932 A1. 21 gen 2016.
[72] LoRa modem with LimeSDR. Available online: https://myriadrf.org/blog/lora-modem-limesdr/
[73] Keysight Technologies. The Internet of Things: Enabling Technologies and Solutions for Design and Test. Application Note 5992-1175EN, Keysight, https://www.keysight.com, 2017.
[74] Tektronix. Wireless Connectivity Test. Application Note 37W-60960-0, Tektronix, http://www.tek.com,2017.
[75] LoRaTM Alliance Members list. https://www.lora-alliance.org/The-Alliance/Member-List
[76] LoRaWAN ™ 101. A Technical Introduction. Available online: https://www.lora-alliance.org
[77] SX1276MB1xAS. Available online: https://os.mbed.com/components/SX1276MB1xAS/
[78] Thiemo Voigt, Martin Bor, Utz Roedig, and Juan Alonso. 2017. Mitigating Inter-network Interference in LoRa Networks. In Proceedings of the 2017 International Conference on Embedded Wireless Systems and Networks (EWSN '17). Junction Publishing, USA, 323-328.
[79] Demodulazione I & Q. Available online: http://infocom.uniroma1.it/rrsn/wiki/uploads/TelecomunicazioniPerLAerospazio/08_TLC_AES_demodulazione_IQ.pdf
[80] What is I/Q? Available online: http://www.ni.com/tutorial/4805/en/
[81] Candès, E.J.; Wakin, M.B. An introduction to compressive sampling. IEEE signal processing magazine 2008, 25, 21 30.
[82] Yu, G.; Zhou, Y. General linear chirplet transform. Mechanical

Systems and Signal Processing 2016, 70, 958 973.
[83] Mann, S.; Haykin, S. The chirplet transform: Physical considerations. IEEE Transactions on Signal Processing 1995, 43, 2745 2761.
[84] Peng, Z.; Meng, G.; Chu, F.; Lang, Z.; Zhang, W.; Yang, Y. Polynomial chirplet transform with application to instantaneous frequency estimation. IEEE Transactions on Instrumentation and Measurement 2011, 60, 3222 3229.
[85] Hsiao, Y.H.; Chen, C.C. Over-atoms accumulation orthogonal matching pursuit reconstruction algorithm for fish recognition and identification. 2016 23rd International Conference onPattern Recognition (ICPR), IEEE, 2016, pp. 1071 1076
[86] Angrisani L., Bonavolonta F., D'Apuzzo M.,Schiano Lo Moriello, R.; Vadursi, M. A compressive sampling-based method for power measurement of band-pass signals. Instrumentation and Measurement Technology Conference(I2MTC), 2013 IEEE International. IEEE, 2013, pp. 102 107.
[87] Blumensath, T.; Davies, M.E. Gradient pursuits. IEEE Transactions on Signal Processing 2008, 56, 2370 2382
[88] KEY CHALLENGES OF THE INTERNET OF THINGS. A Guide to Building IoT Ready Devices. Available online: https://www.tek.com/document/how-guide/6-key-challenges-internet-things
[89] Infographic: The Growth Of The Internet Of Things. Available online: https://www.ncta.com/platform/industry-news/infographic-the-growth-of-the-internet-of-things/
[90] H. Schmidbauer (September 2016). NB-IoT vs LoRa™ Technology. Which could take gold? A White Paper prepared for the LoRa Alliance™.
[91] L. Angrisani, PhD student A. Tocchi, D. Ruggiero, R. S. Lo Moriello, G. de Alteriis and F. Capasso, "Estimation of Instantaneous Frequency in the Presence of Interfering Trajectories," 2020 IEEE International Instrumentation and Measurement Technology Conference (I2MTC), 2020, pp. 1-6, doi: 10.1109/I2MTC43012.2020.9128597.
[92] VI Angrisani, L., Bonavolontà, F., Dassi, C., Liccardo, A., Moriello, R.S.L., PhD Student Tocchi, A. 7006649427;55825402400;57205436107;14631935200;57212675767;57014887400;On the suitability of compressive sampling for lora signals classification (2020) International Review of Electrical Engineering, 15 (3), pp. 187-198. Cited 3 times.https://www.scopus.com/inward/record.uri?eid=2-s2.0-85090686574&doi=10.15866%2firee.v15i3.18129&partnerID=40&md5=

0a26f2246429bfaa0774a606e3e666ba
[93] R. S. Lo Moriello, PhD Student A. Tocchi, A. Liccardo, F. Bonavolontà and G. de Alteriis, "Exploiting IoT-Oriented Technologies for Measurement Networks of Environmental Radiation," in IEEE Instrumentation & Measurement Magazine, vol. 23, no. 9, pp. 36-42, December 2020, doi: 10.1109/MIM.2020.9289067.
[94] Tamburis O, Giannino F, D'Arco M, PhD Student Tocchi A, Esposito C, Di Fiore G, Piscopo N, Esposito L. A Night at the OPERA: A Conceptual Framework for an Integrated Distributed Sensor Network-Based System to Figure out Safety Protocols for Animals under Risk of Fire. Sensors (Basel). 2020 Apr 29;20(9):2538. doi: 10.3390/s20092538. PMID: 32365698; PMCID: PMC7249212.